QUINOL ACTIVITY OF CYTOCHROME AA_3-600 MENAQUINOL OXIDASE FROM *BACILLUS SUBTILIS* CHARACTERIZED BY BIOCHEMICAL AND EPR METHODS

BY

SOPHIA M. YI

DISSERTATION

Submitted in partial fulfillment of the requirements
for the degree of Doctor of Philosophy in Biochemistry
in the Graduate College of the
University of Illinois at Urbana-Champaign, 2016

Urbana, Illinois

Doctoral Committee:

Professor Robert B. Gennis, Chair
Professor Yi Lu
Professor Emeritus Antony R. Crofts
Professor Wilfred A. van der Donk

ABSTRACT

The membrane protein cytochrome (cyt) aa_3-600 menaquinol oxidase from *B. subtilis* is uniquely a heme-copper oxygen reductase that uses substrate menaquinol instead of cytochrome c. The cyt aa_3-600 accepts electrons from menaquinol (or Vitamin K_2) and channels them one-at-a-time to low-spin heme A and finally to the binuclear center where oxygen is reduced to water. In order to characterize the protein-quinone interaction, cyt aa_3-600 has been cloned with a His-tag, expressed and purified from the native system. One equivalent of quinone is found to strongly associate with isolated protein.

The enzyme stabilizes a menasemiquinone radical (SQ) at a high affinity site (Q_h) that is important for catalysis. The molecular details of the stabilized SQ revealed by 1D-, 2D- X-band ^{14}N, ^{15}N electron spin echo envelope modulation (ESEEM) experiments indicate that a nitrogen having the largest hyperfine interaction ($^{14}A \sim 0.9$ MHz) likely belongs to side chain of Arg. In addition, ^{1}H, ^{2}H ESEEM spectra show two strongly coupled exchangeable protons with anisotropic components ($|T| = 5.6$ and 2.9 MHz) that form H-bonds with the SQ. The H-bond interactions involve protonated nitrogen of Arg70 and acidic side chain of Asp74. These residues face one carbonyl group of the SQ ring structure and orchestrate an asymmetric H-bonding around the quinone head group.

The Q_h-site of cyt aa_3-600 contains conserved residues Arg70, Asp74, His94 and Glu97 that are considered functionally important. Several mutations have been introduced at the Q_h-site. Among the Q_h-site mutants, the R70H mutant, showing a strong quinol oxidation activity, was able to generate menasemiquinone radical that was examined further by advanced X- and Q-band EPR. The bound SQ of the R70H mutant exhibits a strong isotropic hyperfine coupling ($^{14}A \sim 2.0$ MHz) with a hydrogen bonded nitrogen. This nitrogen originates from a histidine side

chain, based on its quadrupole coupling constant, e^2qQ/h = 1.44 MHz, typical for protonated imidazole nitrogen atoms. In the wild type cyt aa_3-600, the SQ is instead hydrogen bonded with N_ε from the Arg70 side chain. Analysis of the 2D- X-band ^1H, ^2H ESEEM spectra shows that the mutation also changes the number and strength of the hydrogen bonds between the SQ and the surrounding protein. Despite the alteration in the immediate environment of the SQ, the R70H mutant remains catalytically active. These findings are in contrast to the equivalent mutation in the close homologue, cytochrome bo_3 ubiquinol oxidase from *E. coli*, where the R71H mutation eliminates function.

The current work on cyt aa_3-600 and its mutants suggests that one-site quinone model describes the specific activity values better than the two-site model that has been advocated, thus far. None of the Q_h-site mutants in cyt aa_3-600 is able to eliminate quinol oxidase activity, except for Asp74 mutants that show structural disturbance of low-spin heme A. In the past, the corresponding Q_h-site mutants in cyt bo_3 have shown complete loss of activity, but new evidence suggests that some of the quinol activity can be restored with menaquinol-based substrate, a molecule having low midpoint potential. The differences between the protein-quinol interactions of the bo_3-type ubiquinol oxidase and the aa_3-600 menaquinol oxidase appear to be based on the reactivity of the substrate quinol and the asymmetric H-bonding pattern imposed by the protein structure. A possible mechanism of quinol oxidation is proposed, where the Glu97 in cyt aa_3-600 replaced by Gln101 in homologous cytochrome bo_3 ubiquinol oxidase of *E. coli* is considered to play a significant role. Overall, the evidence leads to structural similarity of the Q_h-sites found in cyt bo_3 and cyt aa_3-600, and cyt bo_3 is remarkable in being able to accommodate both ubiquinol and menaquinol as substrates.

ACKNOWLEDGEMENTS

This has been overall a humbling experience. I am grateful to Bob, my advisor, for his support over the transformative years I have spent under his watch. Without his patience and steadfastness towards the project, it would not have been possible to see it come to fruition. Because of his kind support, I have been able to stay relevant in scientific research.

Both Drs. Sergei Dikanov and Rimma "Marina" Samoilova have been amazing in their expertise of pulsed EPR techniques. They have been also generous and kind in sharing of their time and knowledge. Working with them closely and with other like-minded individuals like Alex T. and Dr. Patrick O'Malley (U. of Mancheser, UK) made it possible to advance progress in understanding protein-quinone interaction.

Gennis Group members have provided valuable support throughout the time devoted to this research project, and I am grateful for their caring, kindhearted gestures that have never been in short supply. I would like to thank Dr. Lu and his group members for allowing me and others from Gennis Group to use instruments and share workspace. Sometimes support comes quietly in unexpected places, and I was very fortunate to have members of thesis committee who made impossible situations possible and who were supportive, despite their hectic schedules. Especially, I owe debt of gratitude towards Jeff Goldberg from Biochemistry Dept. for keeping an oversight over administrative affairs that requires detailed knowledge of rules governing the graduate studies.

Various *Bacillus* expression plasmids originated from van Wachenfelt Group (Sweden), Ordal Group (UIUC) and Dr. Daniel Zeigler from *Bacillus* Genetic Stock Center (Ohio State). The *E. coli* cyt bo_3 expression strain CLY cyoABCD was made accessible by Myat Lin (Gennis Group), and the *Vibrio cholera* strain was received from Hanlin Ouyang (Gennis Group). The Rosetta strain was made available by James Hemp (Gennis Group).

The expression strain for diaphorase was received from Elena Maklashina of Dr. Gary Cecchini's Group (UCSF). Ke Yang (Gennis Group) provided the purified *E. coli* bd I oxidase sample used to evaluate the activity assay. Todd Holland (Crofts Group) offered helpful discussions on potentiometric titration experiment, and Mark Nilges (EPR center) was an incredible resource on EPR spectroscopy. The early exploration of ATR-FTIR and crystallization techniques was possible because of kind assistance from Ahmet Vakkasoglu (Gennis Group) and J.P. Zhu (Gennis Group), respectively. Ziquio "Tim" Ding (Gennis Group) is carrying on the collaboration efforts with Nair Group (UIUC) to crystallize cyt aa_3-600. Recently, Chang "Charles" Sun (Gennis Group) has conducted Q-band ^2H ENDOR experiments of cyt bo_3 and has carried on a collaborative work on molecular dynamic simulation that provided an insight on the SQ interaction with Arg71 in cyt bo_3.

TABLE OF CONTENTS

CHAPTER 1: Introduction

The cytochrome aa_3-600 from *Bacillus subtilis* (*B. sub*) belongs to a superfamily of terminal oxidases that are functionally important as the final electron acceptors of the oxidative phosphorylation, in reducing dioxygen to water and in driving protons across the cytoplasmic membrane to generate a proton motive force. Thereby, cytochrome oxidases perform critical role in the complete metabolism of both carbon and non-fermentable carbon food source and in contributing to energy conservation in the form of ATP synthesis. The modes of binding and reducing oxygen to water and translocating protons across the membrane have been generally accepted to be consistent among the members of this class of enzymes, based on high structural similarities and CO-flash photolysis studies [1-4]. However, two different electron input mechanisms divide the enzyme complexes belonging to this family: quinol and ferrocytochrome c (cyt c).

$$O_2 + 4e^{-1} + 8H_{in}^{+} \leftrightarrows 2H_2O + 4H_{out}^{+}$$

The transmembrane protein *B. sub* cyt aa_3-600 accepts a pair of electrons from menaquinol, lipid-soluble vitamin K_2, a counterpart to ubiquinol in mitochondrial membrane. There is a structural significance associated with this preference in electron-donating substrate. The cyt aa_3-600 does not have the di-copper Cu_A center in its subunit II that is responsible for electron transfer from ferrocytochrome c to low-spin heme A in subunit I [5]. Since the oxygen reduction mechanism is thought to be identical regardless of the electron donor, the menaquinol must sequentially donate electrons to the low-spin heme. However, it is not known whether there is, as in Cu_A center of cyt c oxidase or in the primary quinone-binding site (Q_A site) of the photosynthetic reaction center, any mediation in the electron transfer pathway from quinol to the

low-spin heme or whether quinol can donate electrons directly to low-spin heme A. Further work is needed in clarifying the number and location of quinone or quinol binding sites.

Many proteobacteria contain heme-copper respiratory oxygen reductases that utilize a membrane-bound quinol as the substrate [6]. Among these protein complexes is the well-characterized *E. coli* cyt bo_3 oxidase that depends on ubiquinol as its substrate and shares high sequence identity with cyt aa_3-600. Structural and functional characterization of high affinity quinone binding site (Q_h) in cyt bo_3 has benefited from site-directed mutagenesis, biochemical and inhibition studies and EPR methods. It is the intent of this report to carve out a similar path for cyt aa_3-600 in defining the structure-based function of protein-quinone interaction and in contributing to understanding of the basis for different quinones used by the cytochrome quinol oxidases.

1.1. Research goals

A study of the quinol activity in cytochrome aa_3-600 menaquinol oxidase and determining the functional significance of the quinone binding site, Q_h:

1. Building a cytochrome aa_3-600 expression system in *Bacillus subtilis* (Chapter 2)
2. Developing quantifiable approaches to describe protein-quinone interaction in cyt aa_3-600 (Chapter 3)
3. Characterizing the electron-nuclear hyperfine interaction involving semi-menaquinone radical at the Q_h-site by EPR spectroscopy (Chapter 4)
4. Probing the Q_h-site in cyt aa_3-600 by site-directed mutations, biochemical studies and EPR methods to ascertain its role during electron transfer (Chapters 5 and 6)

1.2. Cytochrome aa_3-600 menaquinol oxidase from *Bacillus subtilis*

The *Bacillus subtilis* (*B. sub*) cytochrome (cyt) aa_3-600 complex is composed of four subunits, and subunits I, II, and III are homologous to the three largest subunits found in the mitochondrial oxidase [7]. The sequence of subunit I from the menaquinol oxidase, as with all other members of the oxidase superfamily, includes the six histidine residues that serve as ligands to heme A and the heme a_3-Cu_B centers [34-38]. However, in the sequence of subunit II of menaquinol oxidase the ligands identified to bind Cu_A in other oxidases have not been conserved and the EPR signal characteristic of the Cu_A center is not observed [5]. The lack of Cu_A is consistent with the inability of cyt aa_3-600 to oxidize cyt c, since Cu_A is proposed to be the initial site of electron entry from reduced cyt c [8].

The cyt aa_3-600 is named after the heme A's present in its redox centers and to indicate the distinctive shift to 600 nm of the alpha-band absorption maximum from 605 nm seen with mitochondrial cyt c oxidase [9]. The low-spin heme A is proposed to perform the role of electron transfer. The heme a_3 also contains heme A, but has only one of its axial ligand positions stably occupied by a histidine residue from subunit I. The other axial position of heme a_3 is available for exogenous ligands to bind, such as the substrate oxygen, or inhibitors, like cyanide. The heme a_3 is closely associated with Cu_B, which is ligated by three histidine residues from subunit I in a position approximately 5 Å from the heme iron of heme a_3. These two metal centers are magnetically coupled and form a binuclear center, heme a_3-Cu_B.

The interaction of heme a_3-Cu_B binuclear center with ligands, such as cyanide and hydrogen peroxide, shows reactivity similar to the mitochondrial enzyme [1, 5, 10, 40]. The heme a_3 and Cu_B binuclear center has been found to resemble in many respects the oxygen

reaction site found in mitochondrial cyt c oxidase. The heme a_3 iron is closely coupled to Cu_B, as revealed by EXAFS spectroscopy [11, 12].

1.3. Issues regarding quinone-mediated electron transfer in cytochrome oxidase

The available information for many quinone-reactive sites in different respiratory and photosynthetic complexes shows very weak sequence and structural similarities [13]. Quinone as electron carrier and its interaction with different proteins with no common protein binding motif is evidence of complexity in protein-quinone interaction and of broad application of quinone redox chemistry in nature.

The menaquinone receives electrons from a variety of dehydrogenases and acts as reductant for cyt bc_1-type complexes [14]. Menaquinol directly donates electrons to a terminal oxidase cyt aa_3-600 in *B. subtilis*, and therefore, bypasses the traditional cyt bc_1 reaction. The cyt bc_1-type membrane protein oxidizes two quinol molecules to regenerate a quinol and reduced cyt c and contributes to proton motive force by using separation of charge across the cytoplasmic membrane through the redox-loop mechanism. This reaction leads to release of four protons at the periplasmic side of the membrane per quinol oxidized. Hence, cyt aa_3-600 may be considered to be less energy efficient than cyt c oxidase, which depends on the redox chemistry performed by cyt bc_1 complex in generating single-electron reduced cyt c.

Not knowing the number and location of quinone binding sites has complicated understanding of substrate specificity in quinone reactive proteins including cyt aa_3-600 oxidase. Generally, quinone binding proteins often have two quinone (or quinol) binding sites in order to facilitate the coupling of one electron redox chemistry to a two-electron donor (or acceptor). For cyt aa_3-600, having two quinone binding sites fits neatly with the mechanism that describes

how menaquinol, a two-electron donor, interacts with cytochrome oxidase that carries out strictly single electron process, where oxygen is reduced to water. The catalytic reaction generates free radicals as intermediate states that could cause damages at scales both small and large, and requires a tight control over the protein-quinone interface and the oxygen binding at the binuclear center. Hence, a potential quinone binding model, satisfying above conditions, would involve one quinone binding site that exchanges freely with the membrane quinol pool and acts as the substrate binding site and the second quinone site that is less mobile with higher affinity and behaves like Cu_A center in cyt c oxidase.

In cyt aa_3-600, a molar equivalent of quinone is present in isolated protein that leads to EPR signal at g-value of 2.0 for semiquinone radical during steady-state enzyme turnover [15, 16]. This observation confirms the presence of a high affinity quinone binding site (Q_h), which has been the subject of extensive investigation in homologous *E. coli* cyt bo_3 ubiquinol oxidase.

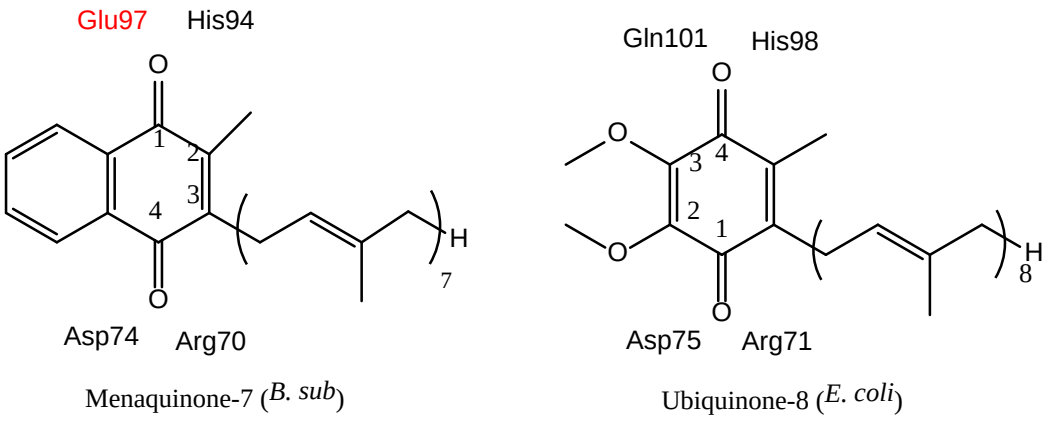

Figure 1.1. Chemical structures of menaquinone and ubiquinone. The residues surrounding each quinol are the conserved residues of Q_h-site in *Bacillus subtilis* cytochrome aa_3-600 and *Escherichia coli* cytochrome bo_3.

The structural characterization of Q_h-site has been enabled by electron paramagnetic resonance (EPR) techniques that detect unpaired electron interacting with its protein surrounding. For cyt bo_3, the location of quinone binding sites could not be elucidated from x-ray structure because quinone was lost during crystallization [17]. However, subsequent EPR studies of site-directed mutations have identified a possible quinone binding site with positive correlation with residues that have high sequence identity among the quinol oxidases [18]. These residues are R71, D75, H98 and Q101 in *E. coli* cyt bo_3 and R70, D74, H94 and E97 in *B. sub* cyt aa_3-600 (see Figure 1.1).

The quinone at the Q_h-site is considered to mediate electron transfer from the quinol oxidation site to low-spin heme A (heme B in cyt bo_3), which directs electrons to heme-copper binuclear center for oxygen reduction [19]. This view has been challenged by quinone-loop mechanism, which is observed in bc_1 complex in photosynthetic bacteria and complex III of mitochondria [20]. The latter mechanism involves two quinone sites in rapid equilibrium with the quinol pool in the membrane, where one site splits a pair of electrons during ubiquinol oxidation and commits one charge to reduce quinone at the second site, eventually regenerating a fully reduced quinol. The former mechanism involving quinones is more plausible for cyt aa_3-600 for several reasons. One obvious reason is the difference in the manner in which the two heme groups are placed in the plane of membrane for cytochrome oxidases, instead of cutting across the membrane as it is found in the bc_1 complex.

While steady state activity of the enzyme has been interpreted in terms of two sites, the work presented, here, suggest a different possibility and different functional capacity for Q_h-site. A two-site theory assumes two different roles for each of the quinones: one site (Q_L) oxidizes quinol and passes the electrons to the second site (Q_h), which then transfers electrons one-at-a-

time to low-spin heme A. However, unlike the Q_h-site, the structural information on quinol oxidation site (Q_L) has remained elusive and has not validated the two-site theory in a satisfying manner. There are no highly conserved residues among the quinol oxidases indicating a possible Q_L-site, and available structural information has been limited and not consistent [21-24]. In addition, the two-site theory is based on tightly bound quinone at the Q_h-site that does not exchange with free quinols in the membrane pool, but there are observations that demonstrate that some exchange can occur, depending on the conditions [24, 26-27]. It is difficult to define the molecular level events during steady state activity assay, but data presented in this report suggest that Q_h-site can participate in the quinol oxidation reaction by cyt aa_3-600. The nature of this association is not clear, but the role of Q_h-site in quinol oxidation cannot be ruled out.

CHAPTER 2: Genetic Cloning and Protein Over-expression of Cytochrome aa_3-600 and Cyt caa_3 Oxygen Reductases from *Bacillus subtilis* in the Native Expression System and Other Expression Strategies in *Escherichia coli* and *Vibrio cholerae*

2.1 Introduction

Generally, low amount of protein and crude quality make it difficult to characterize membrane proteins by biochemical and biophysical methods. Creating the means to grow cells that would express proteins from *Bacillus subtilis* (*B. sub*) in large quantity have been one aspect of my research efforts. This chapter addresses the undertaking that led to building an expression system in *Bacillus* strains based on several prospective plasmid DNAs. His-tag was the choice of method for refining protein samples, because of its role in an efficient and simple purification process. Proteins, cytochrome (cyt) aa_3-600 and cytochrome caa_3 from *B. sub*, were cloned from genomic DNA, consequently His-tagged at potentially favorable sites and made into plasmid constructs for protein expression [38, 50]. Various culture conditions were adjusted for increase in protein yield.

The recombinant protein expression of cyt aa_3-600, using the pET vectors with *Escherichia coli (E. coli)* strains, was examined both in the presence and absence of ctaA gene, heme A synthase, which is absent in the *E. coli* genome. Aside from the possibility of this approach leading to functional protein isolation, this strategy had the potential to naturally introduce different hemes into the recombinant membrane proteins. Conversely, *E. coli* cyt bo_3 was introduced to *B. sub* to further explore the feasibility of replacing native heme co-factors with different types of hemes. Since *E. coli* does not produce heme A co-factor, expressing cyt bo_3 in *B. sub* could potentially allow formation of *E. coli*-based hybrid protein complex with heme A. Lastly, arginine auxotrophs were prepared for additional work in advanced electron paramagnetic resonance (EPR).

2.2 Materials and methods

2.2.1. Cloning of cytochrome aa_3-600 into various expression vectors

B. sub 168 strain was the original template strain from which qoxABCD operon was polymerase chain reaction (PCR) amplified with *Platinum Pfx* DNA polymerase (Invitrogen), using the forward primer, 5'-GCATAACAAAGTACTAGTTAAGGAGGGAGGAAGT**ATG** CAC -3'(qoxASpeI) and the reverse primer 5'GAAGAGGGTTTGGGCCC**TTA**TTCGTTATGG CCTGAATGC -3' (qoxDApaI) (IDT, Coralville, IA). The genomic DNA was prepared from a cell pellet after it was disrupted with 1-2 mg/mL lysozyme (Sigma, St. Louis, USA) at room temperature for 30 min. of incubation. The resulting broken cells were cleaned by Dneasy Blood & Tissue kit by Qiagen. The isolated genomic DNA was stored in 50 – 100 μL aliquots in -20 ˚C. *B. subtilis* genomic DNA was initially digested with restriction digest enzyme EcoRV prior to subsequent PCR reaction.

Initial cloning of cytochrome aa_3-600 into pCR-XL TOPO cloning vector

Earlier attempts to clone the genomic copies of *Bacillus stearothermophilus* (*B. stearo*) cytochrome bo_3 and *B. sub* cytochrome aa_3-600 directly into *Bacillus subtilis* expression plasmids were unsuccessful, largely because the ligation reaction did not yield correct circularized recombinant plasmids. Therefore, another commercially available plasmid that readily ligates with DNA inserts was initially used to mount the cloned genes. This circularized plasmid DNA could be used to generate a high yield of PCR products for ligation reaction into *B. sub* expression system.

A sequence encoding for a ribosomal binding site (RBS) was introduced in the forward primer, 8 bp upstream from the starting codon, and was retained within the DNA reading frame of the DNA fragment upon the restriction digestion. The resulting PCR product of ~4 kbp size

was gel-extracted and purified using Qiagen Gel-extraction Kit. The cleaned DNA insert was ligated into pCR-XL-TOPO cloning vector (Invitrogen), which has a high success rate in ligation due to its linearized single 3'-thymidine (T) overhangs for TA pairing with the 3'-adenine (A) overhangs generated in the DNA insert. Following the PCR reactions with *Platinum Pfx* DNA polymerase (Invitrogen), the PCR products were treated with *Tag* DNA polymerase, in order to generate the 3'-adenine (A) overhangs in the DNA insert. The ligation product was used to transform TOP10 One Shot electrocompetent *E. coli* cells (Sigma). A colony forming unit was grown in a liquid culture overnight for isolation of plasmid and verification of the insert. Once a recombinant plasmid was validated by a colony PCR reaction and double-digestion by restriction digest enzymes (Spe I and Apa I), it was used as the DNA template for subsequent PCR reactions for cloning of cytochrome aa_3-600.

Cloning of cytochrome aa_3-600 into pLala and pEB112 expression plasmids

The original primer set contained restriction sites SpeI and ApaI, and these were designed with the purpose of inserting DNA fragment into the *B. sub* expression plasmid pLala (Lewin 2009). These sites are not indicated on the map of pLala (5,146 bp) in the communication by Lewin et al.; the restriction digest site SpeI occurs upstream of BamHI site, and ApaI occurs downstream of ClaI [33].

The PCR reaction product was double-digested with restriction digest enzymes SpeI and ApaI (Invitrogen). The purified double-digested fragment from PCR reaction and the equally treated vector pLala were in the ligation assay with T4 DNA Ligase (Invitrogen) and incubated at 16˚C overnight. The ligation product was transformed into XL1B *E. coli* cells by electroporation and plated on 12 μg/mL chloramphenicol plate after a rescue with LB medium and 1 hour incubation at 37 ˚C. Electro-competent XL1B cell line was maintained on (15 ug/mL)

tetracyclin and prepared in low salt buffer (10% glycerol). A colony with correct transformant was promptly verified by PCR amplification of the inserted qoxABCD operon using the original primer set. In addition, the presence of correct size band or bands was observed on the 1% DNA gel, when the respective single or double-digested product of the isolated recombinant plasmid was loaded.

2.2.2. His-tag insertion into qoxABCD operon of cytochrome aa_3-600

A His_6-tag was introduced at the C terminus of qoxB or subunit II by PCR method of splicing by overlap extension [30], which utilizes two separate PCR reactions in series. This method requires two sets of primers: an external set, encompassing the entire sequence length of aa_3-600 oxidase, and an internal set, containing the codons coding for six Histidine residues. First, a PCR reaction was performed with pairing of an external forward primer (qoxASpeI) and an internal reverse His-tag primer 5'-CCTGATCAATA**TCA**ATGGTGATGGTGATGGTGTT CTTCTGTATC-3'. This reaction gave ~3k base pair DNA fragment, which was checked by 1% DNA gel agarose and subsequently extracted and cleaned by QIAquick PCR Purification Kit (Qiagen). Another PCR reaction involved the pairing of an external reverse primer (qoxDApaI) and an internal forward His-tag primer 5'- CAGAAGAACACCATCACCATCACCAT**TGA**T ATTGATCAGG-3'. This reaction resulted in ~1kbp DNA fragment, which was handled as described above. These initial PCR reactions were conducted to yield two fragments of DNA sequence of cytochrome aa_3-600, where each DNA fragment contains an external end of the overall construct and an overlap region that contains a six Histidine coding sequence. The final PCR reaction conducted with these two different DNA fragments and the external set of primers (qoxASpeI and qoxDApaI) yielded a full length sequence that incorporated a His_6-tag at the C-

terminus of qoxB. This final construct was gel-extracted and digested with corresponding restriction enzymes and subjected to an overnight ligation reaction. The resulting product along with the double digested pLala plasmid were used to transform XL1B, and the resulting *E. coli* strain was sequence verified by both a PCR reaction with *Tag* polymerase (Invitrogen) and DNA sequencing submission.

2.2.3. Preparation of *E. coli* XL1B competent cells and recombinant plasmid transformation

XL1B *E. coli* strain was used to maintain plasmids that could be isolated and purified later when transforming a *B. sub* strain. An LB medium of 250 mL volume was initially inoculated with 2.5 mL of overnight 5 mL culture with addition of 15 μg/mL tetracyclin. The culture was monitored until the optical density reading reached 0.6 – 0.8 at OD_{600}. This step usually took between 3 – 4 hours. Once the absorbance reading reached 0.6, the culture was collected in 50 mL conical tubes for a spin down at the speed of 4000 rpm for 10 min. The cell pellets were washed with 35 – 50 mL cold distilled H_2O by resuspending the pellet and spinning down the cells. The supernatant was poured off, and the wash step was repeated once. Lastly, the cell pellet was resuspended in 35- 50 mL cold 10% glycerol. The supernatant was poured off, leaving behind ~3 mL liquid volume and the cell pellet. The cell pellet was resuspended and was aliquoted at 50 -55 μL each into microcentrifuge tubes for storage. The competent cells were stored in -80˚C. This procedure yielded +50 electrocompetent cell samples. Alternatively, a smaller scale preparation (i.e. 100 mL LB culture) would yield ~ 30 samples when starting culture is inoculated with 1 mL of overnight subculture. (Tetracyclin was prepared in 50% ethanol and stored in -20˚C.)

2.2.4. Preparation of *B. subtilis* competent cells and transformation strategies

The *B. subtilis* competent cell lines were prepared from a single colony from LB plate or a streak from a glycerol stock on LB plate. It was important to prepare the LB plate on previous day and incubate at 30 °C overnight. Next day, the cells were scraped from the plate and suspended in 5 mL GM1 medium. A sufficient amount of cell suspension was added to 10 mL GM1 medium to give OD_{525} reading of 0.2 - 0.3 (or $Klett_{54}$ = 40 – 50). This cell culture were placed in a shaker at 37 °C for 4.5 hours to yield OD_{525} = 0.6 – 0.8 (or $Klett_{54}$ = 170 – 200). The 5 mL culture then was added 25 – 50 mL GM2 medium and was shaken (200 rpm) at 37 °C for 1.5 hours. At the end of growth, cells were spun down at 4000 rpm (Sorvall, GS-34 rotor) for 10 min. Most of the supernatant was removed, except for 1/10 the original volumes of the supernatant. To this cell volume, 1/10 volume of glycerol was added. The mixture was swirled, and the cells were distributed in 500 μL volumes in microfuge tubes. The cell aliquots were ready for immediate use, and the remaining cells were stored at -80 °C.

Spizizen salts (1 L)

$(NH_4)_2SO_4$	2 g
K_2HPO_4	14 g
K_2HPO_4	14 g
Sodium Citrate	1 g
$MgSO_4 \cdot 7H_2O$	0.2 g

	GM1 medium (100 mL)	**GM2 medium (100 mL)**
Spizizen salts	100 mL	100 mL
20 % Casamino acids	60 μL	20 μL
5X LB	1 mL	0.15 mL
25 % Glucose	2 mL	2 mL
Trp/Phe (5 mg/mL)	1 mL	--
1 M $MgCl_4 \cdot 6H_2O$*	--	0.2 mL
1 M $CaCl_2$*	--	50 μL

*Added just before use.

Trace elements per Liter:

$MgCl_2 \cdot 6H_2O$	125 mg
$CaCl_2$	5.5 mg
$FeCl_2 \cdot 6H_2O$	13.5 mg
$MnCl_2 \cdot 4H_2O$	1.0 mg
$ZnCl_2$	1.7 mg
$CuCl_2 \cdot 2H_2O$	0.43 mg
$CoCl_2 \cdot 6H_2O$	0.6 mg
$NaMoO_4 \cdot 2H_2O$	0.6 mg

There are several strategies for attempting transformation in *B. sub*. Having different tried-and-tested protocols was essential when encountering difficult cases, where repeated attempts using one approach did not give at least one colony. The plasmid DNA was preferable to ligation products when transforming cells. The plasmid constructs initially prepared in *E. coli* system and then isolated for transforming into *B. sub* consistently gave better results than the ligation products. One approach began with dilution of 0.1 mL of frozen competent cells with 1 mL of GM2 (freshly prepared), without $MgCl_2$ and $CaCl_2$. Then 5 – 9 μL of plasmid DNA was added. The transformed cells were incubated at 37 °C for 30 min. and spun down at room temperature (2000 rpm). The cell pellet at the bottom of the microfuge tube was carefully suctioned with pipetman and spread on LB plates with appropriate antibiotics.

Second approach involved using higher volume of cells (900 μL), to which 5 – 9 μL of plasmid DNA was added. No dilution was made prior to plasmid addition. The transformed cells were incubated for 30 min. without shaking at 37 °C. Then 50 μL of 10 % yeast extract was added and incubated for 60 min with shaking. The cell pellet was spun down at low rpm and suctioned by pipetman. Approximately 200 μL of volume of cells were plated. The LB plate was kept upright and incubated overnight at 37 °C.

Third approach also involved using higher density of cells (200 – 250 μL), to which 5 – 9 μL of plasmid DNA was added. The transformed cells were incubated for 30 - 40 min. without shaking at 37 °C. All of the cells were used directly for plating with minimal disturbance.

2.2.5. Optimization of protein expression

The qoxABCD operon, encoding the cyt aa_3-600 menaquinol oxidase, was cloned and expressed from plasmid pLala having chloramphenicol resistance (Cm^r) under the control of the glp promotor. Plasmid pLala replicates both in *E. coli* and *B. sub*. *E. coli* strains transformed with pLala were maintained on LB plates with 12 μg/mL chloramphenicol (Cm). A His_6 tag was introduced at the C-terminus of qoxB to facilitate protein purification by nickel-nitrilotriacetic acid containing resin. The isolated recombinant plasmid pLala was transformed into *B. subtilis* strain LUW143, lacking both aa_3-600 menaquinol oxidase and caa_3-type cyt c oxidase (ΔqoxABCD::kan; ΔctaCD::ble). Liquid cultures were inoculated with *B. subtilis* cells were grown on LB plates containing appropriate antibiotics. Cells were grown in LB medium treated with 5 μg/mL Cm, 7.5 μg/mL neomycin (Neo), and 1.8 μg/mL zeomycin (Zeo) at 37 °C. Enzyme expression was induced by the addition of 20 mM glycerol. Cells were harvested upon reaching a high cell density.

The different growth conditions were screened for pLala recombinant system, which gave the largest protein yield. The time of cell growth and cell collection, temperature, timing of glycerol induction and culture supplementation were examined. The largest amount of protein was isolated from culture that was induced at the beginning of the seeding and grown past its stationary phase. Many other gram-positive plasmid expression systems were prepared, including plasmids pMM1522 having ampicillin resistance (Amp^r) and pMM1525 for expression

in *Bacillus megaterium* (*B. meg*) (Mo Bi Tec), and none gave a comparable yield of protein as the plasmid pLala with its glpD promotor.

2.2.6. Purification of cytochrome aa_3-600

Cell pellets were resuspended in 50 mM K_2HPO_4, 10 mM $MgCl_2$ at pH 7.5-8.2 and disrupted at high pressure (100 kpsi) by using a microfluidizer (Microfluidics Corp., Worcester, MA). Cell debris was removed by brief centrifugation at 8000 X g. The supernatant was the subjected to centrifugation at 180,000 X g for at least 4 hours to collect membranes. The isolated membranes were dispersed in 50 mM K_2HPO_4, pH 7.5-8.2 and homogenized with 1% dodecyl maltopyranoside (DDM by Anatrace) by stirring at 4 °C. The solution was centrifuged at 180,000 X g for 1 hour to remove insoluble fragments and then loaded onto a column filled with Ni-NTA resin for purification. The column was initially equilibrated with 50 mM K_2HPO_4, 40 mM NaCl, 0.05% DDM, pH8.2 for 3-5 column volumes. At least two incremental stepwise washes were performed with buffer containing up to 15 mM imidazole. Cyt aa_3-600 was eluted with buffer containing 100 mM imidazole. The protein was dialyzed overnight against the loading buffer and was concentrated to ~200 μM.

The size of cyt aa_3-600 subunits was verified by SDS-PAGE protein gel. The protein gel was further processed with a protocol for Western blot, where polyvinylidene fluoride (PVDF) membrane was stained with antibodies against His-tag (Supersignal West Hisprobe kit, Pierce, Rockford, IL). The blot was visualized on developed film, and it displayed a single band at ~35 kDa, the anticipated size of subunit B where His-tag was inserted.

2.2.7. UV-visual spectrophotometry of cytochrome aa_3-600

Cyt aa_3-600 contains multiple hemes that give rise to signature spectral features. The protein concentration was estimated from the absorbance difference 600-630 nm in the reduced-minus-oxidized spectra. Various extinction coefficients were reported by others and the conservative value of 28 mM^{-1} cm^{-1} was applied in the calculation according to Beer's Law. The assay was generally reliable and was repeated several times in order to allow for a statistical confidence. The treatment with $K_3Fe(CN)_6$ on the isolated enzyme was found not to affect the determination of protein concentration.

2.2.8. Pyridine hemochromatogen assay

A total amount of heme components in heme-binding proteins can be assessed from pyridine hemochromatogen assay, where isolated hemes form complexes with pyridine. Hence, the absorbance can be assigned by the type of heme. The reaction solution contained the following: 500 μL 200 mM NaOH/40 % pyridine, 450 μL dH_2O, 50 μL diluted protein sample and 5 μL 0.1 M $K_3Fe(CN)_6$. To this mixture, sodium dithionite was added. Several spectra of the reduced pyridine hemochromes were recorded one minute apart. The reduced minus oxidized absorbance spectra allowed calculation of millimolar concentration of each component using extinction coefficients provided by Berry and Trumpower [28].

2.2.9. Adding a His-tag to *Bacillus stearothermophilus* cytochrome bo_3 oxidase and protein expression

A His_6-tag was added to cbaAB genetic operon of *Bacillus stearothermaphilus* (*B. stearo*) cytochrome bo_3 oxidase, a two subunit SoxB-type cyt c oxidase. A direct ligation reaction did not occur between the DNA insert and the following plasmids, pMM1522 (BsrGI and SacI),

pWB995 (PstI and HindIII), despite repeated attempts. Hence, linearized pCRII-TOPO plasmid with 3'A- overhangs were used to create a stable circularized template containing the cba2-His insert. A PCR reaction was run with the DNA template containing HindIII and PstI restriction digestion sites, which had matching sites on pLala and pEB112 expression plasmids for ligation. The recombinant pLala and pEB112 plasmids with cbaAB-His insert were verified by restriction digests and DNA sequencing and transformed into *B. sub* strains (1A1 and LUW143). *B. sub* cells showing successful transformation were verified by DNA sequencing of isolated recombinant plasmids. The cultures were grown in LB medium and were induced with 0.5 mM IPTG per liter of culture for *B. sub* carrying pEB112 vector when the cell density reached ~0.6 at 600 nm (see Figure 2.3). Induction of protein expression with 20mM glycerol occurred at the start of incubation for pLala vector containing strain because the pathway of the induction is long and has slow response time, which involves activating a gene (glycerol-3-phosphate dehydrogenase) in the chromosomal DNA. Purification procedure was as indicated above (2.2.6). Activity assay detecting oxygen consumption was performed in the following conditions: [15 nM] enzyme, [0.4 μM] c-551, [125 μM] N, N, N', N'-tertramethyl-p-phenylenediamine (TMPD), [5 mM] Na-ascorbate in 1 mM $MgSO_4$, 150 mM KCl, 1 mM Na_2HPO_4, pH 6.7 buffer at 42°C.

2.2.10. Cloning of *Bacillus subtilis* cytochrome caa_3 oxidase and His-tag insertions at subunits I and II

The ctaCDEF operon for cytochrome (cyt) caa_3 oxidase was cloned from genomic DNA of *Bacillus subtilis* 168 (*B. sub*) following the protocol from section 2.2.1. A His_8-tag was inserted each at the C-terminus of subunit II (ctaC gene), subunit I (ctaD gene) and N-terminus of subunit I (ctaBCDEFG-CI8H) to improve outcome of protein expression and isolation. The

protocol followed the method of splicing-by-overlap extension (see section 2.2.2), where tag insertion at subunit II occurred by creating two DNA fragments, 3 kDa and 1 kDa, through PCR reaction using two sets of primer pairs (Hisfor/reverse, 3 kDa and forward/Hisrev, 1 kDa). Similarly, the tag insertion at subunit I occurred by creating two DNA fragments with two primer pairs (forward/Hisrev, 3 kDa and Hisfor/reverse, 1 kDa). The ctaCDEF and ctaCDEFG DNA templates, the regions encoding cyt caa_3 from *B. sub*, were flanked by PstI and HindIII restriction digestion sites for ease of ligation with pEB112 and pLala vectors. *B. sub* strains (1A1, LUW143 and LUW142) were transformed with recombinant vectors carrying the correct cyt caa_3 DNA sequence. The transformed *B. sub* strains were evaluated for protein expression and isolation. The growth condition was also examined for different growth media, including supplementation with succinate instead of glycerol or glucose. The plasmids pHCMC2 and pHCMC4 ligated with either ctaCDEF or ctaCDEFG (using restriction digestion sites, BamHI and MluI) did not display a meaningful protein expression level in *B. sub*.

2.2.11. Protein expression of cytochrome aa_3-600 in *E. coli* and *Vibrio cholerae*

A pET17 vector (100 μg/mL ampicillin) carrying qoxABCD operon of cyt aa_3-600 (having restriction digestion sites, SpeIfor and XhoIrev) was constructed for expression in *E. coli* and *Vibrio cholerae (V. cholerae).* The plasmid DNA was transformed into *E. coli* CLY strain (i.e. strain having genetic sequence for cyt bo_3 disrupted, ΔcyoABCD), Rosetta2 strain (Novagen) and *V. cholerae* strain (Lab stock). The transformed CLY strain with 50 μg/mL kanamycin (Kan) was grown in M6 medium supplemented with [100 mg/mL] thiamine, 10 μM $CuSO_4$ and Glucose at 1% inoculation. *V. cholerae* strain with spectinomycin resistance (Spm^r) was grown in Luria broth (LB). Rosetta2 strain was grown using both approaches.

Preparation of E. coli and Vibrio cholerae competent cells and transformation protocols

Competent cell lines for *E. coli* strains C43 and CLY (i.e. ΔcyoABCD) were prepared following the protocol from section 2.2.3. However, the Rosetta2 competent cells (Novagen) were made using a variation of this protocol. A 250 mL Luria broth medium (LB) was inoculated with 1 mL of overnight culture and grown to cell density of 0.3-0.4 OD_{600}. The cells were collected at low speed (3000 rpm, 10 min.) and resuspended in 3 mL Tryptic Soy Broth (TSB), Luria broth medium containing 10 % PEG6000, 5 % DMSO, 10 mM $MgCl_2$, 10 mM $MgSO_4$, 10 % glycerol and pH 6.1. The cells were kept on ice for ~10 min., and 50 μL aliquots of cells were frozen. For transformation of Rosetta2 cells, the following was added to each aliquot of cells: 3 μL plasmid DNA, 10 μL 5x 0.5M KCl, 0.15M $CaCl_2$ and 0.250M $MgCl_2$, and 37 μL dH_2O. The cells were kept on ice for 30 min. and heat shocked at room temperature for 10 min. and returned to ice for 10 min. The cells were rescued with 300 μL LB, shaken at 37°C for 50 min. and spread on a plate.

Vibrio cholerae competent cells were prepared from 50 mL of LB inoculated with ~2 mL overnight culture and grown to ~0.3 OD_{600}. Cells were collected and washed with 25 mL of 1 mM $CaCl_2$, followed by successive washes with 12.5 mL volume and 2.5 mL volume. Finally, the cells were washed with 1 mL of 1 mM $CaCl_2$ and 10 % glycerol and resuspended in 1 mL of the same buffer. Aliquots of 100 μL were frozen and stored. For transformation, 5 μL of plasmid DNA were added to 100 μL of cells and transformed by electroporation.

2.2.12. Constructing recombinant plasmids for co-expressing heme A synthase and heme B synthase with cytochrome aa_3-600 in *E. coli*

Several plasmid constructs were made in order to facilitate expression of *B. sub* cyt aa_3-600 in *E. coli strain.* Since *E. coli* does not carry genomic information required to express heme

A synthase, the ctaA gene (i.e. encoding heme A synthase) was cloned from *B. sub* 168 genomic DNA and was inserted into TOPO-TA plasmid. Using this template plasmid, ctaA gene was copied and added to pETDuet vector at one multiple cloning site (MCS), and qoxABCD, the genetic operon for *B. sub* cyt aa_3-600, was inserted at the second site, where each of the DNA inserts were under the control of a T7 promotor. Second construct was made where ctaA and cta B (i.e. gene encoding heme B synthase) were inserted into plasmid pETDuet downstream from each of its two promotors. Third construct was prepared where ctaA and ctaB were combined into a single DNA sequence using the method of splicing-by-overlap extension (primers were ABXbaIfor and ABPstIrev, 2100 base pairs (bp) DNA fragment) and circularized into pETDuet. The ctaA gene is in the reverse reading frame located upstream from ctaB-CDEF operon for cyt caa_3 in *B. sub* chromosome, and the combined single DNA sequence of ctaA and ctaB genes under the control of one promotor would offer an advantage in protein expression of cyt aa_3-600 [42-43, 45].

The protein expression of *B. sub* cyt aa_3-600 in *E. coli* was performed with CLY, having resistance genetic cassettes for 100 μg/mL ampicilin (Amp) and 50 μg/mL kanamycin (Kan), and Rosetta2 having resistance genetic cassettes for 100 μg/mL Amp and 34 μg/mL chloramphenicol (Cm) strains using expression plasmid pETDuet-A-QoxHis1, which carried DNA sequences for ctaA and qoxABCD genes. The plasmid DNA containing sequences of ctaAB and qoxABCD were also examined for protein expression in CLY strain. Co-expressing *E. coli* cyt bo_3 (pLala cyoABCD) with ctaA gene in a *B. sub* strain was evaluated for the feasibility of forming a functional enzyme when the native hemes B and O are replaced with heme A during protein synthesis.

2.2.13. Construction of *Bacillus subtilis* arginine auxotrophs (ΔargC, ΔargF and ΔargH)

Bacillus subtilis (B. sub) arginine auxotrophs were created with LUW143 (i.e. strain having genetic disruptions for cyt aa_3-600, ΔqoxABCD, and cyt caa_3, ΔctaCDEF in its chromosomal DNA) strain and integration plasmids pBGSC6 (ECE22, Ohio State) and pMutin4 (ECE139, Ohio State) that integrate into chromosome by Campbell-type recombination with the cloned insert. Several genes (argC, argF and argH) encoding for enzymes involved in arginine biochemical synthetic pathway were disrupted. The plasmid pBGSC6 (5 μg/mL chromamphenicol) carrying ~1 kbp argC DNA fragment franked by primers HindIIIfor and BamHIrev was constructed initially. The argC gene was also interrupted with plasmid pMutin4 (or ECE139, having erythromycin resistance cassette) with either ~1 kbp or ~0.6 kbp DNA fragments flanked by primers labeled EcoRIfor and BamHIrev. The expression of argF gene was impeded with plasmid pBGSC6 with ~560 bp insert bordered by primers BamHIfor and EcoRIrev. The argH gene was disrupted with a DNA fragment inserted into plasmid pMutin4. All of the constructs of integration vectors with respective DNA inserts were maintained in Top10 (Invitrogen) *E. coli* strains. The arginine auxotrophs were selected with appropriate antibiotics. The chromosomal DNA *Bacillus* auxotrophs were checked for the disruption of respective gene by isolating the genomic DNA and running PCR reactions with corresponding primer sets with Tag polymerase.

Bacillus competent cell lines were created for each of the auxotrophs. Each of the auxotrophs was examined for growth response to various supplements, especially to arginine, in spizizen growth medium (see Section 2.2.4).

Table 2.1. Growth response of arginine auxotroph with genetic disruption of argC gene (ΔargC) to growth conditions prepared with different growth supplements

Spizizen Supplements	**0**	**1**	**2**	**3**	**4**	**5**
Trace elements [1/10000]	added	added	added	added	added	Added
20 % Casamino acid [100 μL/100 mL]	--	--	--	--	--	--
5 mg/mL Tryptophan [1 mL/100 mL]	added	added	--	added	added	Added
1M Glucose [2.8 mL/100 mL]	added	added	added	added	added	Added
5x LB medium	--	--	--	--	--	--
Thiamine	--	added	--	--	--	--
Arginine [μg/mL]	--	--	2.5	5	10	20
OD_{600}	1.0	0.8	0.8	1.2	1.5	1.7

*Grown from *B. sub* strain LUW143 with integration plasmid ECE139 carrying the DNA insert that has overlapping regions with argC gene.

Table 2.2. Growth response of arginine auxotroph with genetic disruption of argF gene (ΔargF) grown with different growth supplements

Spizizen Supplements	**0**	**1**	**2**	**3**	**4**
Trace elements [1/10000]	added	added	added	added	added
20 % Casamino acid [100 μL/100 mL]	added	---	added	---	---
5 mg/mL Tryptophan [1 mL/100 mL]	added	added	---	added	added
1M Glucose [2.8 mL/100 mL]	added	added	added	added	added
5x LB medium	---	---	---	---	---
Arginine [μg/mL]	---	---	---	25	50
OD_{600} (16 hours)	0.4	0.02	0.06	0.2	0.06

* Grown from *B. sub* strain LUW143 with integration plasmid ECE139 carrying the DNA insert that has overlapping regions with the argF gene (i.e. labeled as argF-4). Varied amounts of arginine were tested.

Table 2.3. Growth screening of arginine auxotroph (ΔargF) by varied amounts of arginine in the present or absence of casamino acid supplementation

Supplements	**0**	**1**	**2**	**3**	**4**	**5**	**6**	**7**	**8**	**9**
Trace elements	a	a	a	a	a	a	a	a	a	a
20 % Casamino acid [μL/100 mL]	--	1	0.5	--	--	--	--	--	1	0.5
Tryptophan [5 mg/mL]	a	a	a	a	a	a	a	a	a	a
1M Glucose	a	a	a	a	a	a	a	a	a	a
Arginine [μg/mL]	--	--	--	25	50	100	150	175	25	25
OD_{600} (16 hours)	0.01	1	1.3	0.4	0.9	1.1	0.2	0.5	1.6	0.8
OD_{600} (19 hours)	0.01	2.3	1.9	1.1	1.9	2	0.9	1.5	2.5	1.6
OD_{600} (22 hours)	0.03	2.6	2.5	2.2	2.2	2.5	1.8	2	2.1	2.1

* Grown from *B. sub* strain LUW143 with integration plasmid ECE139 carrying the DNA insert that has overlapping regions with the argF gene (i.e. having labeled as argF-4). Varied amounts of casamino acid and arginine were tested. 'a' indicates that a particular supplement was added for that specific growth condition.

Table 2.4. Growth response of arginine auxotroph with genetic disruption of argH gene (ΔargH) grown with different growth supplements

Spizizen Supplements	**1**	**2**	**3**	**4**	**5**
Trace elements [1/10000]	added	added	added	added	added
20 % Casamino acid [100 μL/100 mL]	added	---	added	---	---
5 mg/mL Tryptophan [1 mL/100 mL]	added	added	---	added	added
1M Glucose [2.8 mL/100 mL]	added	added	added	added	added
Arginine [μg/mL]	---	---	---	12.5	25
OD_{600} (21 hours)	2.2	0	0.03	0.3	1.1

*Grown from *B. sub* strain LUW143 with integration plasmid ECE139 carrying the DNA insert that has overlapping regions with argH gene sequence.

Table 2.5. Growth screening of arginine auxotroph (ΔargH) by varied amounts of arginine in the present or absence of casamino acid supplementation

Supplements	**1**	**2**	**3**	**4**	**5**	**6**	**7**	**8**	**9**	**10**
Trace elements	a	a	a	a	a	a	a	a	a	a
20 % Casamino acid	--	--	--	--	--	--	--	--	--	--
Tryptophan [μg/mL]	a	a	a	a	a	a	a	a	a	a
1M Glucose	a	a	a	a	a	a	a	a	a	a
Arginine [μg/mL]	60	70	80	90	100	110	120	130	140	150
OD_{600} (21 hours)	1.8	1.9	1.9	1.7	1.6	2.1	2	1.4	1.7	1.6

*Grown from *B. sub* strain LUW143 with integration plasmid ECE139 carrying the DNA fragment that overlaps with argH gene. Varied additions of casamino acid and arginine were tested.

2.3. Results and Discussion

Optimization of over-expression and purification of cyt aa_3-600 in Bacillus subtilis

The cyt aa_3-600 was expressed in *Bacillus subtilis (B. sub)* from several plasmid constructs, carrying the genetic sequence for qoxABCD with His-tag at C-terminus of subunit II. The protein expression in plasmid pLala (having chloramphenicol resistance cassette) yielded ~1 mg protein per liter of culture. Altering the growth conditions and supplementation did not improve this outcome. The protein expression level with pLala construct was higher than levels in protein expression trials using other plasmid constructs. The plasmid pEB112 (having ampicillin resistance cassette) obtained from Ordal Group (UIUC) resulted in ~0.6 mg protein per liter of culture, and the plasmid pWB995 (having neomycin resistance cassette) gave even

lower level of expressed protein. The pHCMC series of expression vectors from *Bacillus* Genetic Stock Center (Ohio State) resulted in limited or no protein expression.

The purified cyt aa_3-600 exhibited clear protein bands in SDS-PAGE gel that could be immediately assigned to subunit I (~43kDa), subunit II (34 kDa) and subunit III (~25 kDa) (see Figure 2.1). These apparent molecular masses were different from the predicted values (74 kDa, 34 kDa and 23 kDa, respectively) probably due to electrophoretic mobility of the subunits stemming from the hydrophobic nature of the protein complex and agreed with figures that were previously reported [31, 32]. Western blot stained with His-tag specific antibodies and developed on a film showed a single intense band that corresponded to subunit II, which carried the His-tag at its C-terminus.

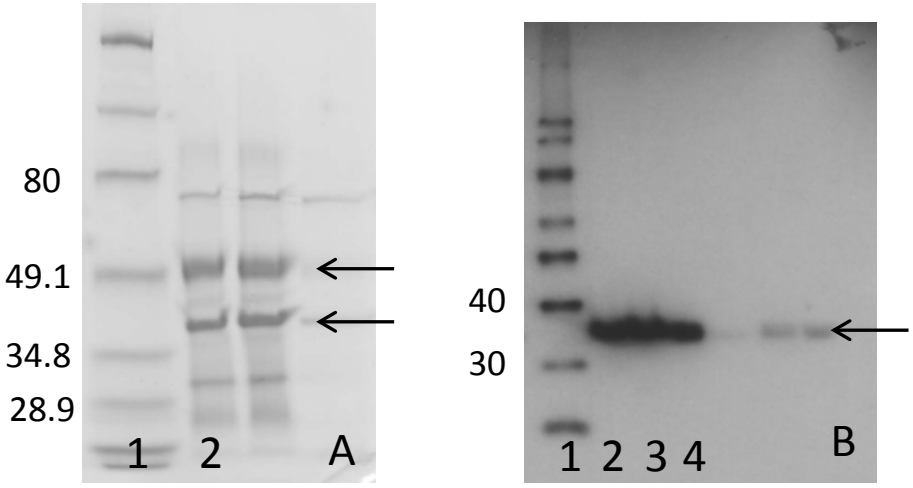

Figure 2.1. A. SDS-PAGE gel of purified *Bacillus subtilis* cyt aa_3-600 oxidase: Lane 1, Broad Range Ladder; lane 2, cyt aa_3-600 (> 5 μg protein). Two intense bands running in gel indicated by arrows are subunit I and II, the two largest subunits. **B.** A film developed from western blot of cyt aa_3-600 cultures with arrested growth at various times points (grown in minimal media supplemented with 0.5 % glucose; grown at temperature of 37 °C initially and at 5^{th} hour of growth switched to 30 °C). Lane 1, Magic Mark ladder (Invitrogen); Lane 2, culture sampled at 5^{th} hour; Lane 3 and 4 reflect culture sampled at 6^{th} and 7^{th} hour of growth. The single dark band between 40 and 30 kDa standard ladder indicated by arrow is the subunit II (34 kDa), having His-tag.

Spectroscopic properties of cyt aa_3-600

The concentration was determined from a reduced-minus-oxidized difference absorbance spectrum of cyt aa_3 that also showed signature features associated with heme A bound to the enzyme (see Figure 2.2). Two distinctive features of the difference spectrum are the soret band at 443 nm and the alpha band at 600 nm. In the air-oxidized sample, there is a single broad peak at ~419 nm that becomes red-shifted in the presence of dithionite.

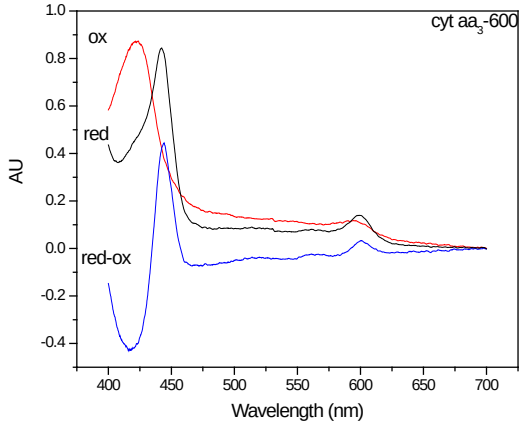

Figure 2.2. Optical spectra of purified wild type cyt aa_3-600. The top spectrum (red) is air-oxidized sample; the middle spectrum (black) is dithionite reduced sample; the bottom spectrum (blue) is the difference spectrum of reduced-minus-oxidized spectra.

Interestingly, an extra peak at 560 nm was present in the reduced spectrum of protein samples obtained from cultures that were harvested prior to reaching the stationary phase or early stationary phase of cell growth. The heme B is generally assigned to this position in the visible reduced spectrum. Its presence suggested that mixture of hemes occupy cyt aa_3-600 in heme binding sites in subunit I. The soret band for these affected samples in the reduced spectrum displayed two peaks, ~419 and 443 nm, instead of one, indicating that mechanism of heme reduction is different. The mixture of hemes observed in cyt aa_3-600 was more prevalent from strains transformed with plasmid pLala construct, the high protein yielding vector, and was

largely absent from other low protein yielding plasmid constructs such as pET112. The synthesis of heme A and consequent correct folding of cyt aa_3-600 appear to occur later in the cell growth and to exert growth pressure on expression strains. Heme A is a downstream product that results from chemical modifications by first adding an isoprenyl group to heme B and followed by transforming a methyl substituent to formyl group in heme O.

Each type of heme from spectra, containing multiple absorbing species, was further explored by pyridine hemochromatogen assay. Total heme content in a sample could be estimated by this approach. The protein concentration calculated from heme A content in a protein sample was consistent with the value determined by UV-visual spectrophotometry for wild type cyt aa_3-600. The pyridine hemochromatogen assay also showed features corresponding to hemes B and A in the protein samples that were processed from prematurely collected cell cultures.

Adding a His-tag to Bacillus stearothermophilus (B. stearo) cytochrome bo_3 and protein expression

A His-tag was added to subunit B of cbaAB genetic sequence and enabled purification of the expressed protein in *B. sub* strain transformed with pEB112 construct. The SDS-PAGE gel showed poor separation of protein bands that were faint and unidentifiable. The relevant bands of 43 kDa and 19 kDa length, the predicted molecular mass of subunit A and B, could not be distinguished [63]. The western blot developed on a film showed very faint bands (~35-40 kDa and ~25 kDa) that could not be immediately assigned. No pertinent protein bands were produced from pLala cba2His transformed into *B. sub*. The reduced-minus-oxidized difference spectrum showed heme B band around 560 nm (see Figures 2.3 and 2.4). No significant polarographic change in oxygen consumption was observed despite increased amounts of reactants in the assay containing c551, TMPD and sodium ascorbate. Often times, the activity of membrane protein

involved in the electron transfer pathway is difficult to evaluate because the electron donor is not known or is not an efficient electron donor. In this case, the lack of a third subunit in the expression vector may have shaped the poor enzyme activity. It is present in the reading frame of the genetic operon and is purported to assist in protein folding or contribute to protein stability.

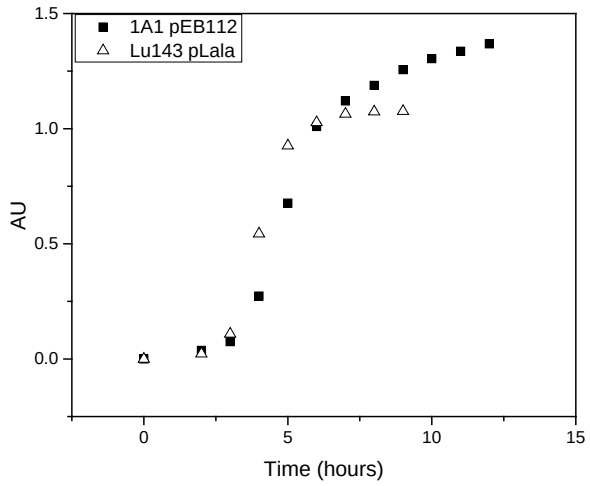

Figure 2.3. Growth curves of two strains expressing *Bacillus stearothermophilus* cyt bo_3. (1) *Bacillus subtilis* strain (1A1) transformed with plasmid pEB112 ligated with genetic sequence of cbaAB-His (shown as black square) for *B. stearo*. cyt bo_3. (2) *Bacillus subtilis* strain (LUW143) transformed with plasmid pLala carrying genetic sequence of cbaAB-His (shown as open triangle). The cultures were grown in Luria broth medium.

Protein expression of B. sub cyt aa_3-600 in E. coli

Several plasmid DNA constructs with DNA insert for *B. sub* cyt aa_3-600 were assessed for protein expression in *E. coli* strains and *Vibrio cholera (V. cholerae).* These strains lack heme A synthase in their genome, and protein expression of *B. sub* cyt aa_3-600 is not expected to occur without some form of complementation that allows for co-expression of heme A synthase [42-43]. Initially, plasmid pET17 with DNA insert for *B. sub* cyt aa_3-600 alone did not lead to expression and purification of functional cyt aa_3-600 in CLY *E. coli* strain. With the purpose of co-expressing ctaA gene of heme A synthase and genetic operon of cyt aa_3-600, plasmid

pETDuet-A-QH1, containing genetic information for heme A synthase and cyt aa_3-600, was transformed into *E. coli* CLY strain, which has the genetic disruption of cyt bo_3 operon in its chromosomal DNA. A large scale culture was grown and processed for isolation of cyt aa_3-600 by applying the isolated membrane to Ni-nitriloacetic acid (Ni-NTA) column that specifically binds to His-tag attached to subunit II of cyt aa_3-600. The SDS-PAGE protein gel displayed smeared background with a faint band at ~34 kDa, which corresponds to an apparent molecular mass of subunit II of cyt aa_3-600. No other protein bands could be assigned to either subunit I or III.

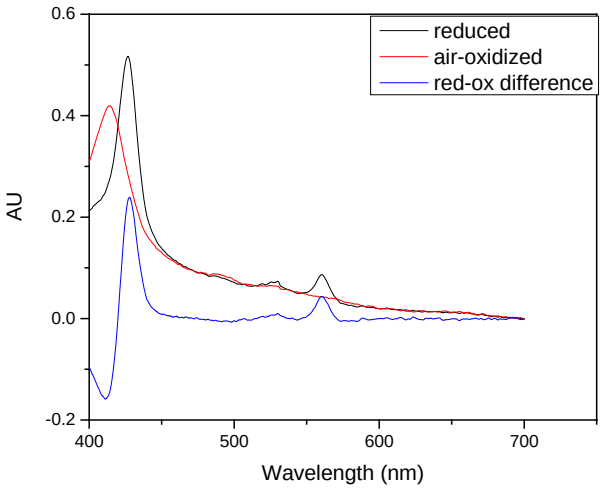

Figure 2.4. UV-visual absorption spectra of purified *Bacillus stearothermophilus* cyt bo_3 (i.e. cbaAB-His). Top spectral line (in black) originated from dithionite-reduced protein sample. The middle spectral line (in red) belongs to air-oxidized protein sample. The bottom spectral line (in blue) is reduced-minus-oxidized difference spectrum. The same sample was used to generate the spectra. The expression strain was *Bacillus subtilis* LUW143 strain transformed with expression plasmid pLala-cbaAB-His that carried the genetic copy for expressing *Bacillus stearothermophilus* cyt bo_3.

The sample itself was very unstable when dithionite was added, and a difference spectrum could not be obtained to investigate the hemes. The air-oxidized enzyme also had altered soret band that stood in contrast from wild type cyt aa_3-600 expressed in *B. sub*.

Transforming the same plasmid construct (i.e. pETDuet-A-QH1) encoding genes for heme A synthase and cyt aa_3-600 oxidase into Rosetta2 strain resulted in isolation of protein that displayed spectral features similar to those of cyt bo_3, which was determined by both pyridine chromatogen assay and dithionite reduced-minus-oxidized difference spectrum. This small amount of protein was likely to be *E. coli* cyt bo_3, because untransformed Rosetta2 strain also produced the same protein that bound to Ni-nitrilotriacetic acid (NTA) resin. There is a natural affinity to Ni-NTA resin column by *E. coli* cyt bo_3 even in the absence of His-tag. The advantage of using Rosetta2 strain in protein expression lies in the fact that the strain carries rare tRNAs, which can facilitate expression of genes that encode rare *E. coli* codons. Any further work with Rosetta2 strain would require disrupting the expression of native *E. coli* cyt bo_3.

Finally, plasmid containing sequences for both heme A and heme B synthases (ctaAB) and cyt aa_3-600 (qoxABCD) (i.e. pETDuet-ctaAB-qoxABCD) was transformed into *E. coli* CLY strain and was found not to express isolatable cyt aa_3-600. Transforming a plasmid carrying genetic operon for *E. coli* cyt bo_3 (i.e. cyoABCD) into *B. sub* also did not lead to a meaningful expression of protein.

Construction of arginine auxotrophs from Bacillus subtilis strain LUW143

Arginine auxotrophs, whose biochemical synthetic pathway for arginine was impeded at argC, argF or argH genes, were constructed from integration plasmids (each having DNA insert that partially overlapped with genetic regions of argC, argF or argH genes) by homologous recombination with *Bacillus subtilis (B. sub)* chromosome of LUW143 strain, having genetic disruption of cyt caa_3 (ΔctaCDEF) and cyt aa_3-600 (ΔqoxABCD). The *B. sub* strains with genetic disruption of arginine biochemical synthesis were monitored for dependence of growth on arginine supplementation in minimal media. The auxotroph altered at argC gene achieved a

strong cell density at 14 hours of growth without arginine supplementation and in the absence of casamino acid and tryptophan supplementation (see Table 2.1). The observation suggested that disruption of argC gene (i.e. ΔargC) in the host cells did not lead to dependence on arginine from an external source, indicating a failed auxotroph. The *B. sub* strain with disruption of argF gene (i.e. ΔargF) displayed a growth dependence on external source of arginine, but the cultures supplemented with arginine did not reach a high cell density initially (see Table 2.2). A secondary screening of *B. sub* ΔargF strain, having disruption in arginine biochemical pathway, confirmed its positive response to arginine supplementation (25 μg/mL) and its potential to achieve a high cell density required for protein expression (see Table 2.3). The *B. sub*, whose genome was disrupted at argH gene (i.e. ΔargH) strain also demonstrated growth that correlated strongly with arginine supplementation in the absence of casamino acid (see Tables 2.4 and 2.5).

Cloning and protein expression of cyt caa_3 from B. sub

The plasmid pLala constructs carrying *B. sub* cyt caa_3 were examined for protein expression in *B. sub* strains and for isolation of pure protein complex. None of the purified samples showed relevant bands in SDS-PAGE protein gel indicating two major subunits I and II (~45 kDa and ~30 kDa). There were many unidentifiable protein bands, despite the His-tags placed at various locations on the genetic operon for ease of purification. The protein sample became unstable when reduced by dithionite, and a meaningful difference spectrum was not obtained. On the reduced-minus-oxidized difference spectrum of isolated *B. sub* cyt caa_3, one would expect to see peaks at 605 nm and 551 nm, respectively for heme A and heme C [32].

Variations of plasmid constructs with cloned sequence for *B. sub* cyt caa_3 oxidase, ctaB-CDEF, ctaCDEF and ctaCDEFG, were unsuccessful on isolating functional enzyme. There is ~100 bp sequence between ctaB gene and ctaC gene that was purported to contain a catabolite

response element and that may play a role in the expression of the cyt caa_3 [44]. The ctaG gene was suggested to assist in the correct folding of the *B. sub* cyt caa_3 complex. It is clear that purification by His-tag alone is not sufficient in isolating functional cyt caa_3 [41].

2.4. Conclusion

A practical, stream-lined process for purifying protein in amount required for biophysical studies have been demonstrated for cyt aa_3-600 from *Bacillus subtilis (B. sub).* However, applying the same approach to other membrane proteins was not met with similar level of success. It still remains a challenge to express and purify functional *Bacillus stearothermophilus* cyt bo_3 and *B. sub* cyt caa_3. Expressing *B. sub* cyt aa_3-600 in *Escherichia coli* strains also failed to yield active protein of good purity. It appears that expressing membrane proteins is not easily replicable from protein to protein using similar protocols and requires distinct handling of each protein. This could reflect the way protein is folded and assembled, polarity and stability of the enzyme complex and the need for specific auxiliary proteins during protein folding and assembly. There is an opportunity for further investigation in the development of efficient process for isolating membrane proteins.

CHAPTER 3: Functional Characterization of Bound Menaquinone in *Bacillus subtilis* Cytochrome aa_3-600 That Co-Purifies With the Enzyme

3.1. Introduction

In this chapter, biochemical and biophysical approaches were explored to establish descriptive parameters for the menaquinone co-factor in *Bacillus subtilis* (*B. sub)* cytochrome (cyt) aa_3-600 oxidase. The measurement of *B. sub* cyt aa_3-600 menaquinol activity by others produced variable figures due to different approaches to protein preparations and assays [15, 29, 31, 39]. Here, an activity assay condition was developed for an efficient reduction of the bound menaquinone in cyt aa_3-600. A coupled-enzyme assay was necessary since a direct detection of the change in menaquinol concentration is not straightforward. An indirect detection of the change occurred by monitoring the depletion of reduced sodium NADH concentration, which has a known extinction coefficient of 6.22 mM^{-1} and shows an absorption band at 340 nm wavelength.

The quinone can assume three different redox states: fully oxidized menaquinone, partially reduced semiquinone (SQ) and two electron reduced menaquinol. The free SQ form is very unstable in solution. However, when it is associated with protein, the stability constant of this intermediate state could increase and could become detectable by electron paramagnetic resonance (EPR) spectroscopy. Consequently, protein samples were treated chemically to stabilize the bound SQ. The optimal condition for determining the electrochemical potential of SQ equilibrated in cyt aa_3-600 was also searched by testing various mediator compounds, buffer conditions and enzyme preparation. The radical signal detected by EPR should titrate as a bell-shaped curve as the electric potential is increased. The curve on the right side of the maximum point would reflect the semiquinone formation. The curve on the left of the peak as the potential is lowered would correspond to reduction of the semiquinone to hydroquinol. The fitting the

titration curves would lead to determination of electrochemical potentials E1 (Q^-/Q) and E2 (QH_2/Q^-) and the midpoint potential of the semiquinone at a given pH.

The implication of a high affinity quinone binding site (Q_h-site) has been that it is likely a two electron to one electron transition point because it has the capacity to hold two electrons and because the *B. sub* cyt aa_3-600 necessarily has a strict single electron catalytic pathway for reducing O_2 to generate two molecules of water. The two-site quinone model has been favored in explaining the role of mediation in electron transfer among the cytochrome quinol oxidases. However, the evidence does not rule out the possibility of Q_h-site being directly involved in quinol oxidation reaction, where there is only one quinone binding site.

3.2. Materials and Methods

3.2.1. Development of activity assay

Screening the conditions for enzyme activity required a systemic determination for an optimal pH, coupling enzyme activity, the amount of NADH, and quinone compounds that gave measurable activity with cyt aa_3-600. A commercially supplied NADH:quinol oxidoreductase, coupling enzyme, gave very little change in NADH consumption in the tested assay conditions (50 mM Tris-HCl or 50 mM KH_2PO_4 buffer in the pH range of 6.5-8.5) with following quinone compounds: menadione (vitamin K_3) in ethanol, menaquinone-4 (vitamin K_2) in hexane, ubiquinone-1, benzoquinone, laprocal, duroquinone and dimethyl naphthoquinone (DMN). When the enzyme reaction showed no change even with DMN, the quinone analog that was reported to show activity with cyt aa_3-600, it became apparent that the coupling enzymes were not able to reduce quinone analogues from NADH, and therefore unable to produce the cyt aa_3-600 activity. A test sample of DT-diaphorase produced observable cyt aa_3-600 activity with

menadione and DMN. While menadione gave weaker activity than DMN, both compounds showed significant autooxidation with increasing concentration and with pH. At milimolar concentrations and at neutral pH, NADH becomes unstable and self-inhibitory in phosphate buffer. Hence, 50 mM Tris-HCl, pH 6.8-7, 0.05 % dodecyl maltopyranoside (DDM) buffer condition was used for enzyme reaction at room temperature.

3.2.2. Optimization of over-expression and purification of diaphorase

The assay performed with diaphorase from the commercially supplied *Clostridium kluyveri* (Sigma, St. Louis, MO) gave little or no activity in the conditions that were specified. DT-diaphorase used in the assay was overexpressed from an *E. coli* strain, which was provided by Gary Cecchini Group (UCSF). The conditions for protein expression and purification of DT-diaphorase required various adjustments in obtaining active enzyme of a high yield.

Functional DT-diaphorase was purified from a culture prepared with Luria broth medium (LB) and 100 mg/mL ampicillin, inoculated at 2.5% in 500 mL volume in a 2-L beveled flask and grown overnight at 30 °C for 24 hours with shaker at 160 rpm. An adequate aeration, requiring a low liquid volume to flask volume ratio, was critical in isolating functional enzyme and in obtaining a high protein yield. No induction was necessary. The harvested cell pellet was resuspended in 50 mL of 50 mM Tris-HCl, 100 mM KCl, pH 7.5 and was disrupted. Once the cell debris was pelleted by centrifugation at 40,000 rpm for 1 hour, the supernatant was bound to blue sepharose resin (Bio-Rad, Hercules, CA). The sample-loaded resin was washed with buffer containing five-fold higher KCl, followed by washes to remove salt. The bound protein was eluted with 10-20 mM NADH. Eluted fractions were combined and buffered exchanged in order to remove excess NADH.

3.2.3. Steady-state activity assay by spectrophotometry

Enzyme activity of *Bacillus subtilis* cytochrome aa_3-600 oxidase was monitored spectrophotometrically in a coupled-enzyme assay, where the coupling enzyme, diaphorase, was used to generate reduced quinone substrate from NADH. This approach avoided the need for preparing reduced quinones prior to setting up the enzyme reaction. Each enzyme reaction volume contained the following: diaphorase in excess amount sufficient to sustain cyt aa_3-600 activity, 100 μM NADH, DMN as substrate, 0.05 μM enzyme in 50 mM Tris-HCl, 0.05% dodecyl maltopyranoside (DDM), pH 6.8 buffer. The respiratory activity was started by reducing DMN in the presence of 100-200 μM NADH and excess amount of purified diaphorase. To this preparation 0.05 μM of cyt aa_3-600 oxidase was added. The reaction was repeated for increasing concentration of DMN in order to determine Michaelis-Menten values. The steady-state activity was monitored by oxidation of NADH at 340 nm with HP Agilent UV/Vis spectrophotometer. Some autooxidation of dimethyl naphthoquinone (DMN) occurred at concentrations above 10 μM, and this deviation was accounted for in the adjusted baseline when quantifying the substrate depletion by the enzyme.

3.2.4. Quinone extraction and isolation by reverse-phase HPLC

Quinone was extracted from the 10 nmol of purified enzyme preparation with 3 mL of solvent containing methanol/petroleum ether (6:4, v/v) by thorough mixing, followed by a brief centrifugation. The organic extraction was repeated three times, and the organic layer was collected in a separate vessel. An equivalent molar amount of standard quinone with various isoprenyl sidechain lengths were added to the protein sample prior to extraction. The organic phase was combined and evaporated under nitrogen stream. The dried, oily residue was re-

dissolved in ethanol. The quinone was isolated by reverse-phase HPLC using a Varian Microsorb-MV 100-5 C18 column (4.6 mm x 25 cm) and a Waters HPLC system. The quinone elution from the C18 column was monitored at 278 nm using a mobile phase of 4:3:3 EtOH: MeOH: ACN. Isoprenoid quinone structure in the elution fraction showing the highest absorption peak was identified by mass spectroscopy (Mass Spectrometry Lab, UIUC).

3.2.5. Potentiometric redox titration of menaquinone radical in the high affinity site in cyt aa_3-600

Redox titrations were carried out at room temperature (~20 °C) [48]. The ~1.5 mL 50 μM enzyme or membrane solution was prepared in either 100 mM Tris buffer, 20% glycerol, 0.05% DDM at pH 8.3 or 200 mM CHES at pH 9.0. The samples were poised electrically at defined redox potentials in anaerobic chamber, quickly sampled at 150 μL-200 μL aliquots and transferred into argon evacuated EPR tubes. The redox potential was initially poised at a high potential endpoint (~100 mV) and then reduced step-wise with dithionite or was oxidized incrementally using ferricyanide $K_3Fe(CN)_6$ from a low potential endpoint (~ -200 mV). Both screening approaches yielded weak or no EPR signals.

The experimental set-up utilized a calomel electrode with Zobell solution (E_h) in place of the standard hydrogen electrode, which maintained ~250 mV difference from the observed electric potential (E_{obs}). A set of mediators were added to the enzyme solution to stabilize the semiquinone during sampling. The redox mediators (10 μM) were: 9,10 anthraquinone-2,6 disulfonate (-184 mV); 1,2 naphthoquinone (127 mV); duroquinone (5 mV); n-ethyl phenozonium (PES, 55 mV); PMS (80 mV); anthraquinone (-100 mV); resorufin (-51 mV).

3.2.6. Generating a stable semiquinone (SQ) radical in cyt aa_3-600

The EPR samples were in the final buffer conditions consisting of 100 mM Tris, 10 mM EDTA, 10 % glycerol, 0.05 % DDM, pH 7.5 – 8.2 with enzyme concentration of ~ 200 μM. The protein samples were concentrated and buffer exchanged using Amicon centrifugal filters (Millipore, Bedford, MA). The semiquinone was generated with NADH in semi-anaerobic condition and was rapidly frozen in liquid nitrogen. Slow reduction with sodium ascorbate over various time points over several hours gave no semiquinone signal. The quinone radical generation with dithionite ($Na_2S_2O_4$), a strong reductant, yielded small signals, inadequate for advanced EPR experiments.

3.2.7. Spin quantification

Double integration of the semiquinone EPR spectrum against 4-oxo-tempo standard gave an estimate of the radical concentration to be approximately 30% of wild type (WT) enzyme concentration in the presence of NADH. This was the maximum unpaired spin concentration achieved for cyt aa_3. Hence, all of the advanced EPR measurements were performed on samples similarly prepared.

3.2.8. Preparation of quinone-free cytochrome aa_3-600 sample film for ATR-FTIR experiment

A thin dehydrated protein film depleted of detergent was difficult to prepare and usually fell apart during a full programmed scan (> 6 hours) of cyt aa_3 sample. Absorbance at amide I and II regions and backbone carbonyl groups (~1750 cm^{-1}) were monitored for the presence of protein on the surface of sample holder. Weak signals and large shifts and distortions associated with protein denaturation made it challenging to observe menaquinone vibrational modes.

3.2.9. Screening for crystallization of cytochrome aa_3-600

For crystallization, 100 μL of 80-100 μM purified cyt aa_3-600 was buffered exchanged into 50 mM Tris, pH 7.4. Initially, the crystal drops were prepared in solutions made up of 21% to 26% PEG400 in 100 mM MES at pH 6.5 with 0.1% decyl β-D maltopyranoside (DM) that contained high homogeneity in alpha form of the anomeric carbon. To these drops, 3 mM of $MgCl_2$ or CdCl of high purity were added in 1:1:2 (precipitant: solution: enzyme) ratio on crystallization wells that were filled at the bottom with 1 mL crystal solution. This initial screening at 4°C led to large round crystals that did not diffract. Hence, additional screenings were performed with Hampton's crystallization screening kit at 1: 2 ratio of crystallization solution to enzyme. In order to refine conditions for cyt aa_3-600 crystals further steps were taken. The purity of the enzyme was improved by additional wash steps with gel filtration (Superdex 200 HR 10/30, 10 kDa - 600 kDa molecular range). Different additives (e.g. Mg/Cd mixture, ZnCl or Hampton's additive) varying conditions (i.e. buffer concentrations, buffer pH, inhibitors, temperature changes and different detergents) were examined.

3.3. Results and Discussion

Steady-state activity of Bacillus subtilis cytochrome aa_3-600

The activity of cyt aa_3-600 was measured by spectrophotometry, which indirectly monitored the quinol oxidizing capacity of this enzyme. The developing the working assay required the use of low potential quinone compounds such as menadione (vitamin K_3) and dimethyl naphthoquinone (DMN) that readily dissolve in ethanol, instead of high potential ubiquinone (Q-1). These reduced forms of the low potential quinone derivatives are unstable even in the anaerobic condition, and low pH buffer condition (pH 6.5-7) kept the autooxidation

at bay with its contribution to less than 10% of observed time traces of the enzyme activity. The commercially available coupling enzyme (*C. kluyveri*) was unable to reduce naphthaquinone-based compound, which made it difficult to determine enzyme activity initially. DT-diaphorase can reduce DMN, but it showed variability with cyt aa_3-600 activity for different batches of diaphorase preparations. This variance in activity was correlated with isolation and purification of functional diaphorase in high concentrations. Hence, the growth conditions and purifications of diaphorase were reworked and tested extensively. The largest activity values observed for wild type cyt aa_3-600 are k_{cat} of 180 DMN/s and K_m of 89 μM (see Figure 3.1). In the previous work by Mattatall et al. [15] the Michaelis-Menten fitting of the quinol oxidase activity obtained with dimethylnaphthoquinone (DMN) as substrate did not reach saturation of enzyme activity even at 400 μM DMN concentration and reported K_m of 300 μM with maximal electron turnover number of 63.5 s^{-1}. The main difference between these two sets of values and other previous reports of single-point concentration activity assay arise from the different protein or membrane preparations used in the assay. Based on the experience of repeated quinol activity assay with substrate DMN, there is variability in K_m and k_{cat} values associated with reagents, DT-diaphorase and protein samples purified at different times. Hence, comparative analysis was performed for assays carried out on the same day with same reagents and protein samples whenever possible (see Chapter 5).

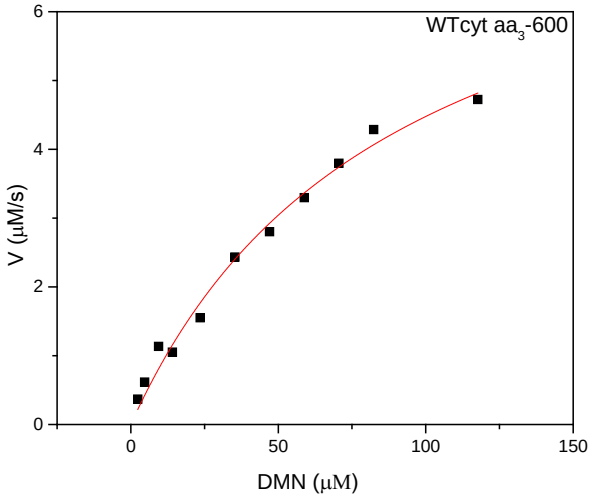

Figure 3.1. Quinol oxidase activity of wild type cytochrome aa_3-600 monitored by change in substrate dimethylnaphthoquinone (DMN) concentration in the presence of DT-diaphorase, a coupling enzyme, and reduced NADH. Buffer conditions: 50 mM Tris-HCl, 0.05% dodecyl maltoside (DDM), pH 6.8.

Direct reduction of quinone substrate with other reductants such as dithionite, dithiothreitol (DTT) and its epimer (DTE) gave no significant development in the time trace that could be assigned to enzyme activity. Cyt aa_3-600 activity with DMN was higher than with menadione. However, *E. coli* cyt bo_3 ubiquinol oxygen reductase showed stronger DMN activity than for cyt aa_3-600 or *E. coli* cyt bd I oxygen reductase. The activity with DMN was higher than for activity with menadione for all oxygen reductases examined. Both of the *E. coli* oxygen reductases (cyt bo_3 and cyt bd enzymes) also react with ubiquinone-1 (Q-1), whereas cyt aa_3-600 does not.

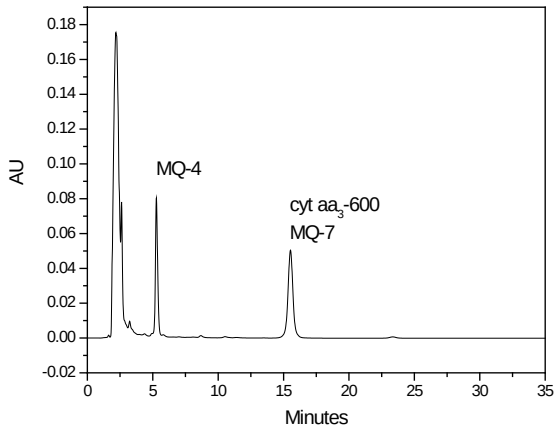

Figure 3.2. HPLC extraction of bound menaquinone-7 from purified protein sample of cytochrome aa_3-600. The first peak that eluted was associated with residues of denatured protein and detergent dodecyl maltopyranoside. The second peak labeled MQ-4 is the standard peak with measured concentration of 10 nM menaquinone-4 having 4 units of isoprenyl group. The third peak to elute from the applied sample injection to HPLC column was the hydrophobic menaquinone-7 that was extracted from cytochrome aa_3-600.

Generation of stable semiquinone radical

Approximately, one equivalent of menaquinone per molar enzyme concentration (1.1-1.2) was extracted from cyt aa_3-600 and applied to reverse-phase HPLC (see Figure 3.2). The isolated menaquinone fraction revealed ionized fragments by mass spectrometry that could be traced to menaquinone-7, which is produced by *Bacillus subtilis*.

This bound menaquinone would participate in single electron transfer steps that would lead to reduction of dioxygen at the heme-copper binuclear center in cyt aa_3-600. Hence, the high-affinity quinone site (Q_h) is a critical juncture where the semiquinone (SQ) state would be stabilized with respect to the quinol and quinone states during enzyme catalysis. Unfortunately, the SQ state of the bound menaquinone in cyt aa_3 was found to be unstable as it was difficult to observe an EPR signal by potentiometric titration at all points of electric potential sampled at pH 8.3. The instability of mena-semiquinone reflects its low midpoint potential and its low stability

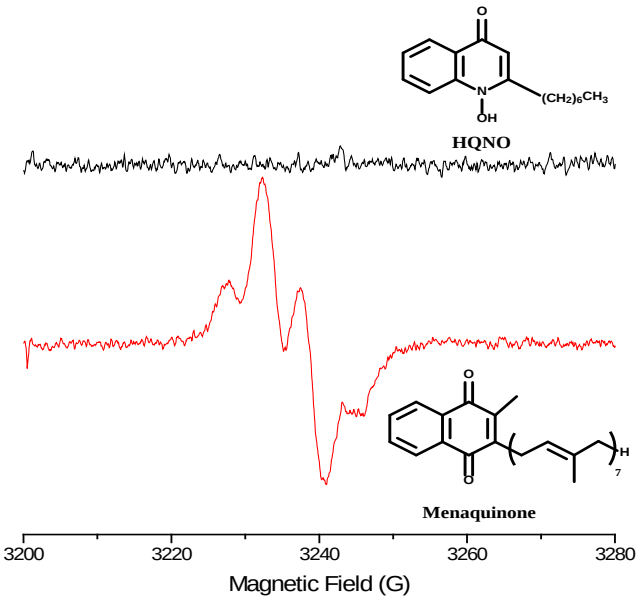

Figure 3.3. Continuous-wave electron paramagnetic spectroscopy (EPR) of wild type cytochrome aa_3-600 in the presence and absence of inhibitor 2-n-heptyl-r-hydroxyquinoline N-oxide (HQNO). The EPR sample was prepared using ~100-200 μM of protein in the presence of NADH and dimethyl naphthoquinone (DMN). Top spectrum was prepared with at least two molar equivalents of HQNO. Bottom spectrum was prepared without the inhibitor. EPR parameters were: modulation amplitude (MA), 0.2 mT; microwave (mw) power, 30 dB; mw frequency, 9.087 GHz, temperature 105 K.

constant at the Q_h-site. Certain changes such as an improved management of air evacuation, higher buffer concentration at a higher pH (e.g. pH 9 or greater) could enhance this technique.

Because it was difficult to poise SQ in cyt aa_3-600 with dithionite, a strong reductant, alternative avenues were explored to stabilize this intermediate state. While sodium ascorbate (~60 mV) was successfully used to stabilize SQ in *E. coli* ubiquinol bo_3 oxidase [46, 47], the same method unsurprisingly did not generate SQ EPR signal in cyt aa_3-600 sample. However, NADH in the presence of dimethyl naphthoquinone (DMN) was able to produce SQ radical in cyt aa_3-600 in a semi-anaerobic condition. The maximum spin concentration of paramagnetic radical formed in pH 7.5 buffer was approximately 30 % of the enzyme concentration of cyt aa_3-600.

The SQ EPR signal (having g-value of 2.0) and is approximately ~12 MHz in line width and contained partially resolved hyperfine structure that has been tentatively assigned to nonequivalent methyl ring substituent (see Section 4.3.2). No redox mediators or other species likely to produce radicals were present in the sample, and the likelihood of highly unstable free semiquinone radical giving rise to such intense EPR spectra under these conditions was small. Advanced EPR experiments displayed evidence for a single species. Hence, the species observed was assigned to bound mena-semiquinone radical.

The effects of the inhibitor 2-heptyl-4-hydroxyquinoline-N-oxide (HQNO) on the stabilization of SQ at this site were evaluated. 1 μM HQNO inhibited electron transfer to 0.05 μM cyt aa_3-600 in the presence of 10 μM dimethyl naphthoquinone (DMN), but was less effective than aurachin C1-10 (AC1-10), which showed inhibition at nanomolar concentrations. Also, addition of HQNO prevented the SQ formation when exposed to over a period of a few minutes (see Figures 3.3 and 3.4). Similar inhibitory effects were reported for *E. coli* cyt bo_3 and suggested competitive interaction at Q_h-site in *Bacillus subtilis* cyt aa_3-600 [24, 45]. Previously, Yap et al. (2010) had described a two-site quinone model, but one-site model cannot be ruled out in explaining the observations.

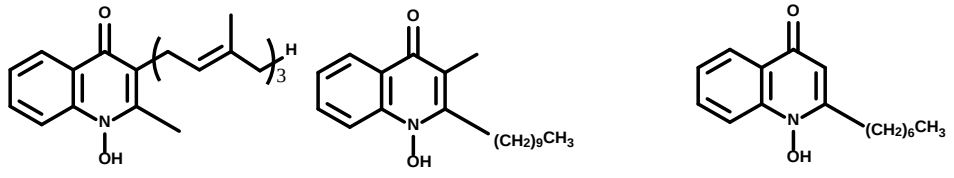

Aurachin C **Aurachin C1-10** **HQNO**

Figure 3.4. Chemical structures of inhibitors for *Bacillus subtilis* cytochrome aa_3-600. Aurachin C1-10 is a modified version of aurachin C that has its ring substituents switched in position at ring carbons 2 and 3 (ubiquinone numbering). 2-heptyl-4-hydroxyquinoline-N-oxide (HQNO) has shown micromolar inhibitory activity for ~ 0.05 μM enzyme preparations. Aurachin C1-10 has shown nanomolar inhibitory activity at same enzyme preparation (see Section 5.3.3).

3.4. Conclusions

The enzyme activity of cyt aa_3-600 was demonstrated with spectrophotometric assay. The assay condition was developed for an optimal enzyme performance in the presence of NADH, dimethyl naphthoquinone (DMN) and DT-diaphorase. It was important to express diaphorase in large quantity and to rework the purification procedure for isolation of functional enzyme, because different batches of diaphorase gave different results. Reducing compound such as dithiothreitol (DTT) was a poor substitute as electron donor to cyt aa_3 and in generating enzyme turnover.

The spectrophotometric activity at a single concentration of DMN (e.g. 10 μM) revealed that the DMN activity was the strongest with cyt bo_3 (*E. coli*) than cyt bd I (*E. coli*) or cyt aa_3-600 oxidases. The significance of this observation is discussed further with additional experiments in Chapter 5. Notably, cyt bo_3 is the dominant oxygen reductase in *E. coli* during active growth and readily accepts electrons from ubiquinol, which has a higher midpoint potential than $DMNH_2$.

The inhibitor HQNO disturbed the stabilization of semiquinone at the Q_h-site, suggesting its specific interaction with cyt aa_3-600. Crystallization efforts by Gennis group in collaboration with Nair Group, thus far, have led from low resolution crystals of >5 Å to more recently ~3.5 Å crystals that show x-ray diffraction.

CHAPTER 4: Exploring the Menaquinone Binding Site (Q_h) Of Cytochrome aa_3-600 by CW and Pulsed EPR Techniques

4.1. Introduction

In Chapter 3, it was demonstrated that cytochrome (cyt) aa_3-600 can stabilize semiquinone (SQ) when chemically reduced in semi-anaerobic condition. A SQ radical is an intermediate state of menaquinone that reflects enzymatic changes as cyt aa_3-600 undergoes catalysis. A striking feature in the continuous-wave (CW) EPR spectrum of cyt aa_3-600 was partially resolved hyperfine structure from protons of methyl group that was associated with the protein-quinone interaction. Studying the molecular details by advanced EPR techniques, such as 1-dimensional (1D) and 2-dimensional (2D) Electron Spin Echo Envelope Modulation (ESEEM) and Hyperfine Sublevel Correlation Spectroscopy (HYSCORE) at X-band (~9.7 GHz), could further elucidate specific interactions between SQ and cyt aa_3-600.

Currently available protein-quinone models have suggested different influence the protein structure has on the SQ radical. These include Q_A and Q_B of photoreaction center, A_1 of photosystem I, bc_1 complex and *Escherichia coli* (*E. coli*) nitrate reductase. These protein complexes have different functional roles when interacting with the substrate quinone or quinol, signifying the importance of protein environment of the quinone sites.

The well-characterized cyt bo_3 ubiquinol oxidase from *E. coli* is uniquely a heme-copper oxidase that offers a comparative basis for understanding the menaquinol oxidase activity of cyt aa_3-600. The ubiquinone bound at the high affinity quinone binding site (Q_h-site) of cyt bo_3 also forms a stable SQ when the protein is partially reduced [45, 51]. A combination of x-ray crystallography, site-directed mutagenesis and pulsed EPR methods have been used to define the residues at the Q_h-site and details of the interactions between these residues and the bound semiquinone [18, 47, 52-53]. Four polar residues have been implicated in binding to the quinol

at the Q_h-site in cyt bo_3: Arg71, Asp75, His98 and Gln101. Among the many sequences of quinol oxidases examined, Arg71, Asp75 and His98 are totally conserved. Gln101 is totally conserved in sequences from proteobacteria but is often replaced by a glutamic acid in the homologues in the firmicutes, including the *Bacillus subtilis* (*B. sub*) cyt aa_3-600 menaquinol oxidase.

Pulsed EPR methods have revealed several salient features of the interactions between the residues at the Q_h-site of cyt bo_3 and the SQ that offer insights when interpreting results from similar studies performed, here, with cyt aa_3-600. 1) The hydrogen bonding to the SQ is highly asymmetric, with strong hydrogen bonds to carbonyl O-1 and weaker interactions at carbonyl O-4 side [46]. 2) There is one strong hydrogen bond between the ε-nitrogen of Arg71 and carbonyl O1 of the SQ, resulting in a substantial transfer of unpaired electron spin to this nitrogen. 3) There is a strong hydrogen bond between Asp75 and carbonyl O1 of the SQ. 4) There is a weak interaction between His98 and carbonyl O4 of the SQ with a small amount of spin density found on the nitrogens of His98.

The Chapter 4 details the efforts to characterize the molecular interactions associated with the SQ: Identifying nitrogen couplings and the number and strengths of hydrogen bonds. The SQ stabilized in the ^{14}N and uniformly ^{15}N labeled *B. sub* cyt aa_3-600 was examined using continuous-wave and pulsed EPR methods, which were performed in collaboration with Drs. Sergei Dikanov and Rimma (Marina) Samoilova. The results show a distinctly different pattern of hydrogen bonding between the protein and SQ species in the menaquinol oxidase than that observed with the *E. coli* cyt bo_3 ubiquinol oxidase.

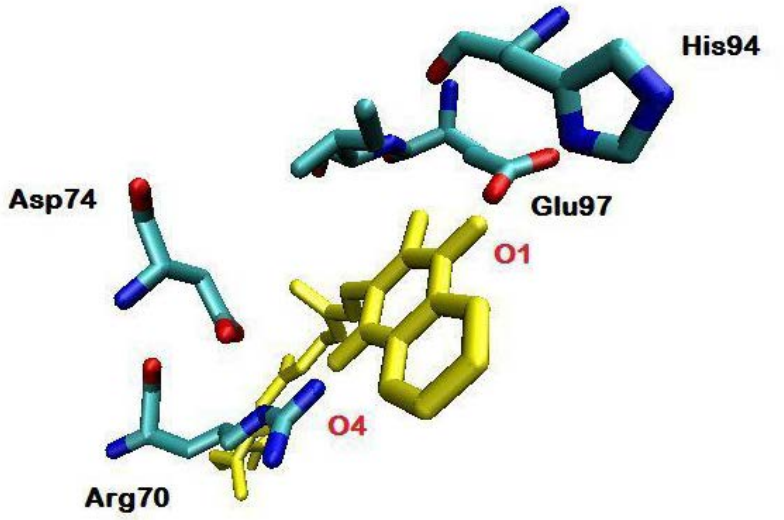

Figure 4.1. Model of the quinone binding at the Q_h site of the cyt aa_3-600.
The figure was generated according to the model based on the x-ray crystal structure of cyt bo_3 [17] using VMD [54] and Swiss Model [55]. Carbonyl oxygens of menaquinone are indicated in red labels. In ubiquinone, the labeling assignment for the carbonyl oxygens is reversed in order. The placement of the menaquinone (MQ) in the model is hypothetical.

4.1.1. Introduction to Electron Paramagnetic Resonance (EPR) spectroscopy

The development of EPR spectroscopy as a research tool in inorganic, bioinorganic, and radical bioorganic molecules has its origin in the advancement of microwave technology during 1940s. From this period, microwave source, such as klystron vacuum tube, became widely available for basic research, repurposed from military usage. For EPR spectroscopy, a fixed microwave source, a klystron, meant using resonant cavity with high sensitivity to irradiate samples, where the corresponding wavelength fits the resonator dimensions. It is the primary reason for keeping the microwave frequency constant while varying the magnetic field in an EPR experiment. The intent of section is to provide only a general introduction and summarizes from the detailed information available from other in-depth resources [56-60].

In continuous wave (CW) EPR experiment, the sample containing paramagnetic species is irradiated by microwaves, and the magnetic field is varied to search for the microwave absorption. This technique is based on the principle that electron has intrinsic spin and orbital angular momentum. Since electron is charged and has angular motion, this movement of charged particle generates magnetic field and associated magnetic moment. The spin magnetic moment has no preferred orientation in the absence of magnetic field. In the presence of external magnetic field, electron aligns itself along the z-axis in two quantum spin states: m_s = ½ or m_s = -½. The orientation parallel to magnetic field, B, is energetically higher than the antiparallel one. This difference in energy, ΔE, is exactly matched by the electromagnetic radiation absorbed when the electron flips its orientation. The observation of this change, the resonant transition, is monitored in EPR spectroscopy. In general, the sample is irradiated with microwave power (9.5 GHz) in the X-band range at a resonance field of 3400 Gauss (G).

$$\Delta E = h\nu = g\beta B_o \qquad (1)$$

where h is Planck's constant, ν is frequency, g is proportionality constant for free electron, β is the Bohr magneton, and B_o is magnetic field.

The protein samples were frozen for EPR spectroscopy, which fixed molecules in all possible orientations. Such an orientation-disordered sample produced a powder spectrum, which contained summation of contributions from all orientations. In this case, the unpaired electrons are not aligned in any specific direction (e.g. a single crystal) or are not rotating rapidly thereby averaging out the direction dependent interactions (e.g. a low-viscosity solution). Hence, the powder sample such as frozen protein in solution has an added complexity to g-factor anisotropy, a deviation of the measured g-factor from the free electron.

This change in g-factor results from the spin and orbital angular momenta mixing through spin-orbit coupling, leading to orientation dependence in the molecule. For every molecule, principal g-factors referred to as g_x, g_y, and g_z can be determined.

In a powder sample, three types of g-factor anisotropy are used to approximate molecular symmetry: *isotropic*, *axial*, and *rhombic*. This assignment is associated with the degree of symmetry in the principal g-factor components. In *isotropic*, all of the principal g-factors are equal ($g_x = g_y = g_z$). In *axial*, there is a discernable symmetry in two of the axis directions ($g_x = g_y \neq g_z$), which leads to two observable features on EPR spectrum. The g-factor along z-axis is considered to be parallel with the x-y plane, and is called $g_\parallel$, where $g_z = g_\parallel$. The equivalent g-factors in the x-y plane, $g_x = g_y = g_\perp$, are perpendicular to $g_\parallel$. In the *rhombic* anisotropy, all of the g-factors are different ($g_x \neq g_y \neq g_z$), and three different spectral features are present on EPR spectrum.

For quinones, only a single line is observed from the X-band (~9.7 GHz) EPR isotropic spectrum because the resolution is limited at the low field range for powder samples. However, at higher frequency Q-band (~35 GHz) EPR, the g-tensor components are resolved for semiquinone (SQ) signal, and three distinct components of rhombic symmetry are observed (see Section 4.2.4). This is clearly demonstrated in cyt aa_3-600, where menasemiquinone signal is better resolved in Q-band spectrum (see Figure 4.2).

Many nuclei listed in the periodic table possess a spin I and an associated magnetic moment. The spin quantum number (I) can be integral or half-integral between ½ and 6. This report addresses hyperfine interactions involving the nuclei of nitrogen atoms (^{15}N and ^{14}N) and hydrogen atoms (^{1}H and ^{2}H), having nuclear spin values (I) of ½ or 1. The interaction of the nuclear spin with magnetic field is described by the nuclear Zeeman frequency,

$$\nu_I = \frac{-g_n \beta_n B}{h} \qquad (2)$$

where g_n is nuclear g-factor, β_n is nuclear magneton, B is the magnetic field and *h* is the Planck's constant. Each magnetic nucleus can be assigned a nuclear Zeeman frequency (ν_I) that is a characteristic of energy associated with spin-inversion at a given magnetic field and fixed microwave frequency (e.g. B = 350 mT at ~9.7 GHz). The nuclear Zeeman frequency is about 10^3 times weaker than the electron Zeeman interaction in the same magnetic field due to larger proton mass. Therefore, in most EPR experiments the nuclear Zeeman interaction is isotropic.

4.1.2. Electron Spin Echo Envelope Modulation (ESEEM)

The utility of EPR technique is in the information one can obtain about the chemical composition, structure, and bonding of paramagnetic species in its protein environment. These chemical characterizations are interpreted from the analysis of g-value, hyperfine coupling constants, and quadrupole coupling interaction for nucleus of spin value $I \geq ½$. Except for g-tensor values, most of the detailed structural information is not obtainable from CW EPR because of inhomogenous broadening of the spectrum. Hence, the nuclear hyperfine and quadrupole splitting of nuclei interacting with the paramagnetic center are not resolved in the EPR spectrum. Fortunately, advanced EPR technique such as ESEEM is able to recover information on electron and nuclear spin interaction by monitoring spin echo modulation. Chemical information such as ligand identity, orientation, and strength of interaction can be determined for weakly coupled interactions.

In ESEEM experiment, echo intensity is measured as a function of the time interval τ between pulses. Unlike CW EPR where the magnetic field component of the microwave field is kept constant as the static magnetic field is swept, in pulsed EPR the microwave pulses of

defined duration are incident upon the sample, while magnetic field is fixed at a position defined from the absorption spectrum. Two factors influence the echo intensity. The first is the magnetic relaxation process resulting from monotonic decay of the echo signal as time, τ, is increased, mainly from electron spin-spin relaxation constant, T_2. The second factor is the interaction of the unpaired electron spins with surrounding magnetic nuclei. Combined together, they contribute to periodic variations of echo intensity as τ is changed. Since ESEEM experiment presents data in time domain, Fourier transformation of the echo intensity is performed to convert the data into frequencies, where the nuclear interactions can be determined.

Different pulse sequences are available for various ESEEM experiments. Two-pulse sequence gives the simplest echo, called Hahn echo, which is essentially a trace of two free induction decays back-to-back. Free induction decay (FID) signal is generated when the sample is excited by the intense microwave pulse. This microwave signal is detected in the resonator as currents and voltages, as the net magnetization vector (or the vector sum of all the magnetic moments) of the sample is rotated into –y-axis from z-axis position, which is parallel with the magnetic field. The magnetization vector precesses in the x-y plane at the resonant frequency until it dissipates completely.

Instead of FID, Hahn echo is monitored in ESEEM study because FID diminishes in the order of 80 ns period after the microwave pulse, within the time frame of instrument dead time. The 2^{nd} pulse is needed to restore the magnetization and extend the signal lifetime by allowing the FID to recover. This refocusing pulse produces electron spin echo at time τ after the 2^{nd} pulse, which is followed by new defocusing of the magnetization vector in the x-y plane. Two-pulse echo is subject to phase memory time, T_m, which occurs in the order of 1μs and arises from spin-spin relaxation, spectral diffusion, spin diffusion and instantaneous diffusion. This

decay time is shorter than relaxation time of stimulated echo, which is generated in three-pulse and four-pulse experiments, and limits the length of time when the signal modulations can be obtained. The stimulated echo in three-pulse and four-pulse experiments leads to less intense frequencies, but gives better resolution than Hahn echo.

The effect that a microwave pulse has on the magnetization during pulsed EPR experiment can be described in the following manner. The static magnetic field, B_o, along the z-axis, is used to establish the equilibrium condition, and an additional magnetic field B_1 is used to perform the experiment. Hence, the detection coils must lie in the x-y plane so that magnetic effects from the sample are not masked by the external field. The B_1 components of microwave field pulses have specific tip angles (which depend on the duration of the pulse) that will rotate the magnetization about the x-axis. For instance, a $\pi/2$-pulse (90°) will tip the magnetization, originally aligned to the external field along the +z-axis, into the x-y plane, and a π-pulse (180°) will invert the magnetization into -z-axis. Upon tipping the magnetization with $\pi/2$-pulse microwave pulse, the magnetization is stationary in the rotating frame of reference, and the spins establish phase coherence (or merge together). Because the electron spins interact with their surroundings, the transverse magnetization (i.e. magnetization having an x-y component) will decay away and return to equilibrium (i.e. magnetization having component along z-axis) through relaxation processes, generating signal.

Several different pulse sequences are available to manipulate the magnetization produced by the microwave pulses and consequently to detect the magnetic behavior during its return to equilibrium. In three-pulse sequence ($\frac{\pi}{2} - \tau - \frac{\pi}{2} - T - \frac{\pi}{2} - \tau$), the stimulated echo signal appear at the end of the pulse run (i.e. after 2τ+T) and is recorded as a function of the time T and fixed time τ. An advantage that three-pulse experiment has over other pulse sequences is that the

three-pulse echo modulation contains only the fundamental nuclear transition frequencies (i.e. ν_α and ν_β, where $\Delta m_I = \pm 1$) and do not produce their combinations that could complicate the ESEEM spectrum. In the experiment involving 4-pulse sequence ($\frac{\pi}{2} - \tau - \frac{\pi}{2} - t_1 - \pi - t_2 - \frac{\pi}{2} - \tau$), the stimulated echo is inverted by π-pulse and is measured as a function of times t_1 and t_2, which are increased stepwise at a fixed time τ.

The four-pulse ESEEM is used to measure the sum and difference ($\nu_\alpha \pm \nu_\beta$) combinations of basic nuclear transition frequencies in different m_s manifolds of the electron spin. This detection is important because the combination peaks appear as narrow features in the spectrum, owing to the fact that the orientation-dependent hyperfine interactions are partially refocused. This is one way to overcome the broad and weak ESEEM signals that are difficult to resolve in disordered samples, such as frozen protein solutions. However, four-pulse technique is limited by the selection of the time τ, which influences the amplitude of the different harmonics in three- and four-pulse experiments different ways. As a consequence, some frequencies or ESEEM signals can be suppressed at a particular τ. In order to avoid the loss of some information, spectra can be recorded at several times for different τ values.

Another way to capture information without the blind spots in the detection method is to employ a two-dimensional ESEEM method or hyperfine sublevel correlation spectroscopy (HYSCORE). HYSCORE has equal spectral resolution in each dimension and its phase sensitivity. The advantage of the HYSCORE technique is the creation of two dimensional spectra with off-diagonal cross-peaks (ν_α, ν_β) and (ν_β, ν_α), whose coordinates are nuclear frequencies from opposite electron spin manifolds. For nuclei with I = ½, the model numerical simulations of contour line shape (i.e. the outline of the cross-peaks on a contour plot) in HYSCORE have been useful in characterizing the relative values of nuclear Zeeman and the

isotropic and anisotropic hyperfine interactions [63-64]. This approach has been effectively applied in characterizing ^{1}H nuclei involved in hyperfine interactions with the unpaired electron in frozen cyt aa_3-600 samples [65].

Hyperfine and nuclear quadrupole interactions

A hyperfine coupling between electron spin (S = ½) and a nucleus with nuclear spin value I consists of the isotropic contribution (A_{iso}) and the anisotropic contribution described by the dipolar coupling tensor (T). The isotropic component arises from the electron spin density at the nucleus and describes a Fermi contact interaction. The anisotropic component is produced by the interaction between an electron and nucleus acting as magnetic dipoles. Because anisotropic hyperfine interaction depends on the distance between electron and nucleus, it can provide information about their relative orientations.

$$T = \frac{\mu_o g_e g_n \beta_e \beta_n}{4\pi h r^3} \qquad (3)$$

where r is the distance between the nucleus and the electron and μ_o is the magnetic permeability constant. The full axial hyperfine interaction tensor has principal values (A_{iso} – T, A_{iso} – T, A_{iso} + 2T). The parameter A_{iso} of the nitrogen interacting with the SQ can be derived from X-band (~9.7 GHz) ^{14}N and ^{15}N ESEEM measurements, while the determination of T requires additional experiments (e.g. X-band ^{1}H ENDOR and ^{15}N matching condition in S-band ^{15}N ESEEM).

A ^{14}N nucleus (I = 1) has a quadrupole moment that interacts with the electric field gradient at the nucleus due to surrounding electrons. This interaction can be uniquely described by two parameters: 1) the ^{14}N nuclear quadrupole coupling constant (K) and 2) the asymmetry parameter (η). The K is a measure of the strength of the interaction between the nuclear quadrupole moment and the electric field gradient at the ^{14}N nucleus due to non-spherical charge distribution. The η is a measure of the deviation of the charge distribution from axial symmetry.

Both K and η are sensitive to atomic and chemical bond arrangements and are great probes for the identification of bonding geometry and of the chemical group.

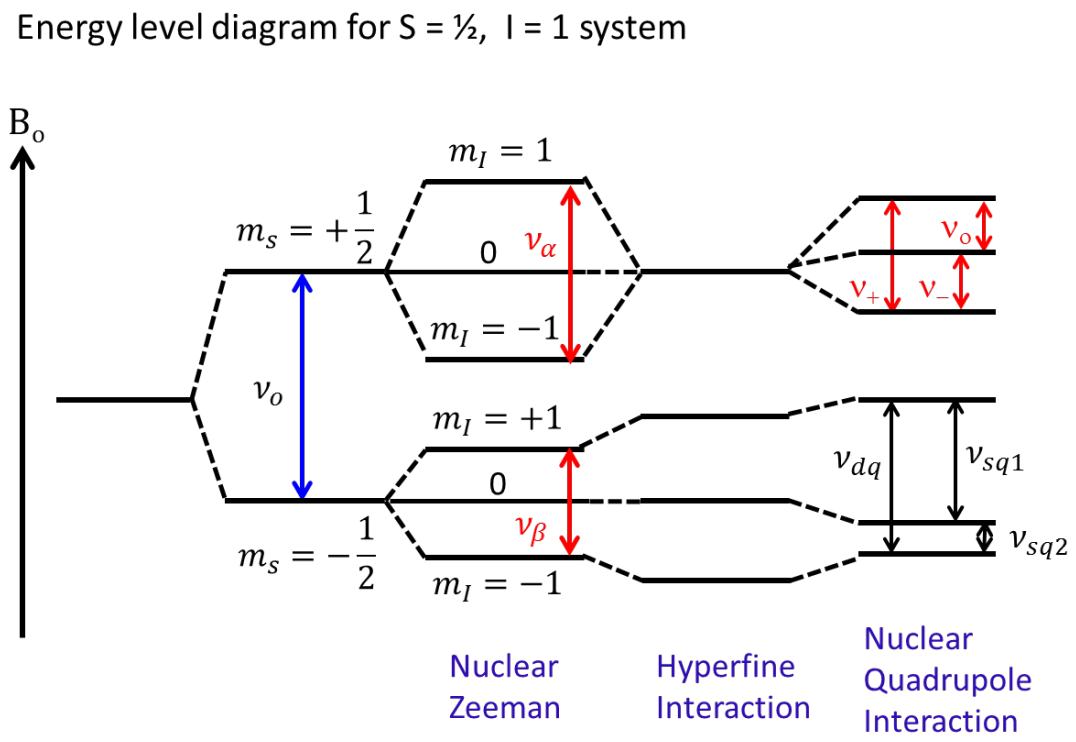

Figure 4.2. A simplified diagram displaying the energy level splitting in an external magnetic field of an unpaired electron (S=1/2) interacting with one ^{14}N (I = 1) nucleus in the region of exact cancellation. The nuclear Zeeman interaction and hyperfine interaction contributions cancel out and leaving behind only the fundamental nuclear quadrupole transition frequencies.

Identifying nitrogen atoms of different chemical groups by ^{14}N and ^{15}N ESEEM spectra

A ^{14}N nucleus has spin value of I = 1 and has quadrupole interactions due to non-spherical charge distribution in the system. Hence, the ^{14}N nucleus interacting with an unpaired electron spin (S = ½) can produce up to six lines in an ESEEM spectrum (see Figure 4.2). These lines are the nuclear transition frequencies from the three nuclear energy sublevels in each of the

two electron spin manifolds with $m_s = \pm ½$. Because of differences in orientation dependence, not all transitions contribute equally to the spectra in ESEEM measurements of power-type samples (e.g. frozen protein solution). The ESEEM spectrum expected from ^{14}N with a predominantly isotropic hyperfine coupling is determined by the ratio between the effective nuclear frequency in each manifold, $\nu_{ef\pm}$, and the quadrupole coupling constant, K.

$$\nu_{ef\pm} = \left| {}^{14}\nu_N \pm \frac{{}^{14}A}{2} \right| \qquad (4)$$

$$K = \frac{e^2 Qq}{4h} \qquad (5)$$

The ${}^{14}\nu_N$ and ${}^{14}A$ are the Zeeman frequency and hyperfine coupling of ^{14}N nucleus, respectively.

For $\frac{\nu_{ef\pm}}{K} \sim 0$ (i.e. ${}^{14}A \cong 2\nu_I$), the nuclear Zeeman and hyperfine splitting cancel in one electron spin manifold. Thus this situation is called the "cancellation condition," where the three nuclear frequencies from a corresponding manifold will be close to the three pure nuclear quadrupole resonance frequencies of ^{14}N (see Figure 2). In the case of exact cancellation, three sharp transitions (ν_+, ν_- and ν_o) are observable from one manifold, whereas only the broadened ν_{dq} is observed from the other manifold in the three-pulse ESEEM spectrum.

$$\nu_+ = K(3+\eta) \qquad \nu_- = K(3-\eta) \qquad \nu_o = 2K\eta \qquad (6)$$

These frequencies have the following relationship ($\nu_+ = \nu_- + \nu_o$). The ESEEM transitions are broadened as $\frac{\nu_{ef\pm}}{K}$ departs from 0 and thus, become difficult to resolve, but can appear in the spectrum up to a ratio of $\frac{\nu_{ef\pm}}{K} \sim 0.75 - 1$ [64-65].

If $\frac{\nu_{ef\pm}}{K} > 1$, only a single line is expected, without pronounced orientation dependence from each corresponding manifold. This line is produced by a transition at the maximum frequency, which is a double-quantum transition between the two nuclear outer states with m_I = -

1 and +1. The frequencies of double-quantum transitions in the powder spectra are described by the equation,

$$\nu_{dq\pm} = 2[\nu_{ef\pm}^2 + \kappa]^{1/2} \qquad (7)$$

where $\kappa = K^2(3 + \eta^2)$ and η is the asymmetry parameter. The two single quantum transitions usually do not show any resolved peaks because of significant orientation dependence from quadrupole interaction. In this case, an estimate of the hyperfine coupling with the ^{14}N nucleus can be obtained from the following formula,

$$^{14}A = [(\nu_{dq+})^2 - ((\nu_{dq-})^2]/8\nu_I \qquad (8)$$

where ^{14}N Zeeman frequency is $^{14}\nu_I$ = 1.066 MHz at X-band (~9.7 GHz). The values for double-quantum transitions can be ascertained directly from the HYSCORE spectrum. Then the estimated hyperfine coupling value, ^{14}A, calculated from this equation can be used to solve for effective nuclear frequency ($\nu_{ef\pm}$) and quadrupole coupling constant (K) by applying the relations shown in above equations.

For cyt aa_3-600, the ^{14}N cancellation condition is not satisfied, and the HYSCORE spectrum shows only cross-peak features whose coordinates correlate to two double-quantum transitions. For such situation, the relative strength of the hyperfine coupling and the Zeeman nuclear frequency can be varied by changing the frequency of the microwave radiation used for pulsed EPR experiments. One strategy is to reach the cancellation condition for ^{14}N nucleus (I = 1) for signal detection at S-band (~3.6 GHz) frequency.

For ^{15}N with nuclear spin value of I = ½ interacting with electron spin (I = ½), only two transitions with frequencies ν_α and ν_β are observed in the ESEEM spectrum, which correspond to two different spin states m_s = ±½. The frequencies depend on the vector sum of the applied magnetic field and the local magnetic field induced at the nucleus by the isotropic and

anisotropic hyperfine interactions with the electron spin. For I = ½, it has been shown that the relative magnitude of the hyperfine and nuclear Zeeman interactions determines the shape of the ESEEM spectra. In HYSCORE spectra of I = ½, the cross-ridges reveal the interdependence of ν_α and ν_β at a given orientation. Hence, analysis of the contours allows for direct, simultaneous determination of the nuclear isotropic and anisotropic hyperfine coupling constants [61]. For strong isotropic couplings, the two coordinates at the maximum intensity of the cross-ridge can be used for the first-order estimate of the hyperfine coupling by taking the difference of the nuclear transitions from opposite spin manifolds (i.e. ν_α - ν_β).

For frozen protein suspensions or powder spectrum, the frequencies of the ν_α and ν_β transitions span the range between

$$\nu_{\alpha(\beta)\perp} = \left|{}^{15}\nu_I \pm \frac{A_\perp}{2}\right| \quad \text{and} \quad \nu_{\alpha(\beta)\parallel} = \left|{}^{15}\nu_I \pm \frac{A_\parallel}{2}\right| \tag{9}$$

which correspond to the perpendicular and parallel orientations of the axial hyperfine interaction tensor, respectively. The ${}^{15}\nu_I$ is the Zeeman frequency of ${}^{15}N$ in the applied magnetic field.

$$A_\perp = |a - T| \quad \text{and} \quad A_\parallel = |a + 2T| \tag{10}$$

where A and T are the isotropic and anisotropic hyperfine coupling constants.

4.2. Materials and Methods

4.2.1. Generating semiquinone radical of cytochrome aa_3-600

The semiquinone was generated as described in Section 3.2.6.

4.2.2. Screening minimal medium growth conditions for *Bacillus subtilis*

Cells were grown in natural abundance of ${}^{14}N$ in Luria broth medium (LB) for unlabeled and deuterated samples. Initially, the M6 medium was tested for the *Bacillus subtilis (B.sub)*

growth and was found not to sustain a good cell density even with three additional supplementations (i.e. thiamine, $CuSO_4$ and glucose) which were shown to support a high cell density in the expression of *E. coli* cyt bo_3. Therefore, other medium formulas were considered. Overnight 50 mL-culture prepared with Cap assay minimal medium gave low growth with OD_{600} = 0.36. Spizizen-based medium with glucose, 5-fold concentrated Luria broth medium and casamino acid supplementations with starting inoculation of cultures at 1% and 5% of 500 mL medium gave respective optical density (OD_{600}) values: 0.202 and 0.521 for 6 hours of growth (see Section 2.2.4). Adding 100x sporulation mixture (i.e. trace elements) to the same medium-based culture with inoculation of cell density at 5% and 7.5% of 500 mL medium gave corresponding OD_{600} of 1.56 and 1.52 for 7 hours of growth.

M63 minimal medium per Liter:

K_2HPO_4	3 g
KH_2PO_4	7 g
NH_4Cl	2 g
$FeSO_4$	8.3 mg
100 mg/L Thiamine	500 μL
1 M $CuSO_4$	50 μL
1 M Glucose	6 mL

Cap assay minimal medium per Liter:

50 mM Phosphate, pH 7	
K_2HPO_4	7 g
KH_2PO_4	3 g
1 mM MgCl2 (MW: 203)	0.2 g
1 mM NH_4SO_4 (MW: 132)	0.1 g
1:1000 sporulation salts	
*autoclaved	

Table 4.1: Screening Spizizen-based minimal medium growth conditions with different supplemental additions of either thiamine and/or concentrated Luria broth medium*

Spizizen Supplements	**0**	**1**	**2**	**3**
Trace elements (1/10000)	Added	Added	Added	Added
20 % Casamino acid (100 μL/100 mL)	Added	Added	Added	Added
5 mg/mL Tryptophan (1 mL/100 mL)	Added	Added	Added	Added
1M Glucose (2.8 mL/100 mL)	Added	Added	Added	Added
10 mg/mL Thiamine (100 μL/100 mL)	---	Added	Added	Added
5X LB medium	---	---	0.2 %	0.4 %
OD_{600} *(14-hour Growth)*	1.9	1.9	0.3	0.3

*The cultures grown in minimal medium of Spizizen-based salts (see Section 2.2.4) for 30 mL cultures. The supplemental additions were made in small volumes that resulted in less than 0.5 mL aliquots. The added amount of each supplement was based on protocol in section 2.2.4. Each growth condition was labeled 0, 1, 2 or 3. 5X LB medium is a five-fold concentrated preparation involving the general Luria broth protocol and was sterilized by either autoclaving or filtering with 0.44 μm membrane. These cultures were monitored for optical cell density of cultures at 600 nm at the 14th hour of growth.

Table 4.2: Screening Spizizen-based minimal medium growth conditions with additions of various supplements*

Spizizen Supplements	**0**	**1**	**2**	**3**
Trace elements (1/10000)	Added	Added	Added	Added
20 % Casamino acid (100 μL/100 mL)	Added	Added	Added	Added
5 mg/mL Tryptophan (1 mL/100 mL)	Added	---	Added	Added
1M Glucose (2.8 mL/100 mL)	Added	Added	Added	Added
10 mg/mL Thiamine (100 μL/100 mL)	---	Added	Added	---
5X LB medium	---	---	---	Added
OD_{600} *(10-hour Growth)*	1.3	0.2	1.3	1.5
OD_{600} *(13-hour Growth)*	2.3	0.2	2	0.3

*See notes under Table 4.1. The cultures were monitored over time that resulted in two time-point observations: 10th hour and 13th hour of growth for defined culture conditions 0, 1, 2 or 3. These cultures were monitored for optical cell density of cultures at 600 nm at various time-points.

Table 4.3: Screening Spizizen-based minimal medium growth conditions with different supplemental additions of either thiamine and concentrated Luria broth medium or only the concentrated Luria broth medium as supplement, while concomitantly varying the glucose concentrations (i.e. 1%, 2% or 3%)*

500 mL Culture	**0** *(OD_{600})*			**2** *(OD_{600})*		
Time points of growth** *(Hours)*	**1 %**	**2%**	**3 %**	**1%**	**2%**	**3%**
4	0.6	0.8	0.9	0.7	0.8	0.9
6	1.1	1.6	1.7	1.2	1.3	1.6
10	2.3	2.1	2.1	2.1	2.3	2.3
11	1.9	---	---	1.7	---	---

*The two defined culture conditions (i.e. labeled 0 and 2) from Table 4.2 were further examined for growth response at three different concentrations of glucose (i.e. 1%, 2% or 3%). ** These cultures were monitored for optical cell density of cultures at 600 nm at various time-points (i.e. 4, 6, 10 and 11th hour of growth). Culture labeled '0' was grown in the absence of thiamine and 5-fold concentrated Luria broth medium based supplement; culture labeled '2' was grown in the presence of thiamine only.

4.2.3. Isotopic labeling of cytochrome aa_3-600 with $^{15}NH_4Cl$

Isotopically labeled samples were prepared from purified proteins grown in minimal medium with Spizizen salts, supplemented with 1 g of NH_4Cl (^{15}N, 99%) per 500 mL (Cambridge Isotope, Andover, MA). Culture was grown in 500 mL of minimal medium in 2-L beveled culture flask, and the following components were added to achieve high cell density: 300 μL of 20 % casamino acids, 10 mL of 50% glucose (weight/volume), 4 mL of 5 mg/mL tryptophan, and 4 mL of 100x trace metals [49, 104]. Each culture flask was inoculated with 4 mL of overnight subculture (37 ˚C), was induced with 4 mL 50 % glycerol (volume/volume) at the start of incubation with shaking, and was grown slowly for 11 hours at 37 ˚C. The protein expression level declined in cultures grown in minimal medium in comparison to those prepared in LB, and generally 6-L of culture was required to prepare an isotopically labeled EPR sample.

4.2.4. Continuous wave (cw) X-band spectroscopy

The samples containing semiquinone radical were examined at microwave frequency of 9.7 GHz at optimized power of 30 mW. The signal amplitude generally increases with power, but declines as the power saturation is reached, where the resonance line becomes distorted and broadens. For most quinone radicals, power range of 20-40 mW produces acceptable signal strength, and power level of 30 mW was selected for consistency. Although the modulation amplitude of 2–5 G was tested for samples, a lower value of 2 G was the preferred instrument setting, because signal's unresolved hyperfine structure, originating from the 2-methyl protons of the quinone head group, was more pronounced. A higher level of modulation amplitude gave larger signal intensity, but resolved the signal poorly because it exceeded the line width of the

signal. The best signal-to-noise ratio was achieved for samples containing semiquinone radical at temperatures between 70 –110 K with liquid nitrogen.

EPR spectral scan is observed as a first-derivative spectrum rather than as an absorption trace, due to additional modulation of the signal. In addition to phase sensitive detector, the magnetic field is modulated with a small set of Helmholtz coils around the sample to enhance the sensitivity of the EPR spectrometer. The changes amount to 0.01 – 20 G modifications at a frequency of 100 kHz. The signal is observed when changes in amplitude accompany changes in the magnetic field.

4.2.5. Pulsed EPR experiments (ESEEM and HYSCORE)

The pulsed EPR experiments were carried out using an X-band Bruker ELEXSYS E580 spectrometer equipped with Oxford CF 935 cryostats. Several types of experiments with different pulse sequences were employed with appropriate phase-cycling schemes to eliminate unwanted features from the experimental echo envelopes. Among these experiments were one- and two-dimensional three-pulse and four-pulse sequences [52]. Spectral processing of three- and four-pulse ESEEM patterns was performed using Bruker WIN-EPR software, including subtraction of the relaxation decay (fitting by 3-6 degree polynomials), apodization (Hamming window), zero filling, and fast Fourier transformation. Pulsed electron-nuclear double resonance spectroscopy (ENDOR) spectra of the radicals were obtained using Davies and Mims sequences with different pulse lengths. The specifics of these experiments are described in [47, 56].

The contour line shape in the powder 2-dimensional (2D) spectrum from the ^{1}H atom having nuclear spin I = ½ and the Zeeman frequency ν_I for axial hyperfine interactions was described in detail by Samoilova et al. [66] and elsewhere [46-47, 61-62]. The analysis of

HYSCORE spectra for nitrogen atoms interacting with the protein stabilized SQ has been previously described by others [64, 47, 67] and is briefly discussed in Section 4.1.2.

4.3. Results and Discussion

4.3.1. Screening for minimal medium growth condition for *B. subtilis*

Various minimal medium conditions were examined for culture growth. The spizizen-based minimal medium showed the most potential to sustain a strong cell growth in the presence of trace elements and in the absence of 5-fold concentrated Luria broth medium based supplement (5X LB), compared to other media (see Table 4.1) [49]. Since the standard medium formula required adding supplements that could interfere with isotopic labelling, the growth condition was screened systematically and modified to remove components that did not impact cell growth negatively. For instance, thiamine and 5X LB supplemental addition were not necessary for growth, but casamino acid was required to achieve a necessary cell density (see Table 4.2). The supplemental components made up a small contribution to the overall culture volume and did not contribute to ^{14}N contamination in uniformly ^{15}N labelled samples, determined by 2D-ESEEM spectra.

4.3.2. CW EPR spectrum of semiquinone stabilized by cyt aa_3-600

The semiquinone (SQ) in cyt aa_3-600 produces X-band EPR spectrum containing a single feature with g value of 2.0047 ± 0.0001. As shown in Figure 4.3A, the spectra display partially resolved hyperfine structure consisting of four components with approximate relative intensities 1:3:3:1 and a splitting of ~12 MHz. This EPR signal is tentatively assigned to three equivalent non-exchangeable protons interacting with the unpaired electron, originating from the methyl

substituent of the quinone ring. Q-band spectrum, measured at higher microwave (mw) field frequency (~35 GHz), resolves the g-tensor anisotropy with components g_{xx} = 2.00642, g_{yy} = 2.0054, g_{zz} = 2.00228 (see Figure 4.3B). Additional hyperfine structure is present near g_{yy} field position that is not completely resolved. Experiments at microwave frequencies ~95 GHz (W-band) or higher could provide better analysis.

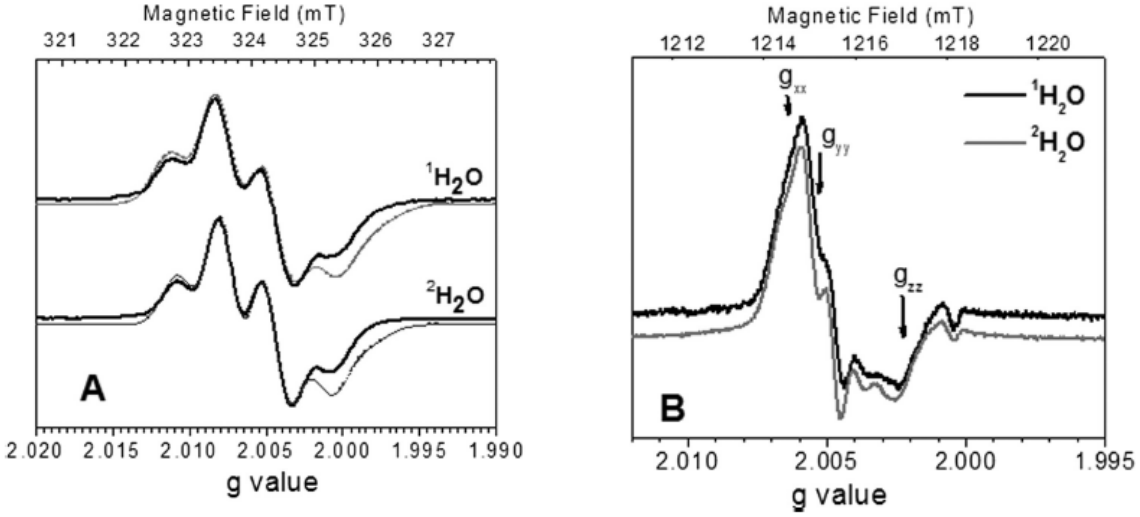

Figure 4.3. A, X-band EPR spectra of SQ in cyt aa_3-600 in ^1H_2O and ^2H_2O. EPR instrument parameters were: modulation amplitude (MA), 0.16 mT; microwave (mw) power, 40 dB (20 mW); mw frequency, 9.087 GHz; temperature, 105 K. The grey lines correspond to the simulated spectra. The simulated spectra were obtained with components of the g-tensor, determined from Q-band spectra and isotropic hyperfine coupling 0.49 mT with three equivalent protons. **B**, Q-band EPR spectra of SQ in cyt aa_3-600 in ^1H_2O and ^2H_2O. EPR instrument parameters were: MA, 0.3 mT; microwave (mw) power, 5.3 mW; mw frequency, 34.106 GHz; temperature, 90 K. 2, 2-diphenyl-1-picrylhydrazyl with g-value of 2.00351 was used as field marker. *Arrows* indicate magnetic field positions used for the determination of the g-tensor principal values.

4.3.3. Nitrogens interacting with the SQ

An unambiguous assignment of nitrogens interacting with the SQ was made from HYSCORE and three-pulse ESEEM experiments. These experiments were performed with wild type cyt aa_3-600 containing natural abundance of ^{14}N (99.16%) and with uniformly ^{15}N-labelled protein. From the ^{14}N HYSCORE powder spectrum of the SQ, the major cross peaks 1

correlated two double-quantum transitions $\upsilon_{dq+} = 4.5\ MHz$ and $\upsilon_{dq-} = 3.5\ MHz$ from opposite m_s manifolds of the ^{14}N nucleus (see Figure 4.4). These had intensities that significantly exceeded other minor features that appear in the area of peaks 2-4 in the experimental spectrum. These nuclear transitions also possess low orientation dependence and produce the most intensive cross-peaks in the HYSCORE spectra.

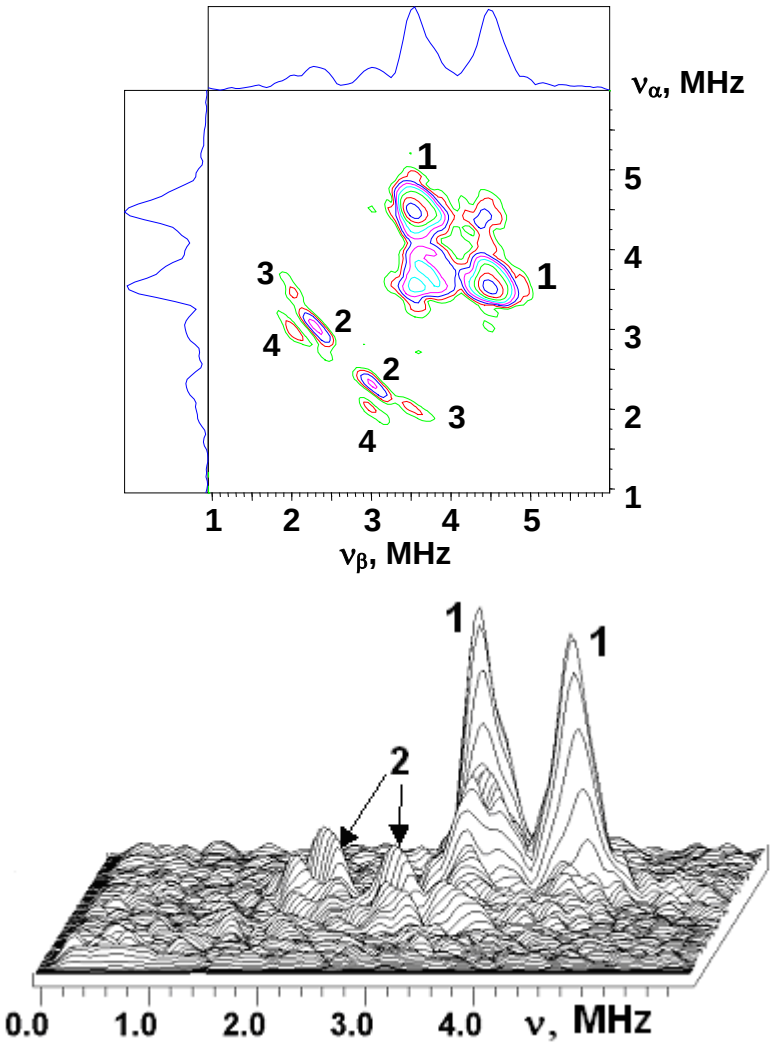

Figure 4.4. ^{14}N HYSCORE spectrum of the semiquinone (SQ) at the Q_h-site of cyt aa_3-600 in contour (top) and 3D-stacked presentations (bottom). EPR instrument parameters were: magnetic field, 346.4 mT; time between first and second pulses, τ = 136 ns; mw frequency, 9.713 GHz.

However, the hyperfine coupling of major cross peaks 1 does not satisfy the cancellation condition that prevented an immediate assignment of the three pure (zero-field) nuclear quadrupole resonance frequencies with ^{14}N transition from three-pulse ESEEM spectra. Hence, equations from section 4.1.2 were applied to estimate EPR parameters that characterize nitrogen interacting with the SQ. Initially, a hyperfine coupling ^{14}A = 0.94 MHz was estimated from the frequencies of double-quantum transitions defined by cross peaks 1 in HYSCORE spectra using Eq. 8. The shape of these nuclear transitions in three-pulse and HYSCORE spectra indicated that the isotropic constant provides the major contribution to the hyperfine coupling. Using this estimated value of ^{14}A, a quadrupole coupling constant (qcc) K = 0.82 – 0.95 MHz was determined from Eq. 7 for substituted values of η, asymmetry parameter, from 0 to 1.

Knowing the quadrupole coupling constant (qcc) of the ^{14}N atoms is quite useful because range of values have been attributed to different chemical groups. This assignment can be used for identification of the nitrogen and characterization of the hydrogen bond to the SQ. The quadrupole coupling constant, K = 0.82 – 0.95 MHz, determined above is consistent with the qcc of ~0.9 – 1.0 MHz of nitrogens from the NH and NH_2 groups in primary aliphatic and aromatic amines and amides [46]. This effectively ruled out histidine as a hydrogen bond partner to the SQ of cyt aa_3-600. However, nitrogen from arginine side chain could participate in the interaction, based on selective isotope ^{15}N labeling study of cyt bo_3, which shares high sequence similarity with cyt aa_3-600. The arginine N_ε in the Q_h-site of *E. coli* cyt bo_3 was determined to have qcc of 0.93 MHz (κ = 2.82 MHz^2) and gave rise to the nitrogen possessing the largest hyperfine coupling [52]. The close coincidence of the quadrupole parameters (κ) suggested that the N_ε of Arg-70 in cyt aa_3-600 (κ = 2.7 MHz^2) is also a primary candidate for the role of the

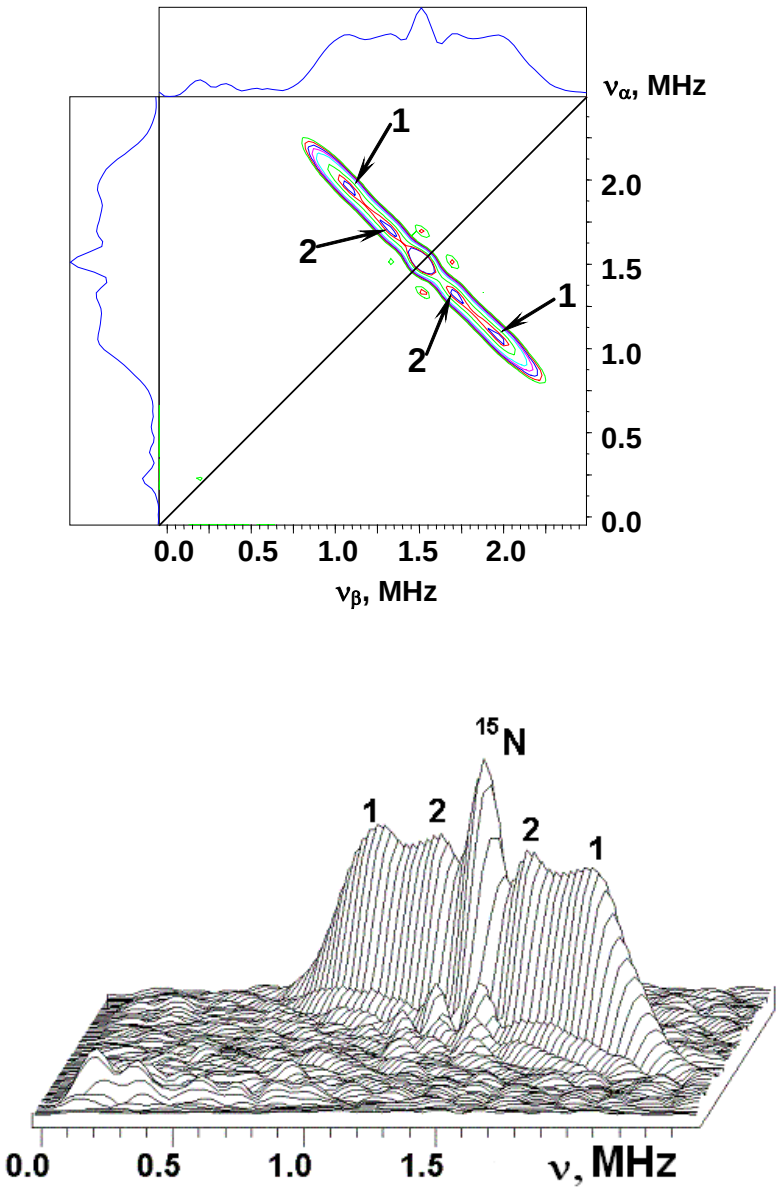

Figure 4.5. ^{15}N HYSCORE spectrum of the semiquinone (SQ) at the Q_h site of cyt aa_3-600 in contour (top) and 3D-stacked presentations (bottom). EPR instrument parameters were: magnetic field, 346.1 mT; τ = 136 ns; mw frequency, 9.706 GHz.

nitrogen carrying the largest unpaired spin density and thus, involved in H-bond formation with the SQ.

The ^{15}N nucleus is a spin ½ system and does not possess the nuclear quadrupole moment that affects the ^{14}N ESEEM spectra and that masks certain signals. Because of the absence of nuclear quadrupole contribution in the spectra, ^{15}N labelled protein offers an advantage in being able to observe all of the nitrogens that magnetically interact with the unpaired electron spin of the SQ. In particular, this method gave an opportunity for an alternative view of weakly coupled nitrogens indicated by cross peaks 2-3 in ^{14}N HYSCORE spectrum. An estimated values of the ^{14}A ~ 0.4 - 0.6 MHz and quadrupole coupling constant (qcc) K = 0.36 - 0.6 MHz suggested cross peaks 2 from ^{14}N HYSCORE spectrum originated from nitrogen of histidine sidechain. This nitrogen could belong to His98 residue in close proximity to one of the quinone carbonyl groups.

The ^{15}N line-shape in the HYSCORE spectra of cyt aa_3-600 showed an extended contour with the shoulders extending ~1.5 MHz (see Figure 4.5). This was consistent with a nitrogen hyperfine coupling of ^{15}A ~1.26 MHz recalculated from ^{14}A ~0.94 MHz, although even the largest resolved coupling, ^{15}A ~ 0.96 MHz for peaks 1 was significantly smaller than this value. Two factors could explain this difference. First, the positions of line maxima in powder spectra for the double-quantum transitions of ^{14}N and single-quantum transitions of ^{15}N, used to estimate ^{14}A and ^{15}A, were determined by different factors. This resulted in effectively different couplings in the presence of the anisotropic contribution to the hyperfine coupling. The difference would be greater as the anisotropic hyperfine interaction (hfi) gets larger. Second, because the total length of the ^{15}N resonance line exceeded typical values of the anisotropic hyperfine interaction for protein nitrogens interacting with a SQ [69], it was likely that the

extended ^{15}N line-shape in the HYSCORE spectra with two resolved splittings was formed by the spectra from several, probably more than two, nitrogens possessing partially overlapped intervals of nuclear frequencies and thus, producing an extended resonance contour. Overlap of the spectra from different nuclei could produce the resolved maxima at the new frequencies, shifted from the frequency of the maximum intensity in the individual spectrum of each of the contributing nitrogen.

Further work is needed to clarify the situation, utilizing ^{15}N-selective labeling to characterize the individual isotropic and anisotropic hyperfine couplings with the side chain and peptide nitrogens of different residues. In addition, pulsed EPR experiments at lower microwave frequencies (3-4 MHz; S-band EPR) could better satisfy the cancellation condition for the ^{14}A couplings and, therefore, allow for an accurate determination of the nuclear quadrupole tensors of the ^{14}N nuclei [68]. Thus far, an attempt at S-band EPR experiment was unsatisfactory because the EPR signal intensity was still very weak even with three-fold increase in the SQ signal intensity of the protein sample.

4.3.4. Non-exchangeable protons associated with the semiquinone (SQ) signal

The hyperfine structure, previously observed on CW X-band EPR spectrum of the SQ, corresponded to the quinone ring methyl protons, which was substantiated by data analysis of ^{1}H and ^{2}H HYSCORE spectra. The 2-dimensional ^{1}H spectra contained several pairs of resolved cross-features located symmetrically relative to the diagonal. Among the proton cross-features, the cross-peaks labeled 1 demonstrated the largest hyperfine splitting, a = ~11 MHz (i.e. ^{1}H isotropic hyperfine coupling constant), and were not affected when the sample was prepared in $^{2}H_2O$ buffer (see Figures 4 and 5).

This appreciably large isotropic constant for the non-exchangeable protons was larger than expected compared to anion radical in organic solvents. The naphthoquinone derived compounds in organic solvents gave lower values (7 to 7.9 MHz) for isotropic hyperfine coupling than those associated with protein in the A_1 center of the photosystem I [71-73] and in the Q_h-site of cyt bo_3 (where ubiquinone was replaced with phylloquinone) [73]. This difference could be caused by protein structure, leading to a significant redistribution of the unpaired spin density. The proton isotropic constant in the rotating methyl group is directly proportional to the π-spin density on the attached carbon atom and is described by the McConnell relation, $a = 81\rho_\pi$ [74]. Therefore, the larger isotropic constant observed for cyt aa_3-600 can be related to 1.5-fold to 2-fold larger unpaired π-spin density on the carbon attached to the quinone methyl group, when compared with anionic SQ radicals in solution. One of the resonance structures of the SQ that allows for a higher π-spin density at the quinone methyl group predicts a strong hydrogen bonding at carbonyl O1 (ubiquinone numbering is used), adjacent to the isoprenyl group on the quinone ring, instead of carbonyl O4 (see Figure 4.8).

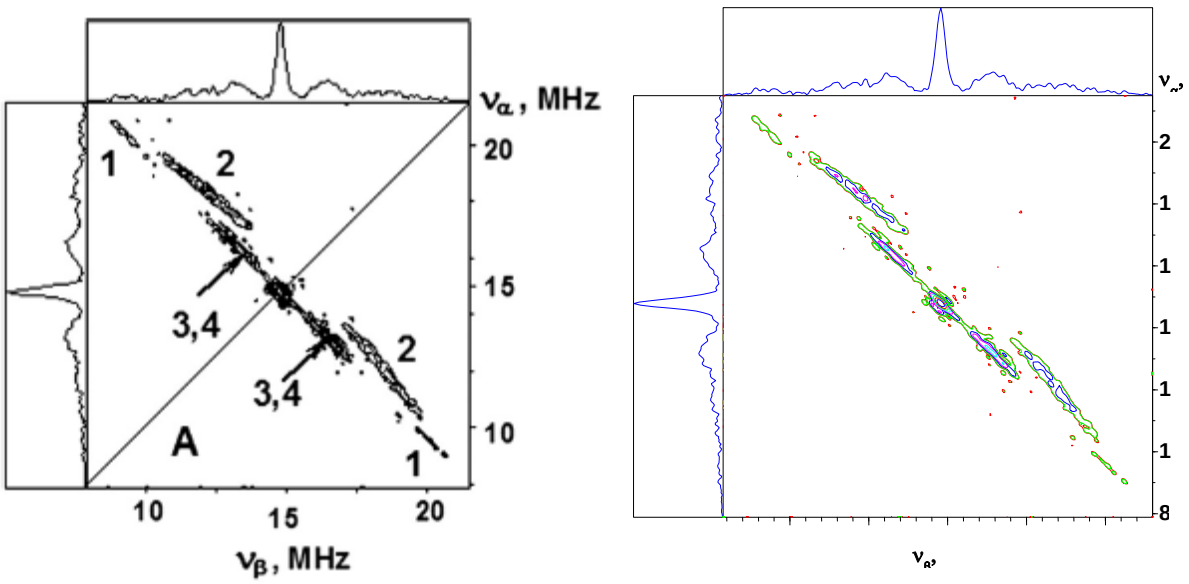

Figure 4.6. Contour presentation of ^{1}H HYSCORE spectrum of the semiquinone (SQ) at the Q_h-site of cyt aa_3-600 in $^{1}H_2O$. EPR parameters were: magnetic field, 346.4 mT; τ = 136 ns with 20-ns stepwise increases; mw frequency, 9.713 GHz. Both spectra (left and right) were produced from the same sample.

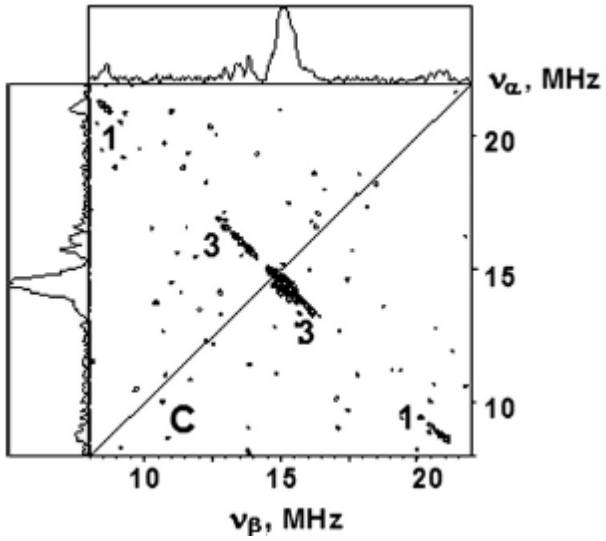

Figure 4.7. Contour presentation of ^{2}H HYSCORE spectrum of the semiquinone at the Q_h-site of cyt aa_3-600 in $^{2}H_2O$. The sample condition and the EPR parameters were the same as those used to perform experiments in Figure 4.6.

The differences in hyperfine couplings between anion radicals in alcohol solutions and SQ radicals in proteins are striking and suggested an asymmetry of hydrogen bonding with the carbonyl oxygens of the SQ in the proteins. This leads to a redistribution of both the spin density and charges within the quinone ring. The couplings for the SQ in cyt aa_3-600 can be explained by a stronger hydrogen bond between the protein surroundings and oxygen O1 (i.e. ubiquinone numbering), compared with O4. The bound oxygen O1, adjacent to isoprenyl group, possessed a larger negative charge to stabilize the interaction with the proton participating in this strong H-bond, and thus, the spin density is partly shifted within the SQ [72, 75]. The result was an increase of the unpaired spin density at C2, which increased the isotropic coupling of the methyl group protons. The evidence for an asymmetry in H-bonding was further supported by exchangeable proton interactions with the SQ in cyt aa_3-600.

4.3.5. Exchangeable protons in close proximity to the semiquinone (SQ)

Two exchangeable protons with distinct differences in the proton hyperfine couplings were determined from ^{1}H and ^{2}H HYSCORE spectra, as cross peaks 2 and 4 (see Figures 4.6 and 4.7). Remarkably, both cross peaks 2 and 4 disappeared from ^{2}H HYSCORE spectrum prepared from sample in ^2H_2O, indicating that these protons freely interact with the solution. Cross peaks 2 possessed the most extended anisotropic contour, with the largest deviation from the diagonal indicating a significant anisotropic hyperfine component. This proton possessed anisotropic hyperfine coupling of |T| ~5.6 MHz, and the cross peaks 4 was determined to have coupling of 2.9 MHz. These anisotropic hyperfine couplings could be correlated with the strength of hydrogen bond interaction with the carbonyl groups of SQ. For the hyperfine coupling of |T| ~2.9 MHz a point-dipole-model estimated a H-bond length of ~ 1.8 Å. This approximation was

consistent with the results of density functional theory calculations (DFT), which also indicated a planar hydrogen bond that forms ~60° angle with a carbonyl group [76].

On the other hand, the exchangeable proton with much larger anisotropic hyperfine coupling |T| ~5.6 Å was likely to participate in a stronger H-bonding to the SQ of cyt aa_3-600. For instance, the point-dipole estimate led to the O…H distance of 1.32 Å for one H-bonded proton (T = 5.2 MHz) from Q_A-site SQ in the photosynthetic reaction center that is functionally similar to Q_h-site of cyt aa_3-600 [77]. According to DFT calculations [76], a hydrogen bond with planar geometry with anisotropic coupling of T ~5.2 MHz would require an O…H bond length of ~1.4 Å. Applying the same rationale, a planar H-bond with a value of T = 5.6 MHz, found in the current work, would correspond to even shorter O…H distance.

The DFT calculations also predict the H-bond involving the proton with |T| ~5.6 Å in cyt aa_3-600 to a significantly out-of-plane geometry with respect to the SQ ring [78]. This deviation of the H-bond out of the SQ plane could be attributed to simultaneous increase of both the isotropic and anisotropic couplings of the H-bonded proton [71]. Indeed, analysis of the proton cross-peak contours in the HYSCORE spectrum showed that the exchangeable proton observed in the SQ of cyt aa_3-600 with |T| ~5.6 Å has one of two possible values for isotropic constant that is quite large, |a| = 5.4 MHz. The simulations of the HYSCORE spectra and locations of the line assigned to $A_\perp$, axial perpendicular tensor component of hyperfine interaction, in the ENDOR spectrum of exchangeable protons support the solution with the unusually large isotropic constant and hence, out-of-plane geometry for the H-bond [63]. Hence, the results indicated that this stronger H-bond is likely to be forced by geometric constraints to be either above or below the ring plane.

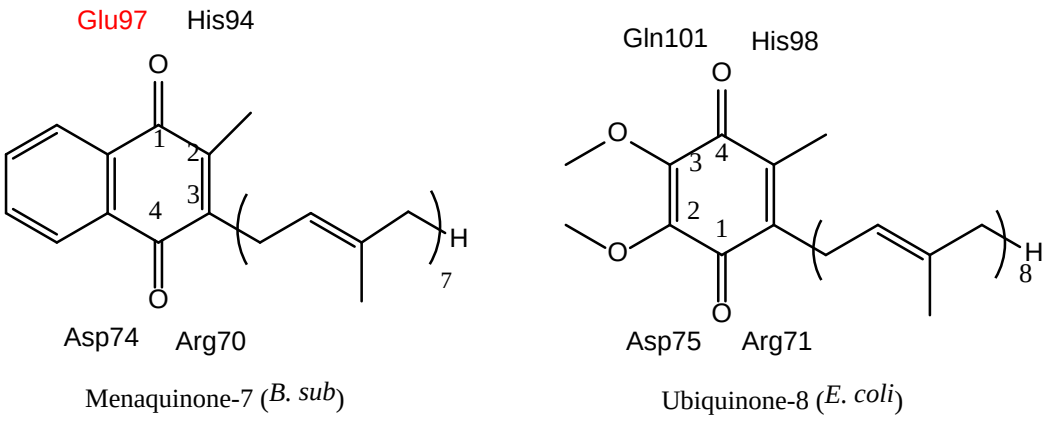

Figure 4.8. Chemical structures for menaquinone (MQ-7) and ubiquinone (UQ-8). The ubiquinone numbering is used throughout the text to refer to corresponding carbonyl positions in menaquinone for ease of comparison. MQ-7 is natural product made by *Bacillus subtilis* that has a hydrophobic tail with seven isoprenyl groups. UQ-8 is natural product made by *Escherichia coli* and has hydrophobic tail consisted of eight isoprenyl groups.

The combined results of proton hyperfine coupling interactions fits a molecular model where asymmetric H-bonding occurs with the quinone carbonyl groups. The observation of two exchangeable protons and evidence of redistribution of the spin density and charges within the quinone ring that favors negative charge at carbonyl O1 (i.e. using ubiquinone numbering) suggest two H-bonds forming with O1. Among the highly conserved residues present at the Q_h-site, Arg70 and Asp74 can potentially form H-bonds with the SQ radical at carbonyl O4 position. The issue of H-bonds being formed as either single-sided (2-0) or double-sided model (2-1) is unresolved, but both the DFT calculations of cyt bo_3 and the experimental results agree on the existence of asymmetry of H-bonding to SQ [79-80].

4.4. Conclusions

This ESEEM study reveals the existence of at least two protein nitrogens coupled to the SQ and carrying the unpaired spin density. This is reflected in the ^{15}N 2D spectrum of the SQ in cyt aa_3-600 showing a poorly resolved line-shape. The largest coupling estimated from the ^{14}N

HYSCORE spectrum is 0.9 MHz and can be tentatively assigned to the N_ε of Arg-70 based on the quadrupole parameter, $K^2(3+\eta^2)$. In the ^{15}N spectrum the largest resolved coupling, ^{15}A, is ~0.95 MHz. This corresponds to a coupling ^{14}A of only ~0.7 MHz, indicating an overlap of the spectra from at least two nitrogens, presumably from Arg-70 and His-94. It is possible that in cyt aa_3-600 there is more spin density transferred to the nitrogens of His-94 than to the corresponding His-98 in cyt bo_3. The mechanism of the transfer of unpaired spin density to His-98 in cyt bo_3 or to His-94 in cyt aa_3-600 is not clear. The nitrogen coupling data indicate a significant difference in the protein interactions with the SQs in cyt bo_3 and cyt aa_3-600. The spin density transfer to the Q_h-site arginine from oxygen O1 appears to be substantially weaker in cyt aa_3-600, and the interaction of the histidine with oxygen O4 may be greater.

Overall, the nitrogen and proton hyperfine interaction data indicate weaker hydrogen bonding of the menaquinone SQ in cyt aa_3-600 in comparison with the ubiquinone SQ in cyt bo_3. In addition, the electronic structure of the SQ in cyt aa_3-600 has more anionic character compared with the neutral SQ state in cyt bo_3.

CHAPTER 5: Surveying the Substrate Interaction of Cytochrome aa_3-600 and High Affinity Quinone Binding Site (Q_h-site) Mutants

5.1. Introduction

The protein-quinone interaction is not well characterized, especially among the heme-copper oxygen reductases that rely on substrate quinols. The cytochrome (cyt) aa_3-600 accepts electrons from menaquinol. The electron flow into cyt aa_3-600 has been poorly understood largely due to uncertainty surrounding the number and location of quinone binding sites and lack of structural data. In Chapter 4, first such attempt to improve the understanding of quinone reactive sites led to molecular level details of menaquinone semiquinone (SQ) stabilized by quinone binding site (Q_h) using advanced EPR methods. This quinone is assumed to be closely associated with cyt aa_3-600 even after the purification step and has shown similar binding characteristics as SQ stabilized by *E. coli* cyt bo_3. The quinone at the Q_h-site is considered to mediate electron transfer from the quinol oxidation site to low-spin heme A (which is heme B in cyt bo_3), which directs electrons to heme-copper binuclear center for oxygen reduction. However, this view is challenged by the specific activity data presented here, which indicate that quinol oxidation occurs at the Q_h-site.

Previously, reports gave conflicting figures for cyt aa_3-600 activity because of different protein isolation protocols and assay conditions. Nevertheless, the steady-state activity was shown to be affected by the redox potential of the analogue, showing greater activity with more reducing substrate [29, 39]. In addition, cyt aa_3-600 activity demonstrated sensitivity to 2-n-Heptyl-4-hydroxyquinoline N-oxide (HQNO) (see Figure 5.3) at equimolar amounts; whereas, other inhibitors such as myxothiazol, antimycin A, stigmatellin were not as effective in diminishing quinol activity when dimethyl naphthoquinone (DMN) was the electron donor. In this chapter, the quinol activity of cyt aa_3-600 is highlighted with biochemical approaches,

including observation of response to various substrates, site-specific mutations and inhibitors. Both quinol oxidation and the oxygen uptake by cyt aa_3-600 are monitored for consistency between the two methods. Mutations are introduced at the Q_h-site that are highly conserved residues among the quinol oxidases and have functional consequence in quinol oxidation reaction.

5.2. Materials and methods

5.2.1. Site-directed mutagenesis in cyt aa_3-600 at the high-affinity menaquinone binding site

The forward primer 5'- GCTGTAATTATGTTATTC**CAT**GGCGGTGTCGACGGTC-3' and the reverse primer 5'-GACCGTCGACACCGCC**ATG**GAATAACATAATTACAGC-3' were used to replace R70 with His. The single amino acid mutation reactions were performed with QuikChange XL Site-Directed Mutagenesis Kit (Agilent, Santa Clara, CA) using the expression plasmid pLala carrying genetic information of cyt aa_3-600 as the template DNA. The resulting polymerase chain reaction (PCR) reaction was initially treated with DPN I (from NEB) to digest parent dsDNA and then transformed into *E. coli* XL1B electrocompetent cells. XL10-Gold ultracompetent cells, which are included in the QuikChange Kit, are not appropriate for transformation because this strain does not allow selection by chloramphenicol. The new recombinant plasmid with desired amino acid mutation was verified by DNA sequencing (UIUC Core Sequencing, Urbana, IL). Next, these new recombinant plasmids were transformed into *Bacillus subtilis (B. sub)* LUW143 strain, whose competent cells were prepared by a protocol involving a medium formula with Spizizen salts, 20% casamino acids, 5-fold concentrated Luria broth medium based supplement (5X LB), 50% glucose, 5mg/mL tryptophan (Trp). Subsequently, resulting colonies were checked for correct single mutations in *B. sub* by DNA

sequencing. This latter step required disruption of cell pellets with 2 mg/mL lysozyme (Sigma, St. Louis, MO), which was followed by isolation of plasmids with the Qiagen Mini-prep Kit (Qiagen, Valencia, CA).

Table 5.1: Primers used to introduce single amino acid mutation to cytochrome aa_3-600 at the high affinity quinone binding site (Q_h-site)[*]

Mutation	Primer Sequence
R70H	5'-GCTGTAATTATGTTATTC**CAT**GGCGGTGTCGACGGTC
	5'-GACCGTCGACACCGCC**ATG**GAATAACATAATTACAGC
R70Q	5'-GCTGTAATTATGTTATTC**CAA**GGCGGTGTCGACGGTC
	5'-GACCGTCGACACCGCC**TTG**GAATAACATAATTACAGC
D74H	5'-GTGGCGGTGTC**CAC**GGTCTGATGATGC
	5'-GCATCATCAGACC**GTG**GACACCGCCAC
D74N	5'-GTGGCGGTGTC**AAC**GGTCTGATGATGC
	5'-GCATCATCAGACC**GTT**GACACCGCCAC
H94F	5'- GCGCTTCCGAATAACAGTTTTTTAGACTCAAAC**TTC**TATAATG
	5'- CATTATA**GAA**GTTTGAGTCTAAAAAACTGTTATTCGGAAGCGC
H94D	5'-GCGCTTCCGAATAACAGTTTTTTAGACTCAAAC**GAC**TATAATG
	5'-CATTATA**GTC**GTTTGAGTCTAAAAAACTGTTATTCGGAAGCGC
E97Q	5'-GACTCAAACCACTATAAT**CAA**ATTTTTACAACTCACGGTAC
	5'-GTACCGTGAGTTGTAAAAAT**TTG**ATTATAGTGGTTTGAGTC
I98M	5'-GACTCAAACCACTATAATGAA**ATG**TTTACAACTCACGGTAC
	5'-GTACCGTGAGTTGTAAA**CAT**TTCATTATAGTGGTTTGAGTC
$R71H_{bo3}$	5'-CGATTGT GATGTTGCTG **CAT**GGTTTTG CTGACGC
	5'-GCGTCAGCAAAACC**ATG**CAGCAACATCACAATCG

[*] The substituted codon is indicated by bold-face and is underlined. Each primer set for each mutation consists of a forward primer and the reverse primer that align exactly with the desired regions of the genetic operon of cytochrome aa_3-600. These mutants are located at the high affinity quinone binding site of cyt aa_3-600. A single *E. coli* cyt bo_3 mutant having R71H phenotype was also prepared.

5.2.2. Sequence alignment of quinol oxidases

Sequence analysis of of ~90 DNA sequences for quinol oxidases from proteobacteria and firmicutes was performed using online tools from NIH/NCBI and other academic resources. The main conclusions drawn from sequence alignments are shown in Table 5.2 and are in agreement with Dr. James Hemp's work (formerly of Gennis Group), who has examined and has kept up with greater number of bacterial and archaeal genomes.

The residue Q101 (*E. coli* numbering) is 70% conserved among quinol oxidases in the sequences reviewed. The valine at times is substituted for isoleucine (I98, *E. coli* numbering). If

valine and isoleucine were considered to be equivalent structurally, then conservation remains 100%. The D100 and Q101 pair in *E. coli* cyt bo_3 has some structural resemblance in corresponding residues N96 and E97 pair in *B. sub* cyt aa_3-600 and may reflect functional significance associated with these positions.

Table 5.2: Conserved residues of the high affinity quinone binding site (Q_h-site) among the sequences of cytochrome quinol oxidases from proteobacteria and firmicultes*

Residue (*Bacillus subtilis* numbering)	Conservation in Firmicutes (%)	Conservation in Quinol Oxidases (%)
R70	100	100
D74	100	100
H94	100	100
E97	80	< 20
I98	60	75

*A sequence alignment of 90 sequences encoding cytochrome quinol oxidases has been analyzed, including *Bacillus subtilis* and *Escherichia coli*.

5.2.3. Optical spectroscopy

(See Section 2.2.7)

Table 5.3: The peak values in the uv-visual absorption spectra of wild type cyt aa_3-600 and its mutants having single amino acid replacement at the high affinity quinone binding site*

Cyt aa_3-600	$Soret_{ox}$ (nm)	$Soret_{ox}$ (nm)	$Soret_{red}$ (nm)	$Alpha_{red}$ (nm)	$Soret_{red-ox}$ (nm)	$Alpha_{red-ox}$ (nm)
WT	420	---	442	598	443	599
R70H	422	---	442	599	443	599
R70Q	420	---	442	599	443	599
D74H	418	439	441	598	443	598
D74N	418	438	441	598	443	599
H94F	421	---	442	599	443	599
H94D	420	---	441	599	442	599
E97Q	422	---	441	599	443	599
I98M	417	---	442	599	443	599

*The air-oxidized spectrum of cyt aa_3-600 and its mutants contain a single soret band. The maxima belonging to this peak has been labeled '$Soret_{ox}$'. Mutations at D74, however, had second peak, which has been labeled as '$Soret_{ox}$' in the second column. The dithionite-reduced spectrum of cyt aa_3-600 and its mutants contain two peaks belonging to a soret band and an alpha band, which are labeled as '$Soret_{red}$' and '$Alpha_{red}$' respectively. The reduced-minus-oxidized difference spectrum of cyt aa_3-600 and its mutants show two peaks labeled as '$Soret_{red-ox}$' and '$Alpha_{red-ox}$'. '$Soret_{red-ox}$' peak value is the difference between $Soret_{red}$ and $Soret_{ox}$. '$Alpha_{red-ox}$' peak value is the difference between $Alpha_{red}$ and $Alpha_{ox}$. The latter value, $Alpha_{ox}$, was obtained from air-oxidized spectrum at the position indicated by 600 nm wavelength.

5.2.4. Steady-state activity assay

Spectrophotometry (See Section 3.2.3)

Oxygen consumption assay

The steady state oxygen reduction activity of cyt aa_3-600 was measured at 25 °C using an YSI model 53 oxygen electrode by Yellow Springs Instruments Co. (Yellow Springs, OH) that is equipped with a temperature-controlled 1.8 mL electrode chamber. Second instrument employed for oxygen reduction activity is Oxygen sensor (Model 1302), a clark-type polarographic sensor, by Warner Instruments, LLC (Hamden, CT).

The activity assay was performed in 50 mM Tris-HCl, 0.05% dodecyl maltopyranoside, pH 6.8. The dithiothreitol (DTT) reduction of wild type cyt bo_3 and $R71H_{bo3}$ was carried out with 130 μM ubiquinone-1, 50 μM dimethyl naphthoquinone (DMN) or 50 μM and 130 μM menadione (vitamin K_3). The substrate reduction with NADH in the presence of diaphorase, a coupling enzyme, was also performed for cyt aa_3-600. The cyanide inhibition of cyt aa_3-600 oxygen reduction activity could not be adequately measured when using NADH/DMN in the assay. In the absence of diaphorase or cyt aa_3-600, there was rapid decline in oxygen saturation level. Both NaCN and KCN were prepared in different buffer pH, and varying working concentrations that added up to > 5 mM were examined.

5.2.5. Quinone extraction

The protocol from Section 3.2.4 was followed.

Table 5.4: Determining the amount of quinone found to associate with purified cytochrome aa_3-600 from *Bacillus subtilis*[*]

Cytochrome aa_3-600	Quinone content (MQ-7/enzyme)	Semiquinone formation
Wild type	1.1	Yes
R70H	1.6	Yes
R70Q	1.4	--
D74H	1.2	Yes*
D74N	0.7	No
H94F	1	Yes
H94D	1.2	--
E97Q	1.4	Yes
I98M	1.6	Yes
Wild type cyt bo_3	1.2	Yes
R71H$_{bo3}$	2.2	No

*The values listed are molar amount of menaquinone-7 (MQ-7) found to associate with molar equivalent of enzyme cyt aa_3-600 or a mutant.

5.3. Results and discussion

5.3.1. Steady-state activity of *Bacillus subtilis* cytochrome aa_3-600 and *Escherichia coli* cyt bo_3

The natural substrate for cyt aa_3-600 is menaquinone-7 (MQ-7), which has a hydrophobic group, consisting of seven repeats of five-carbon isoprenyl group. The presence of a hydrophobic tail on a quinone derived compound decreases its solubility in solution, and makes it difficult to work with in a working assay. Hence, dimethyl naphthoquinone (DMN), which has a methyl group instead of an isoprenyl group and still retains the functionally relevant naphthoquinone head group, was an attractive choice as menaquinone-7 substitute in the activity assay. For *E. coli* cyt bo_3, the natural substrate is ubiquinone-8, which has an eight-chain length isoprenyl group, but ubiquinone-1 with a single unit of isoprene has been applied effectively in monitoring activity. All activity assays were performed using the same buffer and reagents in

tandem, in order to minimize the variability associated with the assay condition and the reagents used. The comparative data analysis was confined to assays conducted only on the same day using the same reagents whenever possible.

The specific activity of cyt aa_3-600 was measured by spectrophotometric assay in the presence of NADH and diaphorase, as the substrate concentration was increased (see Figure 5.1). The steady-state activity values determined for cyt aa_3-600 and *E. coli* cyt bo_3 are shown in Table 5.5. In the optimized assay condition, wild type cyt aa_3-600 achieved k_{cat} of 180 s^{-1} and K_m of 89 μM with dimethyl naphthoquinone (DMN) as the substrate. Exchanging Arg70 to histidine in cyt aa_3-600 did not diminish the enzyme activity. In fact, the R70H mutation showed comparable activity as wild type enzyme with k_{cat} of 227 s^{-1} and K_m of 55 μM DMN. The evidence of any activity from R70H mutant was unexpected, since the corresponding mutation at Arg71 in the homologous cyt bo_3 displayed loss of enzyme activity towards its substrate, ubiquinone-1.

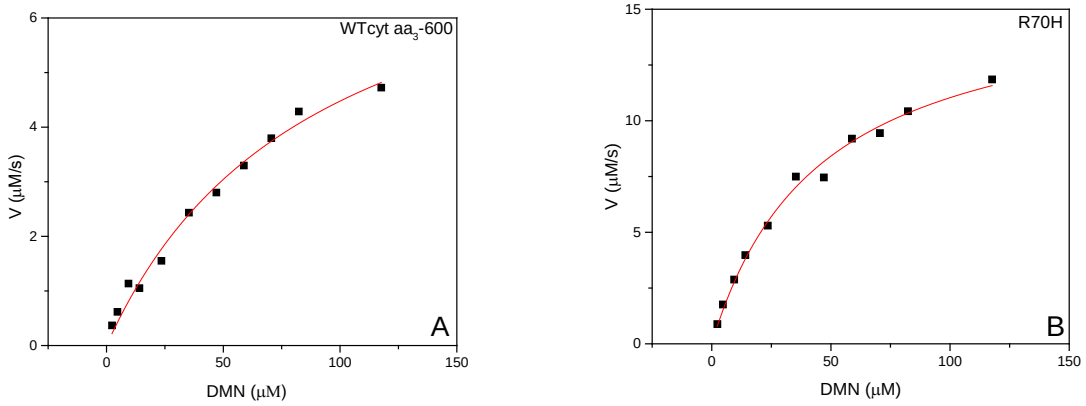

Figure 5.1. **(A)** Quinol oxidase activity of wild type cytochrome aa_3-600 and **(B)** R70H mutant of cytochrome aa_3-600 monitored by change in substrate dimethyl naphthoquinone (DMN) concentration in the presence of DT-diaphorase, a coupling enzyme, and reduced NADH. Buffer conditions: 50 mM Tris-HCl, 0.05% dodecyl maltoside (DDM), pH 6.8.

No oxygen reduction activity was detected for wild type cyt aa_3-600 and R70H mutant when ubiquinone-1 was employed as the electron donor, suggesting that the substrate ubiquinone was not able to donate electrons to the enzymes. This observation was based on a single substrate concentration of 130 μM ubiquinone-1 used to monitor oxygen consumption by the enzymes wild type cyt aa_3-600 and R70H mutant. The determination of this single concentration of substrate ubiquinol was made based on the K_m value of ~50 μM in *E. coli* cyt bo_3 that was calculated consistently for activity measurements made with ubiquinone-1.

Menadione, which has an intermediate midpoint potential (i.e. dimethyl naphthoquinone < menadione < ubiquinone-1) with respect to ubiquinone-1 and dimethyl naphthoquinone (DMN), showed lower activity levels for both cyt aa_3-600 and R70H mutant than 50 μM DMN despite the twice the concentration level used (i.e. 130 μM menadione). These single-point substrate concentrations for DMN and menadione were arbitrarily selected, and the consequent results are limited to preliminary analysis of the enzyme activity. A previous report by Mattatall et al. (2001) has reported K_m of 300 μM for DMN using different assay condition and different protein preparation [15]. The single-point concentration (i.e. 130 μM) for menadione was used to match the concentration used for ubiquinone-1 in single-point oxygen consumption assays for comparison purposes, and the K_m value of menadione with cytochrome oxygen reductases has not been determined.

Using NADH and diaphorase in the assay was essential to reducing low potential quinones (i.e. DMN and menadione) during enzyme reaction. However, it could not be verified independently whether cyanide inhibits dioxygen reduction at the catalytic site of cyt aa_3-600 by this approach. The potassium cyanide interacted directly with NADH and DMN and depleted oxygen saturation level, which was not related to cyt aa_3-600 activity.

Table 5.5: Steady-state dimethyl naphthoquinol activity values for *Bacillus subtilis* cyt aa_3-600 and *Escherichia coli* cyt bo_3 *

Enzyme[1] [0.05μM]	K_m (μM)	k_{cat} (s^{-1})	k_{cat}/K_m
WTaa_3-600	89	180	2
R70H$_{aa3\text{-}600}$	55	230	4
WTbo_3	38	430	11
R71H$_{bo3}$	50	150	3

*Activity was measured by using uv-visual spectrophotometry. Substrate dimethylnapthoquinone was reduced in the presence of NADH and diaphorase in 50 mM Tris-HCl, 0.05% dodecyl maltopyranoside, pH 6.8. The concentrations of *Bacillus subtilis* wild type cytochrome aa_3-600 and R70H mutant were determined in the presence of ferricyanide, which completely oxidizes the enzymes. Similar treatment was found to be unnecessary for wild type bo_3 and R71H mutant in determining the concentration. Multiple repeats of activity assay in saturating condition were performed. There was > 20% variance in activity values obtained for wild type cytochrome aa_3-600.

Table 5.6: Oxygen consumption assay with single-point substrate concentration of ubiquinol-1, menadiol and dimethylnaphthoquinol*

Activity (e-/s/enzyme)	WTbo_3	R71H$_{bo3}$	WTaa_3	R70H$_{aa3}$
Q-1 [130 uM]	1100	4	0	2
Menadione [50 uM]	--	--	0	0
DMN [50 uM]	1000	110	120	120

*Activity (e-/s/enzyme) was measured in 50 mM Tris-HCl, 0.05% dodecyl maltopyranoside, pH 6.8 for single-point concentration of each of the substrates. The substrates were added to assay in oxidized states and were reduced during the assay. 0.05 μM concentration of enzymes was used for each observation of enzyme activity. For wild type bo_3 and R71H mutant, the menadione activity was not determined.

The rate of quinol oxidation by wild type cyt bo_3 was decidedly greater than cyt aa_3-600 regardless of the quinone-derived compound tested in the analysis of preliminary data (see Table 5.6). The rates of oxygen consumption for cytochrome bo_3 were shown to be similar in enzyme activity when DMN, menadione and ubiquinone-1 were substrates in the assay (see Figure 5.3)[1]. In contrast, the activity of R71H mutant of cyt bo_3 was eliminated in the oxygen consumption assay when reduced ubiquinone-1 was the electron donor[2]. The activity of R71H$_{bo3}$ was restored when the assay was conducted with DMN or menadione. Its k_{cat} 153 s^{-1} is less than its

[1] This observation was based on analysis of preliminary activity data that involved only a single-point concentration of 130 μM ubiquinone-1, 130 μM menadione and 50 μM dimethyl naphthoquinone (DMN). Further work is required in measuring activity of cytochrome bo_3 at different substrate concentrations and consequently determining the K_m value for substrate menadione. The K_m for substrate DMN has been determined in this work (see Table 5.5).
[2] Analysis of enzyme activity has not been performed for mutant R71H until this work.

counterpart R70H mutant of cyt aa_3-600, but the demonstration of activity with DMN indicated that with low potential substrates, R71H $_{bo3}$ mutation could overcome energy barrier where ubiquinone-1 could not.

The high potential ubiquinone (~60 mV) could be equally reduced by dithiothreitol (DTT) alone or by NADH with diaphorase (the data not shown). This versatility of ubiquinone-1 seems to be grounded on its relatively stable reduced form in solution and its relatively high midpoint potential. For wild type cyt bo_3, the activity was not affected by how ubiquinone-1 was reduced and by whether quinol oxidation or change in oxygen saturation level was measured. On the other hand, the pH of the buffer influenced cyt bo_3 activity differently based on how ubiquinone-1 was reduced. The substrate ubiquinone-1 reduced with DTT was more sensitive to buffer pH, probably due to sensitivity of DTT to solution pH. The peaked activity value achieved at pH 7.5 fell precipitously at pH 7 and 8.5. The NADH reduced ubiquinone-1 demonstrated equally strong cyt bo_3 activity in the pH range of 6 to 8, revealing more stability. Overall, the activity values for both cyt aa_3-600 and cyt bo_3 were not greatly affected by change in buffer pH for preliminary analysis of enzyme activity involving single-point substrate concentrations (see Figures 5.2 and 5.3). For cyt aa_3-600 and R70H mutant, it was not immediately clear that the observed changes in enzyme activity at different pH were due to actual dependence of pH or due to variability in the assay itself. Further work is needed to provide clarity on this matter.

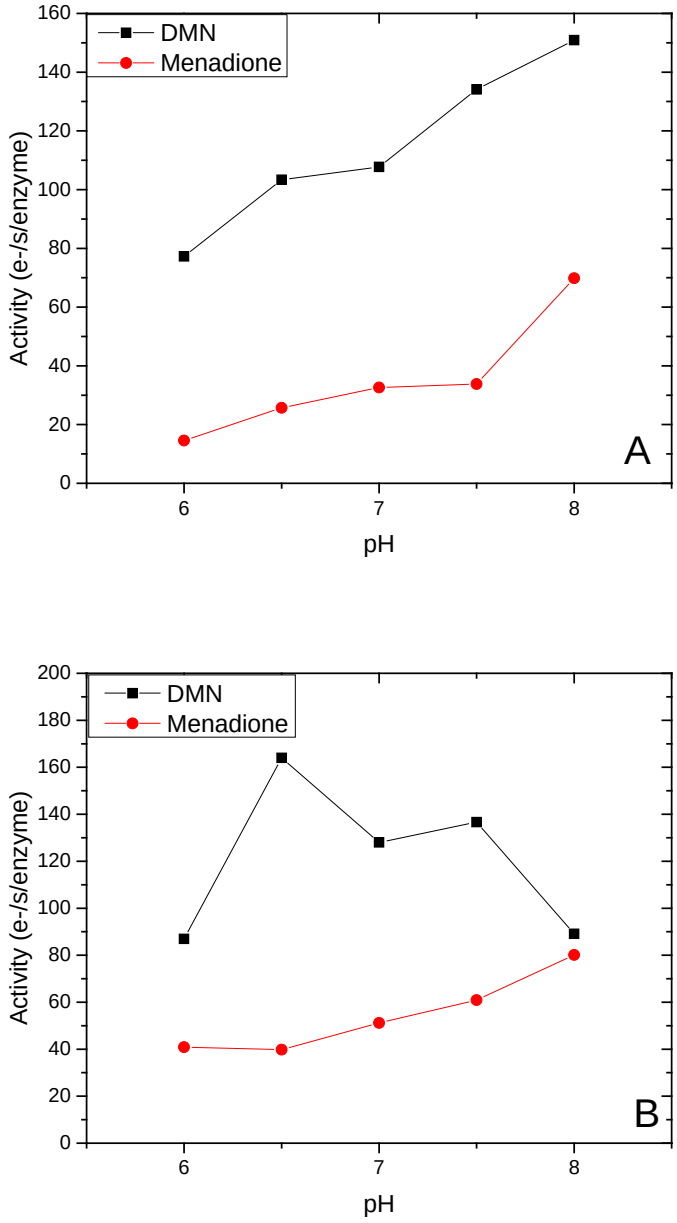

Figure 5.2. (A) pH-dependence of the activity of wild type cytochrome aa_3-600 and **(B)** R70H mutant of cytochrome aa_3-600. Activity was measured in the presence of DT-diaphorase, a coupling enzyme, and reduced NADH. Buffer conditions: 50 mM Tris-HCl, 0.05% dodecyl maltoside (DDM), pH 6.8. Single-point substrate concentrations of 50 μM dimethyl naphthoquinone (DMN) and 130 μM menadione were used.

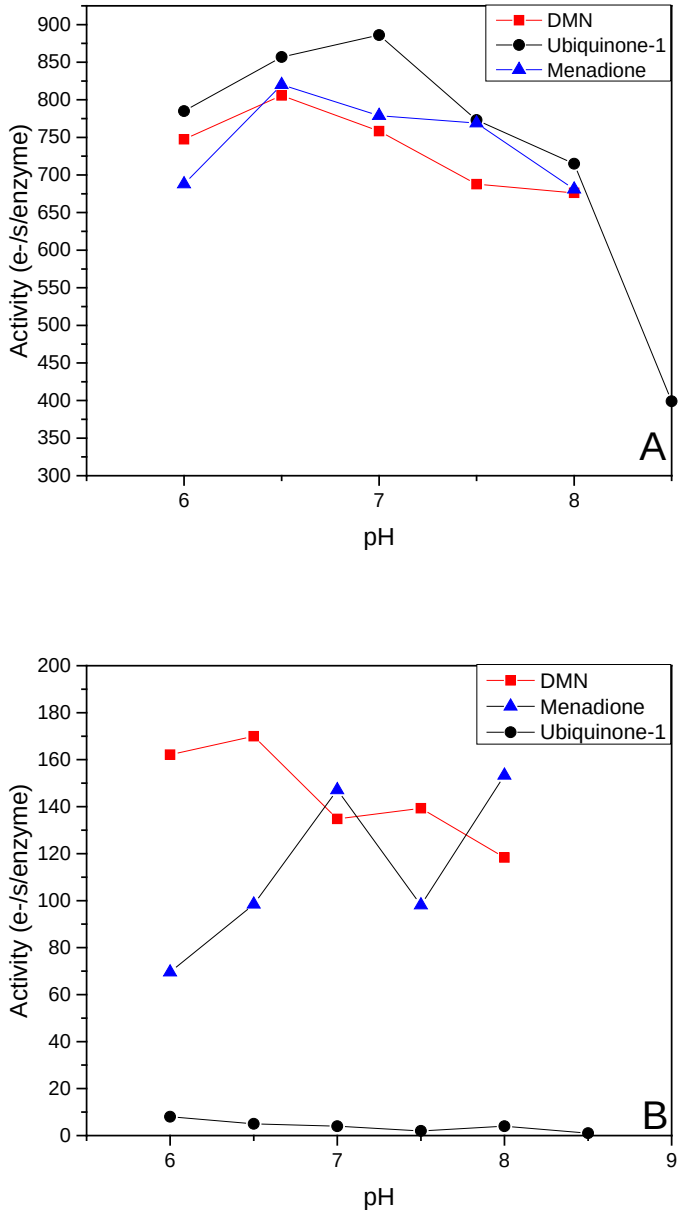

Figure 5.3. (A) pH-dependence of the activity of *Escherichia coli* cytochrome bo_3 and **(B)** R71H mutant. Activity was measured in the presence of DT-diaphorase, a coupling enzyme, and reduced NADH. Buffer conditions: 50 mM Tris-HCl, 0.05% dodecyl maltoside (DDM), pH 6.8. Single-point substrate concentrations of 50 μM dimethyl naphthoquinone (DMN), 130 μM menadione and 130 μM ubiquinone-1 were used.

5.3.2. Steady-state activity and activity inhibition of cytochrome aa_3-600 mutants

Select mutations at high affinity quinone binding site (Q_h-site) were made based on high sequence identity among quinol oxidases. These mutations did not display significantly diminished enzyme activity as anticipated, except for D74 mutants[3] (Table 5.7). Two of the mutants, R70H and E97Q, showed higher enzyme activity compared to the wild type, and the others had declined activity. Only D74H and D74N experienced elimination of activity with DMN. When the electron donating substrate was menadione, there was a steep decrease in activity for E97Q with respect to the wild type protein. All other mutations at the Q_h-site had similar relative activity with respect to the wild type cyt aa_3-600 regardless of dimethyl naphthoquinone or menadione used as the substrate.

Table 5.7: Enzyme activity of cyt aa_3-600 and Q_h-site mutants with single-point substrate concentration of dimethyl naphthoquinol and menadiol*

	DMN (50 μM)	% Activity	**Menadione** (130 μM)	% Activity
WTaa_3	120	100	30	100
R70H	180	150	50	160
E97Q	190	170	10	40
H94F	70	60	20	70
H94D	20	20	2	6
I98M	90	80	25	80
D74H	6	5	0	0
D74N	6	5	6	20

*The single-point concentration of substrates was added to assay in oxidized states and were reduced during the assay with NADH and DT-diaphorase, a NADH dehydrogenase. Activity (e-/s/enzyme) was measured in 50 mM Tris-HCl, 0.05% dodecyl maltopyranoside, pH 6.8 for single-point concentration of each of the substrates. The substrates were added to assay in oxidized states and were reduced during the assay. 0.05 μM concentration of enzymes was used for each observation of enzyme activity.

From the activity results alone, it was not immediately clear which biochemical considerations would adequately characterize the enzyme mechanism involved. All the mutants carried at least one equivalent of quinone bound tightly to protein structure (Table 5.4).

[3] This observation was based on analysis of preliminary activity data that involved only a single-point concentration of 130 μM ubiquinone-1, 130 μM menadione and 50 μM dimethyl naphthoquinone (DMN). Further work is required in measuring activity of cytochrome aa_3-600 at different substrate concentrations and consequently determining the K_m value associated with each substrate.

Apparent disruption of quinone-protein interaction surrounding the head group was not sufficient to displace the quinone. This indicated a potential role of the quinone hydrophobic tail in the strong association of quinone with the protein.

Disturbing the Q_h-site by single amino acid mutations produced notable properties in the optical spectra. The air-oxidized wild type cyt aa_3-600 has a single soret band ~419 nm, and the dithionite reduced spectrum shows a shift of this peak to ~442 nm and appearance of second peak at 598 nm (see Table 5.3 and Figure 2.2). While R70H had spectral features similar to wild type when reduced by dithionite, other mutations experienced visible changes in the spectral features or behaved differently. For instance, the mutant H94F appeared not to have undergone changes in the spectral features, but the air-oxidized enzyme responded to oxidation by ferricyanide (data not shown).

The deviation from wild type cyt aa_3-600 spectra was most obvious for D74H and D74N mutations, where extra peaks (i.e. ~439 nm and 598 nm) appeared in the air-oxidized spectrum (see Table 5.3). These peaks were associated with the partially reduced form of the protein, because the 439 nm peak shifted to the soret band position 441 nm with dithionite, while the 598 nm peak disappeared when the enzyme was treated with ferricyanide. More importantly, the partially resolved hyperfine structure was absent from CW EPR spectrum of semiquinone (SQ) stabilized in D74H mutant (see Figure 5.4). These changes are reflected in the complete loss of enzyme activity for these two mutants and suggested the importance of Asp74 in the quinol oxidation. The quinone at the Q_h-site modulates the flow of electrons into cyt aa_3-600, and the mutations at the site could perturb the electron transfer process to low-spin heme A, one of the redox centers in cyt aa_3-600. In fact, Q_h-site is within a close proximity (~14 Å) of low-spin

heme A, a structural disturbance could explain the change in optical spectra for D74H and D74N mutants in contrast to the wild type cyt aa_3-600.

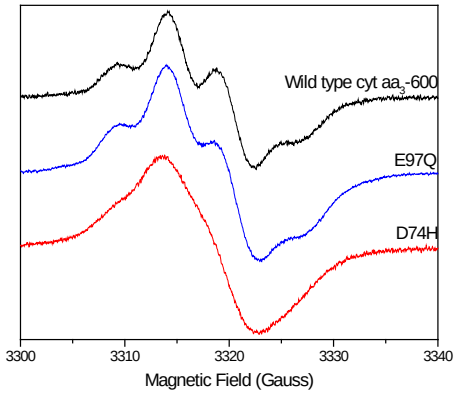

Figure 5.4. Continuous-wave electron paramagnetic spectroscopy (EPR) of wild type cytochrome aa_3-600, E97Q and D74H mutants. The EPR sample was prepared using ~100-200 μM of protein in the presence of NADH and dimethyl naphthoquinone. Buffer conditions were: 100 mM Tris; 10 mM EDTA; 10% glycerol; 0.05%, pH 8.2. EPR parameters were: 0.16 mT modulation; microwave power, 0.2 mW; microwave frequency, 9.29 GHz; 3320 center; 40 G scan range; 40,000 gain; 90 K (liq. N_2).

Previously, the EPR SQ signal of wild type cyt aa_3-600 could not be generated in the presence of inhibitor 2-heptyl-4-hydroxyquinoline-N-oxide (HQNO) (see Figures 3.3 and 5.5). This was further corroborated in the activity assay, where wild type cyt aa_3-600 was completely inhibited by 1 μM HQNO and 30 nM aurachin C1-10 (AC10)[4]. Mutations at the Q_h-site varied in response to the inhibitors. The R70H mutant was sensitive to micromolar amount of HQNO (7 μM) with 8% activity remaining, but the activity was eliminated with 30 nM aurachin C1-10, just as in the wild type.

Other mutations showed resistance to inhibition and maintained relatively strong activity at the inhibitor concentrations that affected activity loss in the wild type. E97Q activity was not

[4] These observations based on preliminary data were elimination of cytochrome aa_3-600 quinol oxidase activity with dimethyl naphthoquinone at single-point concentration of 50 μM. Further work is required to determine inhibition constant for each inhibitor in wild type cyt aa_3-600 and its mutants.

eliminated by 30 μM HQNO (~20 % activity remaining) and 30 nM aurachin C1-10 (~25%). The H94F mutant had ~60% activity remaining with HQNO and AC10. The H94D mutant had 45% activity remaining with 2 μM 2-heptyl-4-hydroxyquinoline-N-oxide (HQNO) and 20% with 30 nM aurachin C1-10. The I98M retained 70% of its activity with either of the inhibitors examined. Specific inhibitors are useful tools for probing the structural and functional properties of the protein-substrate interaction, and additional data on inhibition response could add to understanding of substrate selectivity in this enzyme (i.e. inhibition constant, K_i)

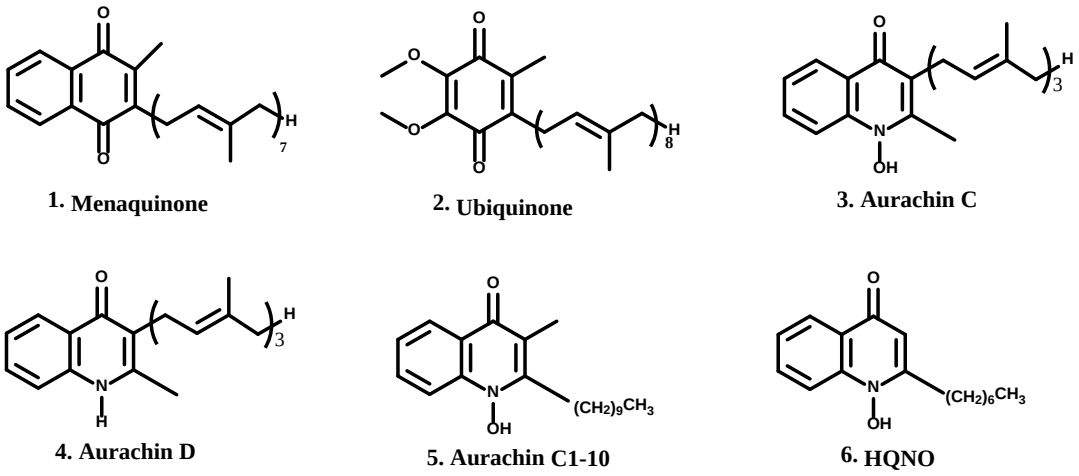

Figure 5.5. Chemical structures of quinone substrates (1-2) and quinone-based inhibitors (3-6). Aurachin C1-10 is the modified version of aurachin C, where the two ring substituents were switched on the naphthoquinone ring structure.

5.3.3. Functional role of Q_h-site in *Bacillus subtilis* cytochrome aa_3-600 and *Escherichia coli* cytochrome bo_3

The quinol oxidation activity is different for cytochrome (cyt) aa_3-600 and cyt bo_3 in strength and in range of response to different quinone-based compounds. A conspicuous difference lies in the incapacity of cyt aa_3-600 to oxidize ubiquinol-1 as the substrate. The ubiquinol-1 reliably elicits a strong response from cyt bo_3 in quinol-mediated dioxygen reduction. Since the natural substrate for cyt aa_3-600 is menaquinone-7, a low midpoint potential quinone,

the evidence supports the view that the quinol oxidase activity of cyt aa_3-600 is restricted to low potential quinone-based substrates. The quinol oxidase activity dependence of cyt aa_3-600 and cyt bo_3 on the electrochemical properties of the quinone substrates is corroborated by a particular mutation $R71H_{bo3}$ in cyt bo_3 that shows no activity with ubiquinone-1, its natural substrate analog. In contrast, this mutation is active with dimethyl naphthoquinone (DMN) and menadione. The restored activity in the cyt bo_3 mutant demonstrates a change in its substrate interaction and possibly substrate specificity. Previously, this mutation in the high affinity site (Q_h) of cyt bo_3 was reported to have no quinol oxidase activity and was found unable to stabilize semiquinone (SQ) [18]. Additional experiments are needed in order to address the questions about the molecular factors responsible for the change in the substrate recognition in the protein-quinone interaction.

When the structural features are probed by observing the effects of quinone-based inhibitors on cyt aa_3-600 quinol oxidase activity, a similar inhibitory response to aurachin C1-10 (AC10) and 2-n-heptyl-r-hydroxyquinoline N-oxide (HQNO) is observed as it has been reported for cyt bo_3 (see Figure 5.5) [81-83]. The AC10 (K_i = 15 nM) was more effective in inhibiting ubiquinol-1 oxidase activity of *E. coli* cyt bo_3 than HQNO (K_i = 0.74 μM) and showed tighter binding (K_d = 15 nM) than other inhibitors (e.g. piericidin A, K_d = 2 μM and UHDBT, K_d = 0.3 μM) examined, including HQNO (K_d = 4 μM) [81, 84-85]. The chemical bond arrangement of AC10 and HQNO indicates that these compounds are acting on the quinol binding site, where the carbonyl group and the hydroxy-substituted heteroatom on the quinone ring structure could facilitate hydrogen bonding.

In comparison, other inhibitors such as p-benzoquinones and substituted phenols were weaker performing inhibitors when ubiquinol oxidation activity of cyt bo_3 was monitored for

residual activity response (i.e. half-maximal inhibitory constant, IC_{50}) [86, 89]. Interestingly, the inhibitory activity of these ring-substituted quinone-related compounds demonstrated asymmetric nature in molecular recognition of the quinol active site in cyt bo_3. This observation coincides with the results from advanced EPR studies of cyt aa_3-600 and cyt bo_3 oxidases that found the respective semiquinone (SQ) stabilized by the enzymes showing asymmetry in H-bonding at the high affinity quinone binding site (Q_h) [46, 63]. The identity of the quinol active site is debatable, because the number and location of quinone binding site(s) are not known in cytochrome oxidase. While it has been considered that the quinol oxidation site exists separately from the high affinity quinone binding site (Q_h), it is noteworthy that the inhibitors acting on the substrate oxidation site would also exhibit asymmetric charge distribution in the aromatic head-groups, just as the SQ at the Q_h-site.

Generally, one molar equivalent of quinone co-purifies with the protein in both cyt aa_3-600 and cyt bo_3 and is considered to bind at the Q_h-site, although it depends on the purification protocol. In the absence of this tightly binding quinone, reconstituting quinone-free cyt bo_3 with exogenous quinone (i.e. ubiquinone-6) was found to cause functional changes in cyt bo_3 that was different from the wild type protein containing native ubiquinone-8 [87]. While quinol activity has been interpreted in two-site quinone model, it appears to be more complicated when deciphering the modes of binding between the synthetic quinones and the wild type cyt bo_3 and cyt aa_3-600 in the assay condition. While the complete exchange between the bound quinone and the free quinone in an assay condition is not likely to occur because of hydrophobic tail, some exchange events could possibly transpire and add complexity in interpreting quinol oxidase activity. The bound quinone has been assumed to bind at the Q_h-site, but the nature of this association requires further scrutiny.

The bound quinone at Q_h-site has been considered to mediate electron transfer to low-spin heme A in cyt aa_3-600 (or heme B in cyt bo_3) from a separate quinol oxidation site (Q_L) where free quinols would make contact with protein from membrane pool. However, a potential involvement of Q_h-site in direct quinol oxidation is suggested by quinol activity data of cyt aa_3-600 mutations at the Q_h-site and forms a new paradigm. Introducing mutations at the Q_h-site in cyt aa_3-600 does not displace the bound quinone and retains quinol activity in most cases with the exception of D74 mutants, where optical spectra of hemes are altered in air-oxidized samples. The mutations of residues at Q_h-site do not eliminate activity, and consequently suggest that the factors that influence quinol activity and quinone recognition by protein structure are not affected by mutations in cyt aa_3-600, compared to cyt bo_3. This difference appears to be rooted in the different quinone-based substrates used by each of the enzymes. The Q_h-site mutants are also less sensitive to inhibitors HQNO and aurachin C1-10 than the wild type protein. The most plausible and satisfying explanation is that the Q_h-site has direct influence on quinol binding and quinol oxidase activity. A strong protein-quinone association has been previously reported and has been attributed to quinone's hydrophobic tail [83,88,90]. These reports agree with the observations made here, which leaves the quinone head group as the key element in quinol activity of protein.

The idea that the Q_h-site directly oxidizes quinol is a simplified and attractive possibility that has been largely dismissed because one equivalent of quinone has been observed to co-purify with some preparations of protein. Such a close structural association with the protein has made it reasonable to accept this bound quinone as an integral part of the protein structure, with a relevant function. Predicting enzyme mechanism with two potential quinone sites also has played into the idea that Q_h-site mediates electron transfer similarly as the Cu_A center in cyt c

oxidase. However, this interpretation may have been misdirected and premature. This bound quinone at Q_h-site could be an evidence of a transitional state of quinol activity, where the quinone ring structure is loosely associated with the Q_h-site after it has donated its electrons.

The Q_h-site would have a higher affinity for reduced quinol than quinone, if it were to act as the quinol oxidation site. The polar residues at the Q_h-site could form H-bonds with quinol and the neutral semiquinone SQ, stabilizing the reactive intermediate, while exhibiting slippage or mismatching events with oxidized quinone due to weak association. Hence, disturbance of hydrogen bond formation could have resulted in elimination of activity in many of the cyt bo_3 Q_h-site mutants and in lower activity in some of the cyt aa_3-600 mutants. The fact that cyt bo_3 mutations at the Q_h-site are more sensitive than the corresponding mutants in cyt aa_3-600 could reflect a looser binding of ubiquinone than menaquinone (MQ), which has a bulkier head group and could provide a tighter fit to the protein scaffold. Indeed, the advanced EPR data have determined that the semiquinone in cyt bo_3 formed stronger H-bonds with Q_h-site residues than in cyt aa_3-600 [46-47]. The Asp74 mutations in cyt aa_3-600 emphasize the significance of H-bond formation and sensitivity to change in side chain pKa in quinol activity of the enzyme. These mutations (D74H and D74N) uniquely have shown no activity both in cyt bo_3 and cyt aa_3-600. The semiquinones in these mutants also do not form asymmetric H-bonding around the quinone head group, reflecting a deviation in the charge distribution over quinone head group compared to the wild type protein. Specifically, these observations have corresponded to the loss of H-bond formation between the semiquinone and Arg70 in cyt aa_3-600 (Arg71 in cyt bo_3). The proton-coupled electron transfer is likely an important component in the quinol oxidation at the Q_h-site that depends on precise and timely H-bond formations between the stabilized semiquinone and Asp74 and Arg70.

5.3.4. A proposed mechanism for menaquinol oxidation in cyt aa_3-600

Any proposed mechanism for menaquinol oxidation at the Q_h-site would need to satisfy following considerations. The H-bonds surrounding the quinone ring structure must display asymmetry, where stronger interactions occur at O1 carbonyl and weaker interactions at O4 (ubiquinone numbering is used). Secondly, the first deprotonation event is an essential initiation step in menaquinol oxidation reaction and involves the proton associated with O4 in menaquinone ring structure. A potential stepwise mechanism could entail following order of events: 1) The menaquinol approaches the Q_h-site and aligns O1 carbonyl with the residues Asp74 and Arg70 and aligns O4 carbonyl with the residues His94 and Glu97. 2) The Asp74 and Arg70 pair forms an ionic bridge[5] in the absence of menaquinone, but this interaction is disrupted when the side chains of Asp74 and Arg70 form H-bonds with fully reduced menaquinol. 3) The strong H-bonding at the O1 side creates a shift in charge distribution over the menaquinol ring that leads to weaker affinity for proton at O4 and hence consequent loss of this proton to polar groups surrounding the O4 carbonyl. 4) An electron transfer to heme A follows the first deprotonation event, resulting in menasemiquinone ($MQH^{\bullet}$) radical. 5) The Asp74 becomes protonated, and the menasemiquinone ($MQH^{\bullet}$) loses its second proton. These events lead to menasemiquinone ($MQ^{\bullet -}$) formation. The steps 4 and 5 are tightly coupled (i.e. first electron transfer and 2nd deprotonation events.) 6) The protonated Asp74 pulls away from menasemiquinone ($MQ^{\bullet -}$) and subsequently, gives up its proton to Arg70 side chain or to surrounding environment (e.g. water molecule). 7) The second electron transfer occurs as the carboxylate side chain of Asp74 displaces Arg70 away from menasemiquinone ($MQ^{\bullet -}$). The menaquinone (MQ) is fully oxidized. Proton rearrangement occurs for His94, which permits

[5] The interpretation of interaction between Asp74 and Arg70 is a speculation based on x-ray structure of *E. coli* cytochrome bo_3 (3.5 Å resolution) [17]. An ionic bridge is likely to form between these charged amino acids; however, the structure has low resolution that does not allow for such interpretation.

restored H-bonding between N_δ of His94 and carboxylate of Glu97. 8) The oxidized menaquinone (MQ) dissociates from the Q_h site and an H-bond is restored between carboxylate of Asp74 and guanidinium of Arg70.

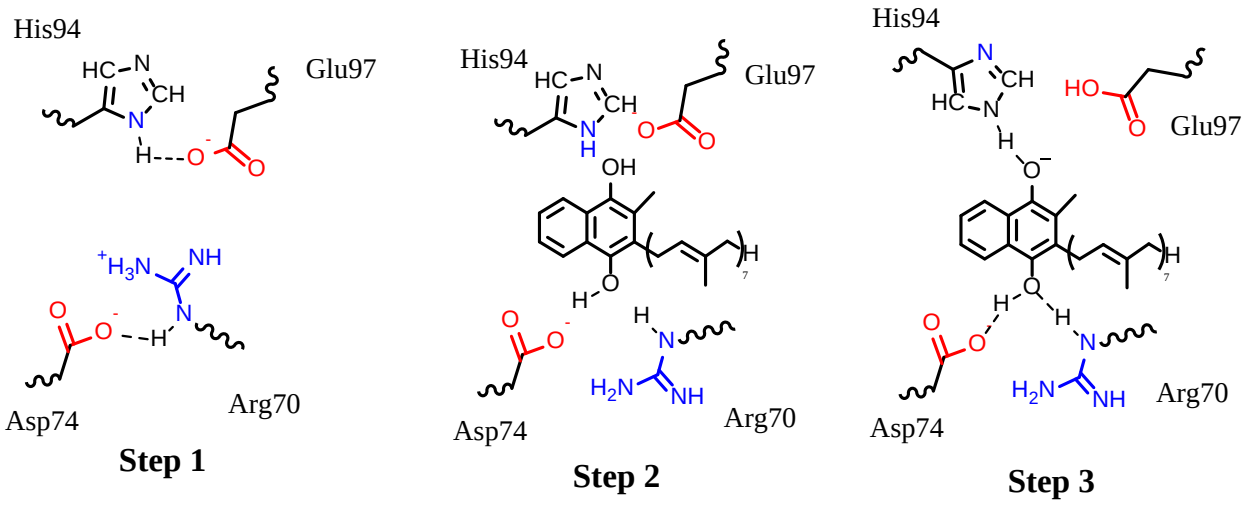

Figure 5.6. A proposed mechanism for menaquinol oxidation by cyt aa_3-600. Steps 1-3 are shown. First deprotonation occurs at Step3. Ubiquinone numbering is used to refer to corresponding carbonyl groups on menaquinone (i.e. O1 faces Asp/Arg pair and O4 faces His/Glu pair).

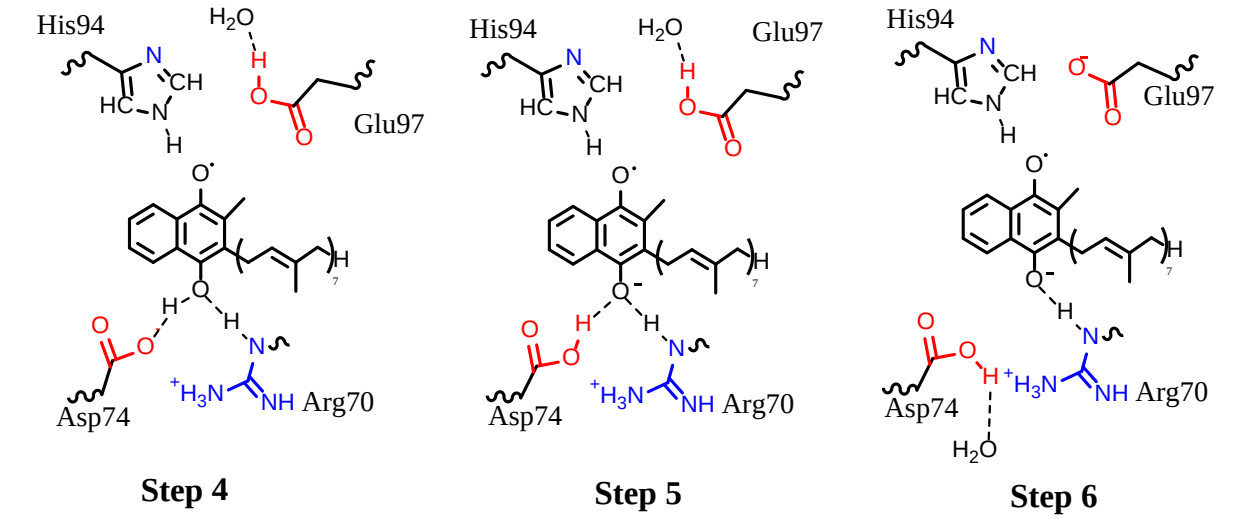

Figure 5.7. A proposed mechanism for menaquinol oxidation by cyt aa_3-600. Steps 4-6 are shown. Steps 4 & 5 are tightly coupled (i.e. first electron transfer and 2nd deprotonation events, respectively).

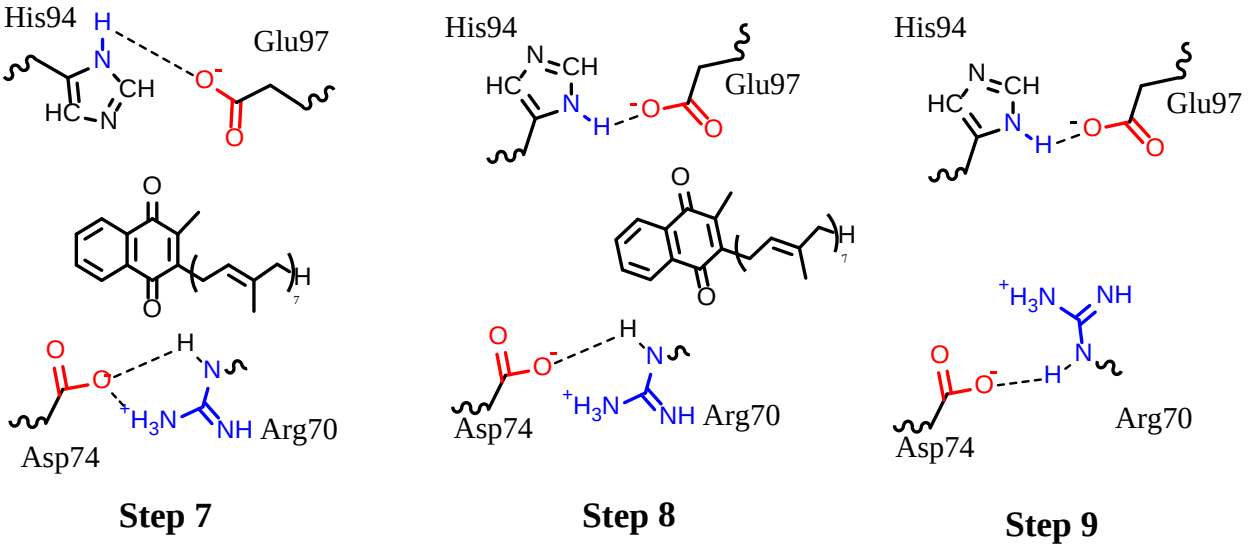

Figure 5.8. A proposed mechanism for menaquinol oxidation by cyt aa_3-600. Steps 7 and 8 are shown. Step 9 is equivalent to Step 1. Second electron transfer occurs at Step 7.

The inactivity of cyt aa_3-600 with ubiquinol (UQH_2) could be explained by the high activation energy required in the first deprotonation step. The residues His94 and Glu97 are within close proximity of each other that they can form a strong H-bond. This association introduces a structural rigidity in the Q_h-site that prevents His94 from rotating about C_β to come into alignment for H-bonding with ubiquinol. The crystal structure of cyt bo_3 shows the corresponding residue (His98) having its imidazyl ring facing away from the Q_h-site. Hence, in order for N_ε to be within H-bond distance with ubiquinol, the imidazyl ring has to rotate ~45-90° about the C_β-C_γ bond. In the past ^{14}N and ^{15}N HYSCORE spectra have shown that N_ε of His98 carries unpaired electron density in its interaction with semiquinone (SQ) and not N_δ [47, 91]. The interaction between the semiquinone and His94 in cyt aa_3-600 is comparable to the corresponding interaction with His98 in cyt bo_3, based on the hyperfine couplings of His nitrogens in both enzymes. The high potential ubiquinol may be unable to cause this necessary reorientation of His94 in cyt aa_3-600, whereas menaquinol does have the additional driving force required to bring about this change. Perhaps, menaquinol could give up first proton to Glu97 directly and thereby disrupt the H-bond interaction between Glu97 and His94. Or, menaquinol could indirectly protonate Glu97 by giving up its first proton to N_ε of His94, which leads to deprotonation at N_δ as Glu97 accepts the imidazyl proton. In an activity assay, the E97Q mutation in cyt aa_3-600, which replaces acidic Glu with polar Gln residue as it is found in cyt bo_3, shows stronger quinol activity than the wild type cyt aa_3-600. Hence, glutamine, a weaker polar residue, participates in weaker H-bonding interactions with His94 and the quinol at the Q_h-site. This weaker association could favor a rapid H-bond formation between menaquinol and His94 and could explain an increased quinol oxidase activity of cyt aa_3-600.

The fact that cyt bo_3 demonstrates quinol oxidase activity with both ubiquinone and dimethyl naphthaquinone (DMN) based substrates suggests that an activation barrier exerting influence in cyt aa_3-600 is either absent or reduced to a weaker component in cyt bo_3. This effect could be related to presence of Glu97 in cyt aa_3-600, which is Gln101 in cyt bo_3. As detailed above, a decrease in asymmetric charge distribution leading to weakened H-bonding interaction at the semiquinone side facing Asp/Arg pair could be one consequence of having acidic residue Glu97 at the opposite carbonyl side of the semiquinone in cyt aa_3-600. Another outcome might be an increased susceptibility of ubiquinol to mismatch pairing with its H-bond contacts in the Q_h-site because of its ring methoxy groups. These substituents on the quinone ring are able to assume different orientations and could be involved in futile H-bonding events, especially with Glu97. Hence, no stable H-bonding would form until the quinone head group correctly orients itself. The MQH_2 is likely to avoid such fruitless binding events.

In a different scenario, substituting Arg70 with His in cyt aa_3-600 has resulted in an improved quinol oxidase activity. The overall retention of asymmetric charge distribution over the quinone ring, despite changes in number and strength of H-bonds, is reflected in the strong activity value of R70H mutant compared to the wild type cyt aa_3-600. The ^{14}N and ^{15}N HYSCORE spectra show a change in asymmetric H-bonding pattern that is strengthened by R70H mutation, compared to the wild type (Chapter 6). In this situation, R70H in cyt aa_3-600 may be locked into a stable conformation with menaquinol, assisted by a strengthened H-bonding with imidazole of His94. The DFR calculations predict three H-bonds: two strong H-bonds on O1 carbonyl of menasemiquinone and one weaker H-bond on O4 side [92]. A possible mode of chemical reaction may involve first proton given up to Glu97 by menaquinol, which frees His94 imidazole to form H-bond directly with the menasemiquinone. While it is not

known whether N_ε or N_δ of His94 participates in the H-bonding with menasemiquinone in R70H, this H-bond formation with His94 would avoid the need for additional energy required to rotate His94.

On the other hand, the equivalent mutation R71H in cyt bo_3 is unable to stably interact with quinol; hence, no stable semiquinone is detected by EPR method [18]. These observations indicate that the protein environment may contribute to different semiquinone interaction in R71H of cyt bo_3 than in R70H of cyt aa_3-600. The asymmetric H-bonding pattern may be diminished, instead, in R71H cyt bo_3, in contrast to what is observed for R70H of cyt aa_3-600. A possible explanation involves a stronger H-bond formation between the ubiquinol and the His101 without the first deprotonation event. The consequence would be an effective disruption of the quinol oxidation reaction where the bound quinol is unreactive. Both $R70H_{aa3600}$ and $R71H_{bo3}$ are active with menaquinone-based substrate. Hence, the inactivity of R71H in cyt bo_3 with ubiquinol indicates that quinol oxidation involving ubiquinone is more sensitive to changes in H-bonding arrangement imposed by the protein structure than menaquinone. The fact that R71H shows activity only with menaquinone-based substrate suggests that 2-1 H-bonds around the carbonyl groups of quinone ring averts activity with ubiquinone-based substrate. Unintended consequence of this (2-1) H-bond pattern could be the reduced charge redistribution over the quinol ring that fails to shift net negative charge to O1 side of the quinone ring. This could hinder the first deprotonation step for ubiquinol at O4 side.

The R71H in cyt bo_3 shows activity with menaquinone-based substrate primarily because the substrate used is low potential menaquinol that quickly gives up a proton to its surrounding. The naphthoquinone ring structure of menaquinone is able to delocalize electron density through its extensive conjugated double-bonds that increases stability particularly for charged states.

This increase in delocalization energy translates to more stable and more acidic molecule. Hence, the reactivity of menaquinol is not likely to be dependent on the protein structure the way ubiquinol reactivity is. This rationale is confirmed by restored activity in R71H mutant of cyt bo_3 with menaquinone-based substrate.

A complete loss of quinol activity resulting from mutations at D74 (i.e. D74H and D74N) in cyt aa_3-600 and corresponding D75 in cyt bo_3 can be explained in the context of the proposed enzyme mechanism above. An acidic residue at this position could be important because it needs to be able to initiate H-bonding with the quinol molecule and participate in the second deprotonation of quinol at the Q_h-site. Residues with side chains having higher pKa values may instead share an H-bond with the bound semiquinone, and also prevent a strong H-bond formation between the semiquinone and Arg70. More importantly, the absence of the H-bonding between the stabilized semiquinone and Arg70 (Arg71 in cyt bo_3) may lock the bound quinone in a state that prevents reaction from going forward. The x-ray structure of cyt bo_3 without quinone suggests that restoration of H-bond formation between Asp75 and Arg71 is an essential part of quinol oxidation reaction cycle that may fail to form in Asp75 mutants or may become significantly weakened. The D74H and D74N mutations in cyt aa_3-600 also disrupt the electron transfer role of heme A that results in a partial reduction of hemes (i.e. high spin heme A). The optical spectra and the low temperature cw EPR spectra of purified air-oxidized protein samples show reduced high-spin heme A (spectra not shown). The structural disturbance introduced by mutations at the corresponding aspartate in both enzymes correlates to reduced asymmetry of the spin density distribution and to loss of quinol activity that is unresponsive to low potential quinol substrate.

5.3.5. Substrate recognition of cytochrome aa_3-600 and cytochrome bo_3

Highly conserved residues at Q_h-site are common to both cytochrome (cyt) aa_3-600 and cyt bo_3, where native menaquinone-7 (MQ-7) and ubiquinone-8 (Q-8) respectively bind. The semiquinone intermediate stabilized at Q_h-site is involved in hydrogen bonding with the surrounding protein environment similarly in an asymmetric manner in both cyt aa_3-600 and cyt bo_3, as illustrated by advanced EPR experiments. The data presented here reveal a correlation between quinol oxidation activity and electrochemical properties of the substrate quinone. The wild type cyt bo_3 displays quinol oxidase activity with both ubiquinol-1 and dimethyl naphthoquinol (DMN) based substrates. On the other hand, wild type cyt aa_3-600 is not reactive with ubiquinol-1. The cyt aa_3-600 Q_h-site mutants display activity that persists with low midpoint potential menaquinol analog (i.e. DMN), whereas the corresponding mutations in cyt bo_3 do not show activity with ubiquinol-1. One possible explanation for these differences in the quinol oxidase activity of two enzymes could be the Glu97 in cyt aa_3-600 menaquinol oxidase replaced by Gln101 in cyt bo_3 ubiquinol oxidase. The fact that cyt aa_3-600 is unable to accept electrons from ubiquinol-based substrate in assay condition could be due to higher energy barrier enforced by the Q_h-site of cyt aa_3-600 that is absent in cyt bo_3. There is a structural basis for binding either ubiquinol or menaquinol in both enzymes. However, the preferential binding of one type of quinone over the other appears to be dependent on substrate availability for *E. coli* cyt bo_3, while *B. sub* cyt aa_3-600 is limited to menaquinone-based substrate because of structural constraint at its Q_h-site.

Some of the *E. coli* membrane proteins are able to interact with both ubiquinone-8 and menaquinone-8 in physiological conditions. Despite lack of direct evidence, data indicate that cyt bo_3 can potentially use ubiquinol-8 and menaquinol-8 as substrates. Previously, the *E. coli*

membranes, lacking ubiquinol-8, have shown significant oxygen uptake that was dependent on endogenous menaquinone-8 content during aerobic respiration [93]. Aside from cyt bo_3, two other oxidases in *E. coli* electron transport pathways could be responsible for this menaquinol-8 activity. Cyt bd-I is the predominant respiratory oxygen reductase that is present in semi-aerobic conditions, and cyt bd-II is expressed in conditions of carbon and phosphate starvation and during the stationary phase of cell growth [96-97]. The cyt bo_3 is expressed by *E. coli* in aerobic growth condition, which coincides with high membrane content of ubiquinone-8 [93-95]. In anoxic conditions, the *E. coli* relies on menaquinol-8 as the electron carrier. The membrane content of menaquinone-8 is still dwarfed by overall contribution of ubiquinone-8 to quinone pool during midpoint exponential growth and the stationary phase. Hence, the native *E. coli* respiration favors pairing of cyt bo_3 with ubiquinol and not with menaquinol based on substrate accessibility. However, different quinone molecules have shown that they can associate with isolated cyt bo_3 in EPR studies [73]. Because *Bacillus subtilis* produces only MQ-7, it is not possible to observe substrate interaction between ubiquinol and cyt aa_3-600 in native culture condition. The cyt bo_3 appears to be distinctive in having structural and functional capacity to interact with both ubiquinol and menaquinol.

5.4. Conclusions

The evidence of Q_h-site having a direct involvement in quinol oxidase activity of cyt aa_3-600 is presented, which leads to a new perspective for an old problem. The mutations at the Q_h-site in cyt bo_3 eliminate activity, while corresponding mutations in cyt aa_3-600 show a decrease or no effect in quinol activity. The greater sensitivity in cyt bo_3 than cyt aa_3-600 to mutations at Q_h-site suggest a higher vulnerability in cyt bo_3 to disturbance in hydrogen bonding between

quinol/SQ and the conserved residues of Q_h-site. A possible rationale for the difference in quinol oxidase activity of cyt aa_3-600 and cyt bo_3 is offered. This difference is suggested to have structural basis. The data presented here also reveal a correlation between quinol oxidase activity and electrochemical properties of the substrate quinone. The Asp74 and Arg70 in cyt aa_3-600 (Asp75 and Arg71 in cyt bo_3) are critical in the quinol activity. There is a structural basis for binding either UQ or MQ in cyt bo_3. The quinol oxidase activity of cyt aa_3-600 at the Q_h-site is not well understood, and the extent and nature of this mechanism are not known and require further investigation.

CHAPTER 6: Structural Characterization of SQ Stabilized in R70H Mutant of Cyt aa_3-600 That Shows Resilience in Specific Activity

6.1. Introduction

The wild type cyt aa_3-600 uses menaquinol as substrate and is able to stabilize semiquinone (SQ). A group of highly conserved residues, Arg70, Asp74, His94 and Glu97, is considered to be important in binding a quinone (Q_h-site) and in generating the SQ EPR signal. For wild type cyt aa_3-600, the nitrogen showing the strongest isotropic coupling with the SQ was tentatively assigned as belonging to sidechain of Arg70 [16]. Weakly coupled nitrogen with significant orientation dependence was proposed as sidechain nitrogen of His94 on the carbonyl oxygen O4 side of menaquinone (ubiquinone numbering is used for comparison purposes). In the absence of studies using selective ^{15}N isotopic labelling of specific amino acids, direct evidence identifying the nitrogen involved in the strong ^{14}N hyperfine coupling with SQ at Q_h-site in cyt aa_3-600 has been lacking. The work detailed in this chapter provides additional evidence that Arg70 is involved in the interaction with the SQ in cyt aa_3-600. In the current work, the Arg70 is replaced with histidine, a residue that has distinctive EPR parameters for its imidazyl nitrogen atoms. This mutation perturbs the interaction between the protein and the SQ and has altered the strongest hyperfine coupling interaction (hfi) involving nitrogen in the 1D-2D- ^{14}N, ^{15}N ESEEM spectra. A similar experiment in homologous cyt bo_3 ubiquinol oxidase involving R71H mutant could not be performed because the SQ was not generated in the mutant [18]. The R70H mutant of cyt aa_3-600 is shown to have changes in the number and strength of H-bonds with the SQ, but the asymmetry in H-bonding to the SQ is not altered.

In this work, it is shown that the weaker hydrogen bonding deduced for the SQ species in the menaquinol oxidase correlates with greater plasticity of the site. Specifically, whereas the R71H mutant in cyt bo_3 is inactive and does not stabilize the SQ, the corresponding R70H

mutant in cyt aa_3-600 remains functional and does stabilize the SQ species. The mutation retains catalytic function despite the considerable disruption of the hydrogen bond network between the protein and SQ species in cyt aa_3-600. These data also provide the first direct evidence that R70 of subunit I in cyt aa_3-600 is hydrogen bonded to the menasemiquinone at the high affinity site. The data presented are the product of collaborative efforts with Drs. Sergei Dikanov (UIUC), Alex Taguchi (UIUC), Rimma Samoilova (Russian Academy of Sciences) and Patrick O'Malley (U of Manchester, UK).

6.2. Materials and methods

6.2.1. Generating semiquinone radical in cytochrome aa_3-600 and Q_h-site mutants

The EPR samples were in the final buffer condition consisting of 100 mM Tris, 10 mM EDTA, 10 % glycerol, 0.05 % DDM, pH 8.1 – 8.2. Purified D74H mutation was oxidized with ~3.5 mM $K_3Fe(CN)_6$ briefly and then desalted by PD-10 column (Amersham Pharm.) and buffer exchanged, prior to generation of semi-menaquinone with NADH (Sigma, St. Louis, MO). However, the semi-menaquinone radical signal was very weak and was not adequate for pulsed EPR experiments. The samples were concentrated, and buffer was exchanged using Amicon centrifugal filters (Millipore, Bedford, MA).

6.2.2. Pulsed EPR experiments (ESEEM and HYSCORE)

The continuous wave EPR measurements were performed at a microwave frequency of 9 GHz (X-band) Varian EPR-E122 spectrometer (110 K) and at 34 GHz (Q-band) Bruker ELEXYSYS 580 (90 K) equipped with a separate Q-band microwave bridge and cavity operating at a 100 kHz modulation frequency. The X- and Q-band pulsed EPR experiments were

performed at 60 K, using Bruker ELEXSYS E580 spectrometer equipped with Oxford CF 935 cryostat. There was no change in the radical signal intensity at 80 K. Field-swept two-pulse ($\pi/2-\tau-\pi-\tau-$echo) echo-detected EPR spectra were acquired to determine field positions for subsequent pulse experiments. One- and two-dimensional three-pulse ($\pi/2-\tau-\pi/2-T-\pi/2-$echo) and four-pulse ($\pi/2-\tau-\pi/2-t_1-\pi-t_2-\tau-$echo) experiments were carried out as described in the previous work [47].

One-dimensional (1D) three-pulse ESEEM data were recorded as 300 time points with increases in 24 ns steps and $\tau = 88$ ns. A second dimension was added to this dataset by repeating scans (~20) with 16 ns step-wise increase for each scan. Two-dimensional (2D) four-pulse ESEEM (HYSCORE) data were collected as 256 X 256 time points defined by two axes. The initial τ value was set at either 136 ns or other delay times with step-wise increases of 16, 20, or 32 ns. Spectral processing of three- and four-pulse ESEEM was performed using Bruker WIN-EPR software. The procedure included subtraction of the relaxation decay (fitting by 3-6 degree polynomials), apodization (Hamming window), zero filling, and fast Fourier transformation. Pulsed ENDOR experiments were accomplished using Davies ($\pi-t-\pi/2-\tau-\pi-\tau-$echo) and Mims ($\pi/2-\tau-\pi/2-t-\pi/2-\tau-$echo) sequences, where a radio frequency (π-pulse) was introduced during time t. Orientation-selective Q-band ^{15}N Davies ENDOR experiments were conducted with microwave $\pi/2-$pulse of 120 ns, $\tau = 500$ ns, and radio frequency (RF) $\pi-$pulse of 70 μs. The details of these experiments are discussed elsewhere [56, 67, 98].

(See Section 4.2.5 for analysis of ^{1}H HYSCORE spectra)

6.3. Results and discussion

6.3.1. Structural characterization of SQ stabilized in R70H mutant of cyt aa_3-600

Nitrogens interacting with the SQ

Figure 6.1 shows stacked plots of the three-pulse ESEEM spectra of SQ in the wild type and R70H cyt aa3-600. The three-pulse ESEEM spectrum of the wild type protein contains only two lines at frequencies 3.5 and 4.4 MHz and does not resolve any other features. These frequencies are correlated in the 2D ESEEM spectrum as belonging to the same nitrogen with hfi coupling of ~0.9 MHz. This nitrogen is tentatively assigned to N_ε of R70 based on the estimated $K^2(3+\eta^2)$ value, which is similar to that determined for N_ε of R71 in cyt bo_3. In the case of cyt bo_3, this assignment was directly confirmed using selective ^{15}N labeling of the nitrogens in the arginine residue.

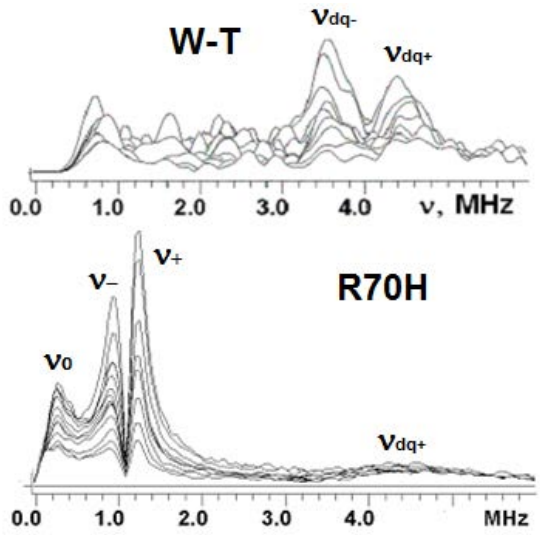

Figure 6.1. Comparison of the X-band ^{14}N three-pulse ESEEM spectra of wild-type cyt aa_3-600 and the R70H mutant. Three lines at low frequencies (0.25, 0.99, and 1.24 MHz) in the spectrum of the mutant indicate ^{14}N with a quadrupole coupling constant K=0.37 MHz, which is typical of a protonated histidine nitrogen.

In contrast, the three-pulse spectrum of SQ in the R70H mutant has a shape typical for a single ^{14}N recorded near cancellation conditions and allows for an immediate assignment of the narrow peaks at ~0.25, 0.99 and 1.24 MHz to three nuclear quadrupole resonance frequencies ν_0, ν_- and ν_+ with the property $\nu_0 + \nu_- = \nu_+$ (see Eqn 6 in Section 4.1.2). There is also a much weaker and broader line at ~4-5 MHz, which can be suggested to belong to the ν_{dq+} transition. This assignment was confirmed by the ^{14}N HYSCORE spectrum in Figure 6.2. The spectrum exhibits cross-peaks correlating ν_0, ν_- and ν_+ with ν_{dq+}, thus indicating that they belong to different electron spin manifolds. They also allow for a more precise determination of the value of $\nu_{dq+} \approx$ 4.3-4.7 MHz from the maximum intensity of the (ν_{dq+}, ν_+) cross-correlation.

Having obtained the frequencies for ν_0, ν_-, ν_+ and ν_{dq+}, equations 6 and 7 (see Section 4.1.2) along with the ^{14}N Zeeman frequency ($^{14}\nu_N$ = 1.06 MHz) were used to determine the quadrupole coupling constant (qcc) K = 0.37 MHz, the asymmetry parameter η = 0.32, and the hfi coupling ^{14}A = 2.18 MHz for the nitrogen nucleus.

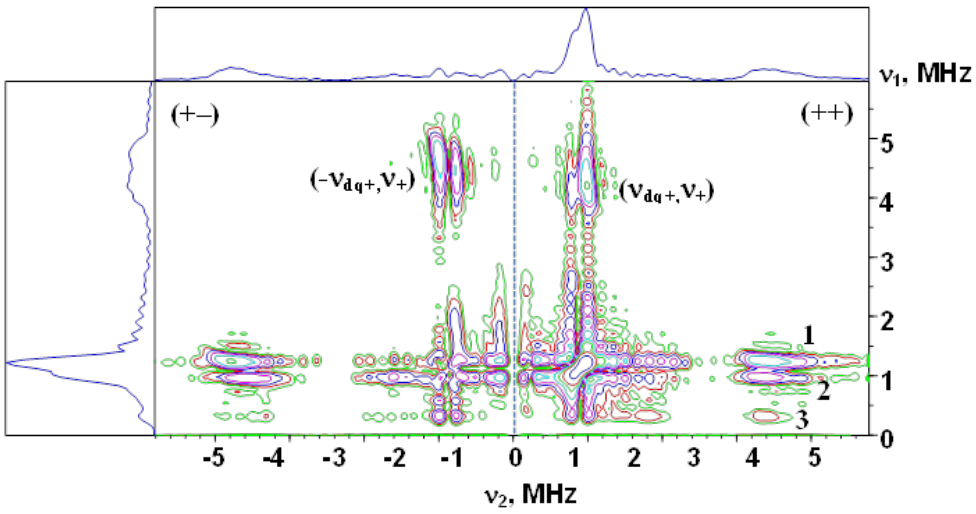

Figure 6.2. Contour representation of the X-band ^{14}N HYSCORE spectrum of SQ_H in R70H cyt aa_3-600. Numbers define the following cross-peaks: 1, (ν_+,ν_{dq+}); 2, (ν_-,ν_{dq+}); 3, (ν_0,ν_{dq+}). Experimental parameters: magnetic field 344.4 mT, time between first and second pulses τ = 136 ns, microwave frequency 9.659 GHz, temperature 80 K, step Δt = 20 ns.

The Q-band ^{14}N HYSCORE spectrum of SQ in R70H cyt aa3-600 shows one intensive pair of cross-peaks 1 in the (++) quadrant at (9.9, 5.3) MHz (see Figure 6.3). The ^{14}N Zeeman frequency in this experiment was 3.75 MHz (1218.7 mT) giving $\nu_{ef-}/K = 7$ and $\nu_{ef+}/K = 13$, thus indicating that the observed cross-peaks correlate dq-transitions from opposite manifolds. These frequencies provide an estimate of the hfi coupling $^{14}A \approx 2.3$ MHz in good agreement with the value determined from the X-band spectra.

In summary, the ^{14}N spectra of SQ in the R70H mutant cyt aa_3-600 oxidase resolve an interaction with only a single nitrogen (N1) possessing significant presumably isotropic hfi coupling resulting from the transfer of unpaired spin density from the SQ via a hydrogen bond bridge. The value of K characterizes the chemical type of the ^{14}N nucleus interacting with the SQ, which is typical for a protonated nitrogen of an imidazole residue [98].

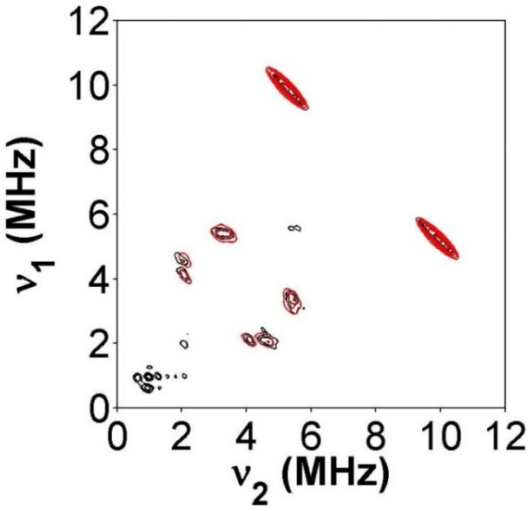

Figure 6.3. Comparison of the experimental and simulated Q-band ^{14}N HYSCORE spectra of SQ_H in cyt aa_3-600 at orientation of the external magnetic field in-plane with the g_Y axis. Spectra are presented in contour mode. Simulations are shown in red. Experimental parameters: microwave frequency 34.166 GHz, time between first and second pulses τ = 136 ns, π/2-pulse length = 28 ns, temperature = 60 K, magnetic field = 1218.7 mT.

The ^{14}N ESEEM spectra do not resolve any lines from other side-chain and peptide nitrogens of the nearby protein environment. These nitrogens are coupled more weakly and do not produce well-defined lines in the ^{14}N powder-type spectra, due to the influence of the nuclear quadrupole interaction (nqi). However, the lines from weakly coupled nitrogens (N_{wc}) can be observed in 2D ^{15}N ESEEM spectra, which are not complicated by the nqi, as shown in our previous experiments with cyt bo_3 and wild type cyt aa_3-600. Furthermore, ^{15}N spectra allow for a more precise determination of the isotropic and anisotropic components of the hfi tensor of the nitrogen nuclei.

The X-band ^{15}N HYSCORE spectrum for SQ in ^{15}N uniformly labeled R70H cyt aa_3-600 is shown in Figure 6.4. The spectrum contains cross-features 1 and 1', located in the (+-) and (++) quadrants, with maxima at (-3.1, 0.2) MHz (1) and (2.8, 0.3) MHz (1'). The first-order estimates of the hyperfine couplings are 3.3 and 3.1 MHz, respectively (2.4 and 2.2 MHz when scaled to ^{14}N). These values are consistent with the coupling estimated from the ^{14}N HYSCORE spectra.

In addition, the (++) quadrant exhibits feature N_{wc} with a maximum near the diagonal point ($^{15}\nu_N$, $^{15}\nu_N$) and accompanying shoulders symmetrically extended up to ~1 MHz along the antidiagonal (see Figure 3). Two resolved splittings, ~0.4 MHz (1_{wc}) and ~0.8 MHz (2_{wc}), can be suggested from an analysis of the shoulder's line shape. The N_{wc} features result from multiple nonequivalent contributions of weakly coupled ^{15}N nuclei in the immediate vicinity of SQ. Comparison of the N_{wc} line shape with the previously published data for SQ in the wild type and D75H cyt bo_3 reveals unique characteristics for each spectrum that reflect differences in the protein environment. To further resolve the individual interactions with the nitrogens in the SQ environment, selective ^{15}N labeling of individual residues needs to be employed.

The 2D-ESEEM studies found a significant difference between the SQs of UQ_8 in cyt bo_3 and MQ_7 in cyt aa_3-600. ^{14}N and ^{15}N ESEEM experiments were performed with the SQ in wild type cyt aa_3-600 containing natural abundance ^{14}N and with uniformly ^{15}N-labeled protein [16]. ^{14}N spectra revealed a nitrogen with hyperfine coupling $^{14}A = 0.94$ MHz and nqi parameter, $\kappa = K^2(3+\eta^2) = 2.7$ MHz^2. For the SQ in the wild type cyt bo_3 the $N_\varepsilon H$ of R71 possesses the largest hfi coupling $^{14}A \approx 1.8$ MHz and an nqi tensor with K = 0.93 MHz and $\eta = 0.51$ [47]. These values give $\kappa = 2.82$ MHz^2, which differs only slightly from the estimated value of $\kappa = 2.7$ MHz^2 for the nitrogen from cyt aa_3-600. This close coincidence of the nqi parameter κ suggests that the N_ε of R70 in cyt aa_3-600 also takes on the role of the nitrogen carrying the largest unpaired spin density and, thus, is involved in H-bond formation with the SQ. The ^{15}N HYSCORE spectrum exhibits extended shoulders with two resolved maxima corresponding to couplings of 0.96 and 0.4 MHz, respectively. It is likely that the ^{15}N line shape with two resolved splittings is formed by the spectra from several (probably more than two) nitrogens that are partially overlapped.

Mutagenesis of the conserved arginine at the Q_h-site indicates a significant difference between cyt bo_3 and cyt aa_3-600. In particular, converting R71 to histidine is lethal for the E. coli oxidase, but the same mutant in *B. subtilis* cyt aa_3-600 is more active than the wild type. Our X-band 1D- and 2D-ESEEM experiments with the R70H mutant show the formation of a H-bond between the SQ and histidine nitrogen possessing the qcc K = 0.36 MHz, typical for protonated nitrogens of an imidazole ring. The isotropic coupling $^{14}A \approx 2$ MHz of this nitrogen exceeds the couplings in the wild type and is comparable to the largest couplings in wild type cyt bo_3 (1.8 MHz) and D75H mutant (2.7 MHz) [47]. In addition, ^{15}N X- and Q-band HYSCORE spectra of R70H clearly show the presence of nitrogen(s) with weaker couplings of ~0.5 MHz.

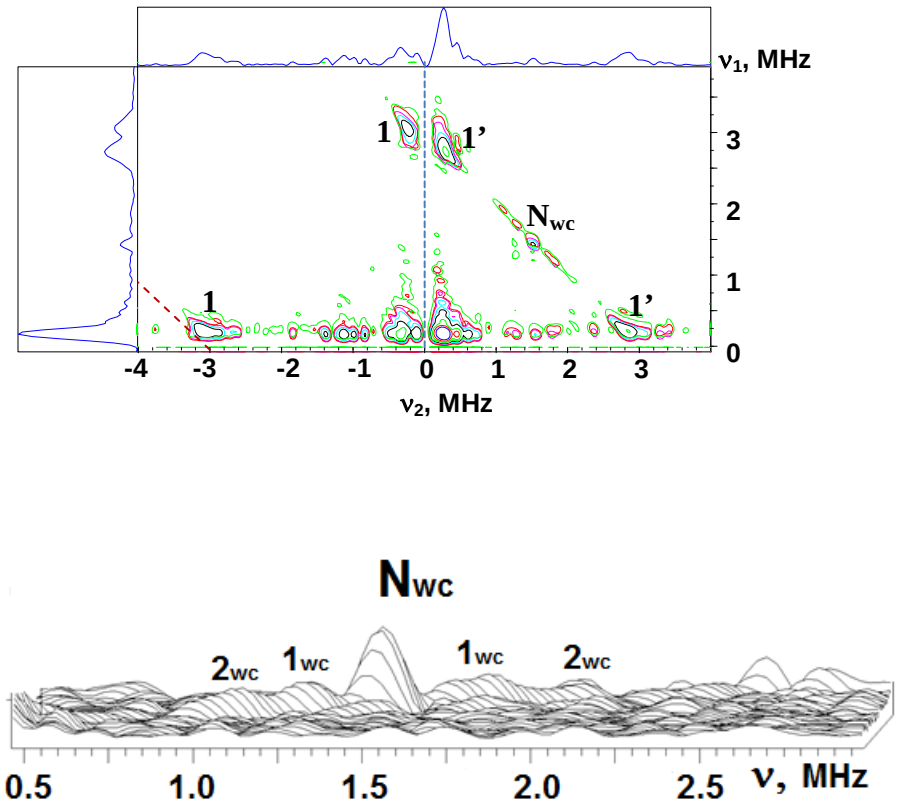

Figure 6.4. Contour (top) presentation of the ^{15}N HYSCORE spectrum of SQ_H in ^{15}N uniformly labeled R70H cyt aa_3-600. Stacked (bottom) presentation of the N_{wc} feature in the (++) quadrant of the spectrum. Experimental parameters: magnetic field = 343.25 mT, time between first and second pulses τ = 136 ns, microwave frequency = 9.625 GHz, temperature = 60 K.

These weakly coupled nitrogens, as well as the nitrogen donors in wild type cyt aa_3-600, are not yet identified. The interpretation and assignment of ^{1}H and $^{14, 15}$ N data are based on the results of DFT calculations because selective isotopic ^{15}N labeling of specific amino acids using auxotropic hosts have not been performed for cyt aa_3-600 and R70H mutant.

X- and Q-band ESEEM/ENDOR experiments with the SQ in the R70H mutant of cyt aa_3-600 have established an interaction with a nitrogen possessing a significant ~2 MHz isotropic hfi coupling. This hfi coupling strength exceeds those found previously in the wild type protein. The qcc of this nitrogen is consistent with the constants reported for the ^{14}N

histidine nitrogens hydrogen bonded with the SQ in other quinone processing sites [98]. Therefore, we conclude that the largest unpaired spin density in the R70H mutant is transferred through hydrogen bonding with the histidine nitrogen.

From a comparative analysis of the hfi and nqi tensor characteristics for the histidine N_δ H-bond donors of SQs in different quinone sites from Table 3 in a previous publication [67], a remarkably good linear correlation between the isotropic hfi constant ^{14}A and the asymmetry parameter η exists [98]. In contrast to N_δ, two points in the graph of A vs. η corresponding to hydrogen bonded N_ε in the Q_i site of the bc_1 complex and the Q_h-site of D75H mutant of cyt bo_3 significantly deviate from the linear plot.

The point corresponding to the H-bonded nitrogen in the R70H mutant also deviates significantly from the linear plot. This suggests that the identity of the H-bond donor from H70 to SQ is the N_ε. Previous studies of the D75H cyt bo_3 mutant have shown that in addition to H75, H98 is also involved in weak H-bonding with the oxygen from the opposite carbonyl through N_ε. Taking into account the similarity of the Q_h-sites, one can suggest that N_ε of H94 is also H-bonded in wild type and R70H cyt aa_3-600. This H-bond would lead to the appearance of the isotropic coupling with the N_ε of the order ~0.5 MHz.

The methyl protons interacting with the SQ

Figure 6.5 shows the ^1H HYSCORE spectra of the SQ in R70H cyt aa_3-600 prepared in ^1H2O. Similar spectra for the SQ in cyt bo_3 and cyt aa_3-600 have been discussed previously [16, 46, 47]. In addition to a diagonal peak at the proton Zeeman frequency ($^1\nu_H$, $^1\nu_H$) ($^1\nu_H \approx 14.7$ MHz), the spectrum contains several pairs of resolved cross-features located symmetrically relative to the diagonal. The cross-peaks assigned as 1_H and 6_H are not eliminated by D_2O (see Figure 6.6). The H/D exchange does affect the intensity of cross-peaks 6_H, thus indicating the

simultaneous contribution of exchangeable and nonexchangeable protons. Additional support for this conclusion was obtained from pulsed ENDOR spectra [98]. The cross-peaks 1_H from nonexchangeable proton(s) possess the largest hfi splitting, of the order ~11-12 MHz, and can be tentatively assigned to the protons of the methyl group stemming from the quinone ring based on previous studies of cyt bo_3 and its mutants and cyt aa_3-600.

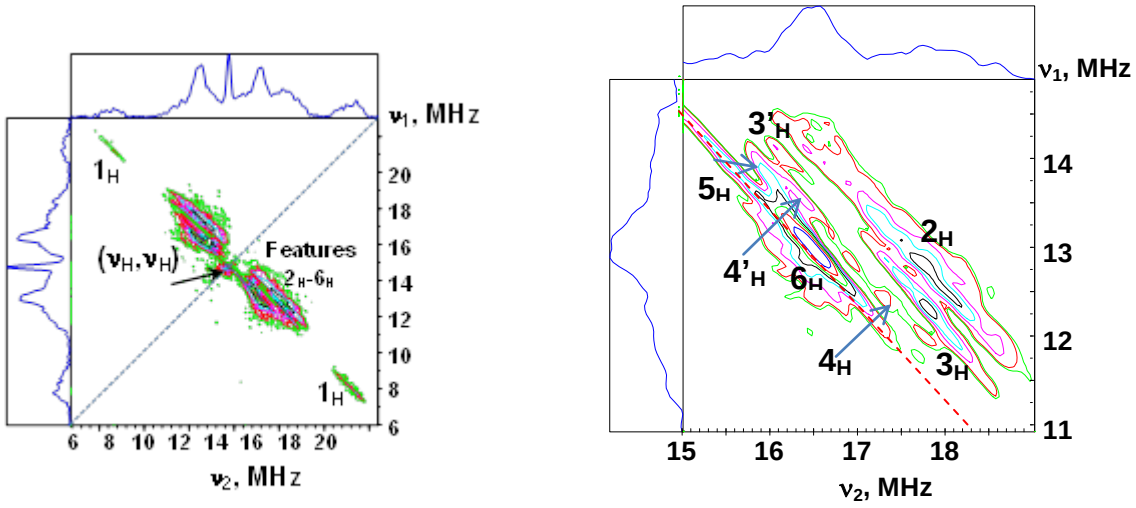

Figure 6.5. ^1H HYSCORE spectrum of the SQ_H from R70H cyt *aa*$_3$-600 in ^1H_2O buffer. The full presentation (left) and an enhanced view of features **2_H-6_H** (right) are shown. The spectrum was obtained after Fourier transformation of the two-dimensional time-domain patterns containing 256x256 points with a 20-ns step. The magnetic field was 345.25 mT, time τ between the first and second microwave pulses was 200 ns, and the microwave frequency was 9.680 GHz.

A simple quantitative measure of the asymmetry in the spin density distribution can be obtained from the ^1H couplings of the methyl group in UQs or 3-methyl-1, 4-naphthoquinones. In contrast to these results, the isotropic constant varies significantly in proteins [98, Table 4]. The hfi coupling A ≈ 10-11 MHz was found for the methyl protons of SQ in cyt bo_3 and cyt aa_3-600 and the A_1 center of the PS I [16, 46, 72, 102]. The couplings ~8-9 MHz in D75E and D75H mutants of cyt bo_3 are still 1.5 times the values in alcohol solutions [101]. By comparison, the SQ in the R70H mutant of cyt aa_3-600 possesses the largest value of the isotropic coupling

for the methyl protons of 12.8 MHz, though an increase of the coupling relative to the corresponding value in frozen solution is still slightly higher for UQ in cyt bo_3 (1.85 ± 0.15) than the MQ in R70H (1.7 ± 0.1). The asymmetrical H-bonding pattern exhibited by the SQ in these proteins is the opposite of that found for the SQ_A in the bacterial RC from *Rb. sphaeroides*. The isotropic coupling of the methyl protons is ~4.5-5.0 MHz in the SQ_A, that is, smaller than that of an anion radical in solution and consistent with the stronger hydrogen bond donation to the O4 oxygen than the O1 oxygen (ubiquinone numbering) [75]. In addition, the methyl protons for the SQ of the MQ-9 in the Q_A site of the reaction center from *Rhodopseudomonas viridis* have an isotropic constant that is not quite as large, ~6.8 MHz [100]. This is even smaller, 5.5 MHz, for MQ-8 in *E. coli* NarGHI (nitrate reductase). These data suggest the same explanation as for SQ_A above. In contrast, the stronger hydrogen bond donation to the O1 oxygen explains the large methyl couplings in cyt bo_3, cyt aa_3-600 and PS I.

In the cases discussed above, several nonequivalent hydrogen bonds are formed between the SQ oxygens and protein residues. A cumulative effect resulting from the common influence of H-bonds of different geometries and strengths leads to the asymmetrical redistribution of unpaired spin density in the SQ. DFT calculations taking into account all H-bonds around the SQ can provide a good model of the spin density distribution as well as an explanation for the experimentally observed hfi couplings.

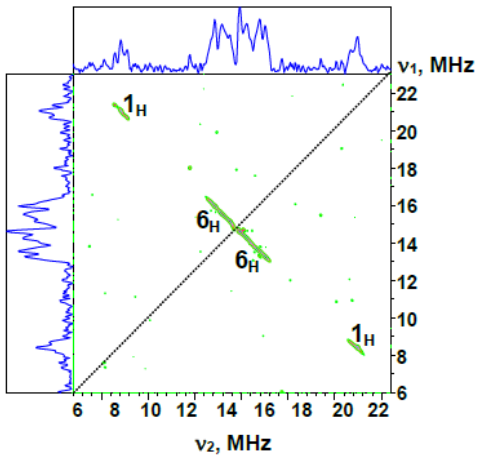

Figure 6.6. ^{1}H HYSCORE spectrum of the SQ from R70H cyt aa_3-600 in D_2O buffer. The spectrum was obtained after Fourier transformation of the two-dimensional time-domain patterns containing 256x256 points with a 20 ns step. The magnetic field was 345.3 mT, time τ between the first second microwave pulses was 400 ns and the microwave frequency was 9.682 GHz.

Exchangeable protons in close proximity to the SQ

In Figure 6.5, the ^{1}H HYSCORE spectra of the SQ in R70H cyt aa_3-600 prepared in $^{1}H_2O$ show cross-peaks 2_H, 3_H, 4_H and $4'_H$, 5_H and $5'_H$. These cross-peaks completely disappear in the HYSCORE spectra (see Figure 6.6) obtained under the same conditions when the sample is prepared in D_2O, showing that they are produced by exchangeable protons [98]. From the spectral features of the exchangeable protons, one can reasonably suggest that the extended ridges 2_H, 3_H and 4_H belong to three unique protons based on differences in the deviation of the cross-ridges from the anti-diagonal passing through ($^{1}\nu_H$, $^{1}\nu_H$). However, the identity of $3'_H$, $4'_H$ and 5_H is not clear and needed to be verified by linear regression of ridges 2_H-4_H in ν_H^2 vs ν_H^2 coordinates. Linear regression analysis of 2_H, 3_H and 4_H can be found in Yi et al. [98]. Extension of the linear fit of 2_H crosses $4'_H$ but its orientation is not coincident with the line defined by 2_H. Moreover, the linear extrapolation of 3_H coincides well with the $3'_H$ and 5_H segments, suggesting that these features belong to the same extended ridge. The remaining

feature 4_H and $4'_H$ align reasonably well by linear regression, although part of the low intensity 4_H ridge deviates substantially from the straight line, which may be explained by the influence of Fourier transform artifacts accompanying the intensive 6_H peak.

Quantitative analysis of the cross-ridge contour line shapes in ν_1^2 vs ν_2^2 coordinates [61, 62] and simulations of the Davies pulsed ENDOR spectra provide the isotropic and anisotropic components of the hfi tensors under an axial approximation for protons H1-H4. The data are summarized in Table 6.1. Cross-peaks 6_H are produced by several non-exchangeable and weakly coupled exchangeable protons and the parameters determined from their formal analysis would not correspond to any real structural characteristics.

Table 6.1: 1Hyperfine tensors of semiquinone (SQ) in R70H cytochrome aa_3-600 in H_2O*

Proton	Cross-ridges	A (MHz)	T (MHz)
H1	1_H	12.8	1.5
H2	2_H	0.7	5.6
H3	3_H-$3'_H$-5_H	0.7	4.5
H4	4_H-$4'_H$	0.5	3.5

*Determined from HYSCORE spectra. Selection of the isotropic couplings for methyl and exchangeable protons is based on analysis of pulsed ENDOR spectra and DFT calculations.

Additional support for the hfi tensors of the exchangeable protons reported above was obtained from the complementary one-dimensional four-pulse ESEEM spectra (see Figure 6.7) [99]. The frequency shifts (i.e. H2, H3 and H4) from $2\nu_H$ proton Zeeman frequency are absent in sample prepared in D_2O buffer (not shown). Similarly, these spectra show the existence of three exchangeable protons with anisotropic couplings $T \approx 5.6$, 4.5 and 3.4 MHz.

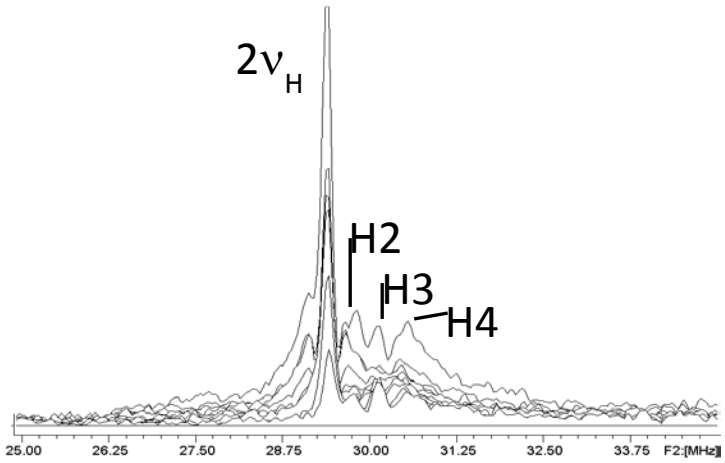

Figure 6.7. Four-pulse ESEEM spectra of the SQ in the R70H cyt aa_3-600 prepared in H2O. The spectra was recorded while time between the second and third or third and fourth microwaves pusles, t1 and t2 (t1 = t2) respectively, was varied. 800 points were accumulated with 12 ns steps at a fixed time τ = 100 ns (farthest trace). The mw frequency was 9.678 GHz and the magnetic field was 345.3 mT.

Comparison of hfi couplings for the exchangeable protons in the R70H mutant indicates that the replacing arginine with histidine has unaffected one strong hfi (5.6 MHz) but strengthened two other couplings up to 4.5 and 3.6 MHz from the value of 2.9 MHz in the wild type protein. Analysis of the 1D- and 2D- ^{1}H ESEEM spectra of SQ in the R70H cyt aa_3-600 indicates three protons with the anisotropic hyperfine interaction constants $|T| \approx 5.6$, 4.6 and 3.8 MHz. In contrast, two exchangeable protons with $|T| \approx 5.6$ and 2.9 MHz were resolved in the spectra of the wild type protein. The deviation of the cross-ridges from the anti-diagonal (ν_H, ν_H) and the shift of the sum-combinations from $2\nu_H$ for $T \leq 2.9$ MHz are close to the resolution limits defined by the individual width of the spectral lines. Therefore, there could be at least one more proton with a similar value in wild type cyt aa_3-600 that was not resolved previously in the spectra.

The hfi couplings can be interpreted in terms of O···H bond distance by point-dipole model estimation and DFT calculations. Protons hydrogen bonded with different SQs in frozen water and alcohol solutions possess the typical value $|T| \approx 2.6 - 2.9$ MHz [77, 101, 103]. DFT calculations show that a hyperfine interaction coupling of $|T| \approx 3$ MHz is consistent for a proton participating in a planar hydrogen bond, forming an angle 60° with the C=O bond, and with a H-bond length ~1.8 Å. A similar bond length can be estimated using a point-dipole model for the O···H bond. One of the H-bonds to the SQ of wild type cyt aa_3-600 involving proton with $|T| \approx$ 2.9 MHz is close to this geometry and can be assumed to have ~1.8 Å H-bond length.

The second exchangeable proton detected in cyt aa_3-600 has a much larger anisotropic coupling, $|T| \sim 5.6$ MHz that suggests an H-bond with the proton located within a shorter distance of the carbonyl oxygen of SQ. However, the point-dipole approximation becomes inappropriate for H-bond distances less than 1.7 Å having $T > 3.5$ MHz. The DFT calculations suggest that the value $|T| \approx 5.6$ MHz would correspond to the distance ~1.3 Å, implying a substantial covalent character for the O-H bond.

The DFT calculations were performed on models using homologous cyt bo_3 Q_h-site x-ray structure, in order to determine the unpaired spin densities on the SQ ring and to simulate H-bonding around the SQ based on calculated hfi couplings. In the absence of accurate structural data for cyt aa_3-600, O'Malley Group (U of Manchester, UK) explored only idealized small models with full or partial geometry optimization [98]. However, by comparing different models, the calculated values have provided valuable insight into understanding how the EPR data reflect structural differences between WT and R70H. For the mutant R70H, three distinct exchangeable protons having T values of 5.6, 4.5 and 3.5 MHz were determined from an analysis of the ^1H

HYSCORE spectrum. The calculated T values for the R70H model are 4.1, 3.3 and 3.9 MHz for H70, H94 and D75, respectively, which are in qualitative agreement with the experiment.

The DFT data show that the hydrogen bonding interaction of the menaquinone SQ with the guanidinium group of the R70 residue in cyt aa_3-600 is weaker than the equivalent interaction between R71 and ubiquinone SQ in cyt bo_3. This can be explained by a longer hydrogen bond formed to R70 in cyt aa_3-600. The R70H mutation in cyt aa_3-600 results in more optimal hydrogen bond to the menaquinol O1, increasing the asymmetry of the spin density distribution in SQ. In contrast, the equivalent R71H mutation in cyt bo_3 forms a less optimal hydrogen bond, which precludes formation of SQ as well as quinol oxidase activity. Although the R71H mutant of cyt bo_3 does not form a stable semiquinone, the D75H mutant of cyt bo_3, which is also inactive, does form a SQ, which does have a more symmetrical spin density distribution based on a comparison of the ^{1}H methyl couplings.

6.4. Conclusions

The current work provides the first direct evidence that R70 of subunit I in cyt aa_3-600 is hydrogen bonded to the menasemiquinone at the high affinity site. The R70H mutant can stabilize SQ at the Q_h-site. X- and Q-band ^{14,15}N pulsed EPR data and DFT calculations show that the SQ interacts with the N_ε of H70 based on its qcc, e^2qQ/h = 1.44 MHz, that is identifiable as protonated imidazole nitrogens. This nitrogen possesses a strong isotropic hyperfine coupling ($^{14}A \approx 2.0$ MHz) resulting from unpaired spin density transferred from the SQ via a hydrogen bond bridge. This hydrogen bond replaces the H-bond with N_ε from the R70 side chain in wild type cyt aa_3-600. The mutation also changes the number and strength of the hydrogen bonds in the SQ environment as determined by the analysis of the ^{1}H 2D-ESEEM spectra. However, the

R70H mutation still retains significant asymmetry in the unpaired spin density distribution as indicated by a strong ^{1}H methyl isotropic coupling equaling to 12.8 MHz. Despite the alterations in the immediate environment of the SQ, the R70H remains catalytically active. This is in contrast to the equivalent mutation in the close homologue, the cyt bo_3 ubiquinol oxidase from *E. coli*, where the similar R71H mutation eliminates function.

7. References

1. Hill, B. C. and Peterson, J. (1998) Spectral and cyanide binding properties of the cytochrome aa_3 (600 nm) complex from *Bacillus subtilis*. *Arch. Biochem. Biophys. 350*, 273-282.

2. Puustinen, A., Verkhovsky, M. I., Morgan, J. E., Belevich, N. P. and Wikstrom, M. (1996) Reaction of the *Escherichia coli* quinol oxidase cytochrome bo3 with dioxygen: The role of a bound ubiquinone molecule. *Proc. Natl. Acad. Sci. 93*, 1545-1548.

3. Trumpower, B. L. and Gennis, R. B. (1994) Energy transduction by cytochrome complexes in mitochondrial and bacterial respiration: the enzymology of coupling electron transfer reactions to transmembrane proton translocation. *Annu. Rev. Biochem. 63*, 675-716.

4. Svensson, M. and Nilsson, T. (1993) Flow-flash study of the reaction between cytochrome bo and oxygen. *Biochemistry, 32*, 5442-5447.

5. Lauraeus, M., Morgan, J. E. and Wikstrom, M. (1993) Peroxy and ferryl intermediates of the quinol-oxidizing cytochrome aa_3 from *Bacillus subtilis*. *Biochemistry 34*, 10245-10255.

6. Garcia-Horsman, J. A., Barquera, B., Rumbley, J., Ma, J. and Gennis, R. B. (1994) The superfamily of heme-copper respiratory oxidases. *J. Bacteriol. 176*, 5587-5600.

7. Santana, M., Kunst, F., Hullo, M. F., Rapoport, G., Danchin, A., and Glaser, P. (1992) Molecular cloning, sequencing, and physiological characterization of the qox operon from Bacillus subtilis encoding the aa_3-600 quinol oxidase. *J. Biol. Chem*. 267: 10225-10231.

8. Chepuri, V., Lemieux, L., Au, D. C.-T. and Gennis, R. B. (1990) The sequence of the cyo operon indicates substantial structural similarities between the cytochrome o ubiquinol oxidase of *Escherichia coli* and the aa_3-type family of cytochrome c oxidases. *J. Biol. Chem.* 265, 11186-11192.

9. Lauraeus, M., Haltia, T., Saraste, M. and Wikstrom, M. (1991) *Bacillus subtilis* expresses two kinds of haem-A-containing terminal oxidases. *Eur. J. Biochem. 197*, 699-705.

10. Hill, B. C. (1993) The reaction of *Bacillus subtilis* aa_3-600 oxidase with oxygen: An aa_3-oxidase lacking the Cu_A site. *Biochem. Biophys. Res. Commun. 192*, 665-670.

11. Power, L., Lauraeus, M., Reddy, K. S., Chance, B. and Wikstrom, M. (1994) Structure of the binuclear heme iron-copper site in the quinol-oxidizing cytochrome aa_3 from *Bacillus subtilis. BBA, 1183*, 504-512.

12. Fann, Y. C., Ahmed, I., Blackburn, N. J., Boswell, J. S., Verkhovskaya, M. I., Hoffman, B. M. and Wikstrom, M. (1995) Structure of Cu_B in the binuclear heme-copper center of the cytochrome aa_3-type quinol oxidase from *Bacillus subtilis*: An ENDOR and EXAFS study. *Biochemistry, 34*, 10245-10255.

13. Fisher, N. and Rich, P. R. (2000) A motif for quinone binding sites in respiratory and photosynthetic systems. *J. Mol. Biol. 296,* 1153-1162.

14. Yu, J., Hederstedt, L. and Piggot, P. J. (1995) The cytochrome bc complex (menaquinone: cytochrome c reductase) in *Bacillus subtilis* has a nontraditional subunit organization. *J. Bacteriol. 177,* 6751-6760.

15. Mattatall, N. R., Cameron, L. M. and Hill, B. C. (2001) Transient-state reduction and steady-state kinetic studies of menaquinol oxidase from Bacillus subtilis, cytochrome aa3-600. Spectroscopic characterization of the steady-state species. *Biochemistry,* 40, 13331-13341.

16. Yi, S. M., Narasimhulu, K. V., Samoilova, R. I., Gennis, R. B. and Dikanov, S. A. (2010) Characterization of the semiquinone radical stabilized by the cytochrome aa_3-600 menaquinol oxidase of *Bacillus subtilis*. *J. Biol. Chem. 285,* 18241-18251.

17. Abramson, J., Riistama, S., Larsson, G., Jasaitis, A., Svensson-Ek, M., Laakkonen, L., Puustinen, A., Iwata, S. and Wikstrom, M. (2000) The structure of the ubiquinol oxidase from *Escherichia coli* and its ubiquinone binding site. *Nat. Struc. Biol. 7,* 910-917.

18. Hellwig, P., Yano, T., Ohnishi, T. and Gennis, R. B. (2002) Identification of the residues involved in stabilization of the semiquinone radical in the high-affinity ubiquinone binding site in cytochrome bo_3 from Escherichia coli by site-directed mutagenesis and EPR spectroscopy. *Biochemistry 41,* 10675-10679.

19. Kobayashi, K., Tagawa, S. and Mogi, T. (2000) Transient formation of ubisemiquinone radical and subsequent electron transfer process in the *Escherichia coli* cytochrome bo. *Biochemistry, 39,* 15620-15625.

20. Musser, S. M., Stowell, M. H. B., Lee, H. K., Rumbley, J. N. and Chan, S. I. (1997) Uncompetitive substrate inhibition and noncompetitive inhibition by 5-n-undecyl-6-hydroxy-4,7-dioxobenzothiazole (UHDBT) and 2-n-nonyl-4-hydroxyquinoline-N-oxide (NQNO) is observed for the cytochrome bo_3 complex: Implications for a $Q(H_2)$-Loop proton translocation mechanism. *Biochemistry, 36,* 894-902.

21. Welter, R., Gu, L.-Q., Yu, L. and Yu, C.-A., Rumbley, J. and Gennis, R. B. (1994) Identification of the ubiquinol-binding site in the cytochrome bo_3-ubiquinol oxidase of *Escherichia coli*. *J. Biol. Chem. 269,* 28834-28838.

22. Tsatsos, P. H., Reynolds, K., Nickels, E. F., He, D.-Y., Yu, C.-A. and Gennis, R. B. (1998) Using matrix assisted laser desorption ionization mass spectrometry to map the quinol binding site of cytochrome bo_3 from *Escherichia coli*. *Biochemistry, 37,* 9884-9888.

23. Sato-Watanabe, M., Mogi, T., Sakamoto, K., Miyoshi, H. and Anraku, Y. (1998) Isolation and characterizations of quinone analogue-resistant mutants of bo-type ubiquinol oxidase from *Escherichia coli*. *Biochemistry 37,* 12744-12752.

24. Yap, L. L., Lin, M. T., Ouyang, H., Samoilova, R. I., Dikanov, S. A. and Gennis, R. B. (2010) The quinone-binding sites of the cytochrome bo3 ubiquinol oxidase from Escherichia coli. *BBA 1797*, 1924-1932.

25. Sato-Watanabe, M., Mogi, T., Miyoshi, H., Iwamura, H., Matshshita, K., Adachi, O. and Anraku, Y. (1994a) Structure-function studies on the ubiquinol oxidation site of the cytochrome bo complex from *Escherichia coli* using p-benzoquinones and substituted phenols. *J. Biol. Chem. 269*, 28908-28912.

26. Sato-Watanabe, M., Mogi,T., Ogura, T., Kitagawa, T., Miyoshi, H., Iwamura, H. and Anraku, Y. (1994b) Identification of a novel quinone-binding site in the cytochrome bo complex from *Escherichia coli*. *J. Biol. Chem., 269*, 28908-28912.

27. Hastings, S. F., Heathcote, P., Ingledew, W. J. and Rigby, S. E. (2000) ENDOR spectroscopic studies of stable semiquinone radicals bound to the *Escherichia coli* cytochrome bo_3 quinol oxidase. *Eur. J. Biochem. 267*, 5638-5645.

28. Berry, E. A. and Trumpower, B. L. Simultaneous determination of hemes a, b, and c from pyridine hemochrome spectra. *Analytical Biochem*. *161*, 1-15.

29. Lemma, E., Simon, J., Schagger, H. and Kroger, A. (1995) Properties of the menaquinol oxidase (Qox) and of qox deletion mutants of *Bacillus subtilis*. *Arch. Micro. Biol. 163*, 432-438.

30. Rumbley, J. N., Nickels, E. F., Gennis, R. B. (1997) One-step purification of histidine-tagged cytochrome bo3 from Escherichia coli and demonstration that associated quinone is not required for the structural integrity of the oxidase. *BBA, 1340*, 131-142.

31. Henning, H., Vo, L., Alvanese, J. , Hill, B. C. (1995) High-yield purification of cytochrome aa3 and cytochrome caa3 oxidases from *Bacillus subtillus* plasma membranes. *Biochem. J.* 309: 279-283.

32. Lauraeus, M., Haltia, T., Saraste, M. and Wikstrom, M. (1991) *Bacillus subtilis* expresses two kinds of haem-A-containing terminal oxidases. *Eur. J. Biochem*. *19*7, 699-705.

33. Lewin, A., Su, X-D., Hederstedt, L. (2009) Positively regulated glycerol/G3P-dependent Bacillus subtilis gene expression system based on anti-termination. *J. Mol. Microbiol. Biotechnol*. *17,* 61-70.

34. Shapleigh, J. P., Hosler, J. P., Tecklenburg, M. M. J., Kim, Y., Babcock, G. T., Gennis, R. B. and Ferguson-Miller, S. Definition of the catalytic sites of cytochrome oxidase: The specific ligands of heme a and the binuclear metal center. *Proc. Natl. Acad. Sci.* 1992, 89, 4786-4790.

35. Varotis, C., Zhang, Y., Appelman, E. H. and Babcock, G. T. Resolution of the reaction sequence during the reduction of O_2 by cytochrome oxidase. *Proc. Natl. Acad. Sci.* 1993, 90, 237-241.

36. Yoshikawa, S., Shinzawa-Itoh, K., Nakashima, R., Yaono, R., Yamashita, E., Inoue, N., Yao, M., Fei, M. J., Libeu, C. P., Mizushima, T., Yamaguchi, H., Tomizaki, T. and Tsukihara, T. Redox-coupled crystal structural changes in bovine heart cytochrome c oxidase. *Science.* 1998, 280, 1723-1729.

37. Proshlyakov, D. A., Pressler, M. A., DeMaso, C., Leykam, J. F., DeWitt, D. L. and Babcock, G. T. Oxygen activation and reduction in respiration: Involvement of redox-active tyrosine 244. *Science.* 2000, 290, 1588-1591.

38. de Vrij, W., van den Burg, B. and Konings, W. N. (1987) Spectral and potentiometric analysis of cytochromes from *Bacillus subtilis*. *Eur. J. Biochem. 166,* 589-595.

39. Lemma, E., Schagger, H. and Kroger, A. (1993) The menaquinol oxidase of Bacillus subtilis W23. *Arch. Microbiol. 159,* 574-578.

40. Varotsis, C. and Vamvouka, M. (1998) Resonance raman and FTIR studies of carbon monoxide-bound cytochrome aa3-600 oxidase of *Bacillus subtilis*. *J. Phys. Chem. B. 102,* 7670-7673.

41. Bengtsson, J., von Wachenfeldt, C., Winstedt, L, Nygaard, P. and Hederstedt, L. (2004) CtaG is required for formation of active cytochrome c oxidase in *Bacillus subtilis*. *Microbiol. 150,* 415-425.

42. Hederstedt, L., Lewin, A. and Throne-Holst, M. (2005) Heme A synthase enzyme functions dissected by mutagenesis of *Bacillus subtilis* ctaA. *J. Bacteriology, 187,* 8361-8369.

43. Svensson, B. and Hederstedt, L. (1994) *Bacillus subtilis* CtaA is a heme-containing membrane protein involved in heme A biosynthesis. *J. Bacteriology, 176,* 6663-6671.

44. Liu, X. and Taber, H. W. (1998) Catabolite regulation of the *Bacillus subtilis* ctaBCDEF gene cluster. *J. Bacteriology, 180,* 6154-63.

45. Ingledew, W. J., Ohnishi, T. and Salerno, J. C. (1995) Studies on a stabilization of ubisemiquinone by *Escherichia coli* quinol oxidase, cytochrome bo. *Eur. J. Biochem*. 227, 903-908.

46. Yap, L. L., Samoilova, R., Gennis, R. B. and Dikanov, S. A. (2006) Characterization of the exchangeable protons in the immediate vicinity of the semiquinone radical at the Q_h site of the cytochrome bo_3 from *Escherichia coli. J. Biol. Chem. 281,* 16879-16887.

47. Yap, L. L., Samoilova, R. I., Gennis, R. B. and Dikanov, S. A. (2007) Characterization of mutants that change the hydrogen bonding of the semiquinone radical at the Q_h site of the cytochrome bo_3 from *Escherichia coli*. *J. Biol. Chem. 282*, 8777-8785.

48. Clark, J. B. 1992. Electrochemical essays: the oxygen electrode. In *Enzyme Assays* (ed. Eisenthal, R. and Danson, M. J.). IRL Press, Oxford, 181-190.

49. Doi, R.H. and McGloughlin, M. *Biology of Bacilli: Applications to Industry*. Boston: Butterworth-Heinemann, 1992.

50. Saraste, M., Metso, T., Nakari, T., Lauraeus, M. and van der Oost, J. (1991) The *Bacillus subtilis* cytochrome-c oxidase. Variations on a conserved protein theme. *Eur. J. Biochem. 195*, 517-525.

51. Sato-Watanabe, M., Itoh, S., Mogi, T., Matuura, K., Miyoshi, H. and Anraku, Y. (1995) Stabilization of a semiquinone radical at the high-affinity quinone-binding site (Q_h) of the *Escherichia coli* bo-type ubiquinol oxidase. *FEBS, 374*, 265-269.

52. Lin, M. T., Samoilova, R. I., Gennis, R. B. and Dikanov, S. A. (2008) Identification of the nitrogen donor hydrogen bonded with the semiquinone at the Q_h site of the cytochrome bo_3 from *Escherichia coli. JACS, 130*, 15768-15769.

53. Grimaldi, S., MacMillan, F., Ostermann, T., Ludwig, B., Michel, H. and Prisner, T. (2001) $Q_h\bullet^-$ ubisemiquinone radical in the bo_3-type ubiquinol oxidase studied by pulsed electron paramagnetic resonance and hyperfine sublevel correlation spectroscopy. *Biochemistry 40*, 1037-1043.

54. Humphrey, W., Dalke, A. and Schulten, K. (1996) VMD: visual molecular dynamics. *J. Mol. Graph. 14*, 33-38.

55. Arnold, K., Bordoli, L., Kopp, J. and Schwede, T. (2006) The SWISS-MODEL workspace: a web-based environment for protein structure homology modelling. *Bioinformatics, 22*, 195-201.

56. Schweiger, A. and Jeschke, G. (2001) Principles of pulse electron paramagnetic resonance, Oxford University Press: UK.

57. Weil, J. A., Bolton, J. R. and Wertz J. E. (1994) Electron paramagnetic resonance. Elementary theory and practical applications, Wiley: New York.

58. Carrington, A. and McLachlan, A. D. (1979) Introduction to magnetic resonance. Chapman and Hall: London.

59. Ralph T. Weber, Ph.D., at Bruker Biospin Corporation: www.bruker-biospin.com

60. Deligiannakis, Y., Louloudi, M. and Hadjiliadis, N. (2000) Electron spin echo envelope modulation (ESEEM) spectroscopy as a tool to investigate the coordination environment of metal centers. *Coord. Chem. Review, 204*, 1-112.
61. Dikanov, S. A. and Bowman, M. K. (1995) Cross-peak lineshape of two-dimensional ESEEM spectra in disordered S = 1/2 , I = ½ spin systems. *J. Magn. Reson. 116*, 125-128.

62. Dikanov, S. A., Tyryshkin, A. M. and Bowman, M. K. (2000) Intensity of cross-peaks in HYSCORE spectra of S = ½, I = ½ spin systems. *J. Magn. Reson. 144,* 228-242.

63. Nikaido, K., Sakamoto, J., Noguchi, S. and Sone, N. (2000) Over-expression of cbaAB genes of Bacillus stearothermophilus produces a two-subunit SoxB-type cytochrome c oxidase with proton pumping activity. *BBA, 1456*, 35-44.

64. Dikanov, S. A., Tsvetkov, Yu. D., Bowman, M. K. and Astashkin, A. V. (1982) Parameters of quadrupole coupling of 14N nuclei of chlorophyll a cations determined by Electron Spin Echo method. *Chem. Phys. Lett. 90*, 149-153.

65. Flanagan, H., Singel, D. J. (1987) Analysis of 14N ESEEM patterns of randomly oriented solids. *J. Chem. Phys. 87,* 5606-5616.

66. Samoilova, R. I., van Liemt, W., Steggerda, W. F., Lugtenburg, J., Hoff, A., Spoyalov, A. P., Tyryshkin, A. M., Gritzan, N. P. and Tsvetkov, Yu. D. (1994) *J. Chem. Soc. Perkin Trans. 2*, 609-614.

67. Taguchi, A. T., O'Malley, P. J., Wraight, C. A. and Dikanov, S. A. (2014) Hyperfine and nuclear quadrupole tensors of nitrogen donors in the Q_A site of bacterial reactions centers: Correlation of the histidine N_δ tensors with hydrogen bond strength. *J. Phys. Chem. 118,* 9225-9237.

68. Spoyalov, A. P., Hulsebosch, R. J., Shochat, S., Gast, P. and Hoff, A. J. (1996) Evidence that ALA M260 is hydrogen-bonded to the reduced primary acceptor quinone Q_A in reaction centers of *Rhodobacter sphaeroides*. *Chem. Phys. Letters 263*, 715-720.

69. Dikanov, S. A. (2013) Resolving protein-semiquinone interactions by two-dimensional ESEEM spectroscopy. *Electron Paramagn. Resonan. 23,* 103-179.

70. Rigby, S. E., Evans, M. C. and Heathcote, P. (1996) ENDOR and special triple resonance spectroscopy of A1.- of photosystem 1. *Biochemistry, 35*, 6651-6656.

71. Teutloff, Ch., Bittl, R. and Lubitz, W. (2004) Pulsed ENDOR studies on the radical pair P_{700}^+ A_1^- and the photoaccumulated quinone acceptor A_1^- of photosystem I. *Appl. Magn. Reson. 26*, 5-21.

72. Niklas, J., Epel, B., Antonkine, M., Sinnecker, S., Pandelia, M. E. and Lubitz, W. (2009) Electronic structure of the quinone radical anion A1*- of photosystem I investigated by adanced pulse EPR and ENDOR techniques. *J. Phys. Chem. B. 113*, 10367-10379.

73. Hastings, S. F., Heathcote, P., Ingledew, W. J. and Rigby, S. E. (2000) ENDOR spectroscopic studies of stable semiquinone radicals bound to the *Escherichia coli* cytochrome bo_3 quinol oxidase. *Eur. J. Biochem. 267*, 5638-5645.

74. McConnell, H. M. (1956) Indirect hyperfine interactions in the paramagnetic resonance spectra of aromatic free radicals. *J. Chem. Phys. 24*, 764-768.

75. Lubitz, W. and Feher, G. (1999) The primary and secondary acceptors in bacterial photosynthesis: III. Characterization of the qinone radicals $Q_A^{-\bullet}$ and $Q_B^{-\bullet}$ by EPR and ENDOR, *Appl. Magn. Reson. 17*, 1-48.

76. Sinnecker, S., Reijerse, E., Neese, F. and Lubitz, W. (2004) Hydrogen bond geometries from electron paramagnetic resonance and electron-nuclear double resonance parameters: density functional study of quinone radical anion-solvent interactions. *J. Am. Chem. Soc. 126*, 3280-3290.

77. Flores, M., Isaacson, R. A., Calvo, R., Feher, G. and Lubitz, W. (2003) Probing hydrogen bonding to quinone anion radicals by ^1H and ^2H ENDOR spectroscopy at 35 GHz. *Chem. Phys. 294*, 401-413.

78. O'Malley, P. J. (1998) A density functional study of the effect of orientation of hydrogen bond donation on the hyperfine couplings of benzosemiquinones: Relevance to semiquinone-protein hydrogen bonding interactions in vivo. *Chem. Phys. Lett. 291*, 367-374.

79. MacMillan, F., Kacprzak, S., Hellwig, P., Grimaldi, S., Michel, H. and Kaupp, M. (2011) Elucidating mechanisms in haem copper oxidases: The high-affinity Q_H binding site in quinol oxidase as studied by DONUT-HYSCORE spectroscopy and density functional theory, *Faraday Discussions 148*, 315-344.

80. Kacprzak, S., Kaupp, M. and MacMillan, F. (2006) Protein-cofactor interactions and EPR parameters for the Q_h quinone binding site of quinol oxidase. A density functional study. *J. Am. Chem. Soc. 128*, 5659-5671.

81. Yap, L. L., Lin, M. T., Ouyang, H., Samoilova, R. I., Dikanov, S. A. and Gennis, R. B. (2010) The quinone-binding sites of the cytochrome bo_3 ubiquinol oxidase from *Escherichia coli*. *BBA, 1797*, 1924-1932.

82. Miyoshi, H., Takegami, K., Sakamoto, K., Mogi, T. and Iwamura, H. (1999) Characterization of the ubiquinol oxidation sites in cytochromes bo and bd from *Escherichia coli* using aurachin C analogues, *J. Biochem. 125*, 138-142.

83. Meunier, B., Madgwick, S. A., Reil, E., Oettmeier, W. and Rich, P. R. (1995) New inhibitors of the quinol oxidation sites of bacterial cytochromes bo and bd. *Biochemistry, 34*, 1076-1083.

84. Matsushita, K., Patel, L., and Kaback, H. R. (1984) Cytochrome o type oxidase from Escherichia coli. Characterization of the enzyme and mechanism of electrochemical proton gradient generation. *Biochemistry, 23,* 4703-4714.

85. Kita, K., Konishi, K., and Anraku, Y. (1984) Terminal oxidases of Escherichia coli aerobic respiratory chain. II. Purification and properties of cytochrome b558-d complex from cells grown with limited oxygen and evidence of branched electron-carrying systems. *J. Biol. Chem. 259,* 3368-3374.

86. Sato-Watanabe, M., Mogi, T., Miyoshi, H., Iwamura, H., Matshshita, K., Adachi, O. and Anraku, Y. (1994a) Structure-function studies on the ubiquinol oxidation site of the cytochrome bo complex from *Escherichia coli* using p-benzoquinones and substituted phenols. *J. Biol. Chem. 269*, 28908-28912.

87. Sato-Watanabe, M., Mogi,T., Ogura, T., Kitagawa, T., Miyoshi, H., Iwamura, H. and Anraku, Y. (1994b) Identification of a novel quinone-binding site in the cytochrome bo complex from *Escherichia coli*. *J. Biol. Chem., 269,* 28908-28912.

88. Sato-Watanabe, M., Mogi, T., Miyoshi, H. and Anraku, Y. (1998) Characterization and functional role of Q_H site of bo-type ubiquinol oxidase from *Escherichia coli*. *Biochemistry 37,* 5355-5361.

89. Sato-Watanabe, M., Mogi, T., Sakamoto, K., Miyoshi, H. and Anraku, Y. (1998) Isolation and characterizations of quinone analogue-resistant mutants of bo-type ubiquinol oxidase from *Escherichia coli*, *Biochemistry 37,* 12744-12752.

90. Nasiri, H. R., Madej, M. G., Panisch, R., Lafontaine, M., Bats, J. W., Lancaster, C. R. and Schwalbe, H. (2013) Design, synthesis, and biological testing of novel naphthoquinones as substrate-based inhibitors of the quinol/fumarate reductase from *Wolinella succinogenes, J. Med. Chem. 56,* 9530-9541.

91. Lin, M. T., Baldansuren, A., Hart, R., Samoilova, R. I., Narasimhulu, K. V., Yap, L. L., Choi, S. K., O'Malley, P. J., Gennis, R. B. and Dikanov, S. A. (2012) Interactions of intermediate semiquinone with surrounding protein residues at the Q_h site wild-type and D75H mutant cytochrome bo_3 from *Escherichia coli. Biochemistry, 51,* 3827-3838.

92. Yi, S. M., Taguchi, A. T., Samoilova, R. I., O'Malley, P. J, Gennis, R. B. and Dikanov, S. A. (2015) Plasticity in the high affinity menaquinone binding site of the cytochrome aa_3-600 menaquinol oxidase from *Bacillus subtilis. Biochemistry, 54,* 5030-5044.

93. Wallace, B. J. and Young, I. G. (1977) Role of quinones in electron transport to oxygen and nitrate in *Escherichia coli*, *Bioch. Biophys. Acta 461,* 84-100.

94. Bekker, M., Kramer, G., Hartog, A. F., Wagner, M. J., de Koster, C. G., Hellingwerf, K. J. and Teixeria de Mattos, M. J. (2007) Changes in the redox state and composition of the

quinone pool of *Escherichia coli* during aerobic batch-culture growth, *Microbio. 153*, 1974-1980.

95. Bekker, M., de Vries, S., Ter Beek, A., Hellingwerf, K. J. and Teixerira de Mattos, M. J. (2009) Respiration of *Escherichia coli* can be fully uncoupled via the nonelectrogenic terminal cytochrome bd-II oxidase, *J. Bacteriol*. 191, 5510-5517.

96. Borisov, V. B., Murali, R., Verkhovskaya, M. L., Bloch, D. A., Han, H., Gennis, R. B. and Verkhovsky, M. I. (2011) Aerobic respiratory chain of *Escherichia coli* is not allowed to work in fully uncoupled mode, *PNAS, 108*, 17320-17324.

97. Brondsted, L and Atlung, T. (1996) Effect of growth conditions on expression of the acid phosphatase (cyx-appA) operon and the appY gene, which encodes a transcriptional activator of *Escherichia coli, J. Bacteriol. 178*, 1556-1564.

98. Yi, S. M., Taguchi, A. T., Samoilova, R. I., O'Malley, P. J., Gennis, R. B. and Dikanov, S. A. (2015) Plasticity in the high affinity menaquinone binding site of the cytochrome aa3-600 menaquinol oxidase from *Bacillus subtilis*. *Biochemistry, 54*, 5030-5044.

99. Reijerse, E. J. and Dikanov, S. A. (1991) Electron spin echo envelope modulation spectroscopy on orientationally-disordered systems: Line shape singularities in S = ½, I = ½ spin systems. *J. Chem. Phys. 95*, 836-845.

100. Gardiner, A. t., Zech, S. G., MacMillan, F., Kass, H., Bittl, R., Schlodder, E., Lendzian, F. and Lubitz, W. (1999) Electron paramagnetic resonance studies of zinc-substituted reaction centers from *Rhodopseudomonas viridis*. *Biochemistry, 38*, 11773-11787.

101. MacMillan, F., Lendzian, F. and Lubitz, W. (1995) EPR and ENDOR characterization of semiquinone anion radicals related to photosynthesis. *Magn. Reson. Chem. 33*, S81-S93.

102. Srinivasan, N., Chatterjee, R., Milikisiyants, S., Golbeck, J. H. and Lakshmi, K. V. (2011) Effect of hydrogen bond strength on the redox properties of phylloquinones: A two-dimensional hyperfine sublevel correlation spectroscopy study of photosystem I. *Biochemistry, 50*, 3495-3501.

103. O'Malley, P. J. and Babcock, G. T. (1986) Powder ENDOR spectra of p-benzoquinone anion radical: Principal hyperfine tensor components for ring protons and for hydrogen-bonded protons. *J. Am. Chem. Soc. 108*, 3995-4001.

104. Harwood, C. R. and Cutting, S. M. (1990) Molecular biological methods for *Bacillus*. John Wiley & Sons Ltd.: West Sussex, England.